9-14-2010 12:00 AM

# Response of a Two-Story Residential House Under Realistic Fluctuating Wind Loads

Murray J. Morrison
*The University of Western Ontario*

Supervisor
Gregory A. Kopp
*The University of Western Ontario*

Graduate Program in Civil and Environmental Engineering
A thesis submitted in partial fulfillment of the requirements for the degree in Doctor of Philosophy

# Response of a Two-Story Residential House Under Realistic Fluctuating Wind Loads

(Spine title: Realistic Wind Loads on the Roof of a Two-Story House)
(Thesis Format: Monograph)

by

Murray J. Morrison

Department of Civil and Environmental Engineering
Faculty of Engineering

A thesis submitted in partial fulfillment
of the requirements for the degree of
Doctor of Philosophy

School of Graduate and Postdoctoral Studies
The University of Western Ontario
London, Ontario, Canada

# THE UNIVERSITY OF WESTERN ONTARIO
# SCHOOL OF GRADUATE AND POSTDOCTORAL STUDIES

## CERTIFICATE OF EXAMINATION

Supervisor

_____

Dr. Gregory A. Kopp

Examiners

_____

Dr. Craig Miller

_____

Dr. Ashraf A. El Damatty

_____

Dr. John R. de Bruyn

_____

Dr. Kurtis R. Gurley

The thesis by
Murray J. Morrison

Entitled

**RESPONSE OF A TWO-STORY RESIDENTIAL HOUSE UNDER REALISTIC FLUCTUATING WIND LOADS**

is accepted in partial fulfillment of the
requirements for the degree of
Doctor of Philosophy

Date_____ _____

Chair of the Thesis Examination Board

# ABSTRACT

Severe wind storms such as tropical cyclones, tornados, downbursts etc. can cause significant damage to infrastructure. Damage surveys following these events have shown that the roofs of residential, wood-frame construction are particularly vulnerable to failures. While damage surveys provide detail information of what components fail, they cannot provide the loads at which these failures occurred or how they initiated. Wind tunnel pressure models provide detailed information of the wind loads on buildings, however, they are not able to predict failures or how these loads are transferred through the structure. In order to better understand the response of wood framed houses when subjected to high wind loads, realistic fluctuating wind loads were applied to a full scale two-story wood frame house. In addition, individual component tests were conducted on toe-nailed roof-to-wall connections to examine their behaviour to fluctuating wind loads. The testing of individual toe-nail connections under realistic fluctuating wind loading has found that the nails are incrementally withdrawn at peak loads. However, the maximum load applied during the fluctuating load tests matches well with the failure capacity determined from ramp loading experiments, even though damage to the connections initiates at much lower loads. Tests performed on the roof of a house have shown that the uplift capacity of the roof is significantly higher than that predicted using the individual connection results. The higher uplift capacity of the entire roof is attributed to significant load sharing between adjacent connections so that failures likely initiate at multiple connections up to the entire roof and the effective tributary area of the roof-to-wall connections is substantially larger than that of a single truss. Since toe-nailed roof-to-wall connections are partially withdrawn during peak wind gusts, how the loads are

transferred through the structural system, to the connections, changes as the connections become increasingly damaged. This implies that while static testing is suitable to determine the capacity of individual toe-nail connections, testing of the full structure must be conducted using realistic fluctuating wind loads. Despite the significant damage accumulated at the toe-nail roof-to-wall connections, there was little evidence of damage to the interior of the house, indicating that there may be significant undocumented damage to homes following tropical cyclones.

**KEYWORDS:** wind loads, low-rise building, structural failures, roof-to-wall connections, full scale testing, structural response

# ACKNOWLEDGEMENTS

The author gratefully appreciates the continuous support and expertise of his supervisor Dr. Gregory A. Kopp throughout his entire post graduate education at the University of Western Ontario. The author would also like to thank Dr. David Henderson for many interesting and invaluable discussions pertaining to his experiences with full scale testing and damage investigations. The author would also like to acknowledge the scholarship support from NSERC Canada and the OGSST program at the University of Western Ontario. The author also appreciates the help provided by Mr. Mitchell Cuddie in the development of the toe-nail rig, as well as the help of Ms. Ana Ruiz and Ms. May El Damatty for their help in conducting the experiments on individual toe-nail connections. In addition, the help of University Machine Services at the University of Western Ontario, and in particular the help of Mr. Chris Vandelaar, is much appreciated. Equipment for this project was provided through grants obtained from the Canada Foundation for Innovation, Ontario Innovation Trust, and the University of Western Ontario.

# TABLE OF CONTENTS

# LIST OF TABLES

# LIST OF FIGURES

# LIST OF APPENDICIES

# NOMENCLATURE

| | |
|---|---|
| $A$ | Area |
| $Cf$ | Force Coefficient |
| $\breve{C}f$ | Peak Force Coefficient |
| $Cm$ | Moment Coefficient |
| $\breve{C}m$ | Peak Moment Coefficient |
| $Cp$ | Pressure Coefficient |
| $Cr^i$ | Reaction Coefficient at connection index *i* |
| $\breve{C}r^i$ | Peak Reaction Coefficient at connection index *i* |
| $\delta$ | Displacement |
| $\delta_i(t)$ | Displacement time series at connection with index i |
| $F_u$ | Uplift Force |
| $F_{A,B}$ | Applied Force at Node A or B |
| $F_{ext}$ | Force due to External Pressures |
| $F_i(t)$ | Force time series at a connection with index i |
| $F_{int}$ | Force due to Internal Pressures |
| $F_{net}$ | Net Force between $F_{ext}$ and $F_{int}$ |
| $F_k$ | Force due to an element with stiffness *k* |
| $Fv$ | Overall Roof Uplift Force |
| $Fv_{HD}$ | Overall Roof Hold Down Force |
| $F_{wt}$ | Factor used to convert wind tunnel pressure coefficients to $GCp_{eq}$ |
| $GCp$ | ASCE7-05 pressure coefficient |
| $GCp_{eq}$ | ASCE7-05 equivalent pressure coefficient |
| $H$ | Mean Roof Height |
| $I$ | Importance Factor in ASCE7-05 |
| $I(x,y,z,\delta)$ | Influence Function |
| $Iu$ | Turbulence Intensity |
| $K_d$ | Wind Directionality factor in ASCE7-05 |
| $K_h$ | Velocity pressure exposure factor in ASCE7-05 |
| $K_{zt}$ | Topographic Factor in ASCE7-05 |
| $k$ | Element Stiffness |
| $k_{crit}$ | Critical Stiffness |
| $L$ | Characteristic Length |
| $M_i(t)$ | Moment time series at a connection with index i |
| $M_{HD}$ | Moment Hold Down |
| $P(x,y,z,t)$ | Surface Pressure |
| $\varphi$ | Roof Slope Angle |
| $q$ | Dynamic Pressure |
| $\rho$ | Density |
| $R_{A,B}$ | Reaction Force at node A or B |
| $R^i$ | Reaction force at connection index *i* |
| $T$ | Total Time |
| $t$ | Time |

| | |
|---|---|
| $\theta_i(t)$ | Rotation at a connection with index $i$ |
| $V$ | Scaling Wind Speed |
| $V(x,y,z,t)$ | Three Dimensional Velocity field time series |
| $V_{10m,O.C.,3s}$ | 3 second gust wind speed at a height of 10 m in an open country terrain |
| $V_{10m,O.C.,3600s}$ | Hourly mean wind speed at a height of 10 m in an open country terrain |
| $V_{H,O.C.,3600s}$ | Hourly mean wind speed at mean roof height in an open country terrain |
| $V_{H,zo,3600s}$ | Hourly mean wind speed at roof height for a terrain with roughness height $z_o$ |
| $V_{H,zo,gust}$ | Gust wind speed at roof height for a terrain with roughness height $z_o$ |
| $V_{net}$ | Net Wind Velocity |
| $\Delta z_{A,B}$ | Change in displacement at node A or B |
| $z_o$ | Boundary Layer Roughness Height |

# SYMBOLS AND ABREVIATIONS

| | |
|---|---|
| 3LP | Three Little Pigs |
| BLWT | Boundary Layer Wind Tunnel |
| CAD | Computer Aided Design |
| C&C | Components and Cladding |
| CTS | Cyclone Testing Station |
| EC | Environment Canada |
| FOS | Factor of Safety |
| HD | Hold Down |
| HDF | Hierarchical Data Format |
| Hz | Hertz |
| IRLBH | Insurance Research Lab for Better Homes |
| mph | Miles per Hour |
| MSU | Mississippi State University |
| MWFRS | Main Wind Force Resisting System |
| N | Newton |
| Re | Reynolds Number |
| PLA | Pressure Loading Actuator |
| PSD | Power Spectrum Density |
| RTWC | Roof-to-Wall Connections |
| SOM | Sum of Moments |
| UWO | University of Western Ontario |
| USD | United States Dollars |

# 1.0 INTRODUCTION

Land falling hurricanes, tropical cyclones and typhoons have caused significant damage and destruction to coastal regions around the world. Cyclone Tracy in 1974 was responsible for the nearly total destruction of Darwin, Australia (Walker, 1975). Hurricane Andrew made land fall in Florida in 1992 causing substantial damage, with estimates of 20 -25 billion (USD) in Florida and an additional 1 billion (USD) in Louisiana (HUD, 1993). Over the past decade, numerous severe hurricanes have made landfall, such as Charley, Katrina, Ike. Annual losses due to hurricanes have been increasing dramatically due to increased population and infrastructure in coastal regions around the world (Pielke et al., 2008). The current upward trend in sea surface temperatures (Trenberth, 2005) is expected to make the worst of these storms stronger (Emanuel, 2005), making mitigation strategies more important than ever (Guikema, 2009 and Board on Natural Disasters, 1999). Post event damage investigations have provided an indication of common failures. These have shown that residential wood-frame structures are particularly vulnerable to high winds and represent a large proportion of the losses (HUD, 1993 and Walker, 1975). Failures to such structures nearly always involve portions of the roof, a fact which is not surprising since it is the roof that experiences the highest wind loads. Roofs become particularly vulnerable when there are openings on windward walls. These openings, which cause substantial increases to the wind loading because of internal pressurization (Kopp et al., 2008), are common in hurricanes due to windborne debris impacts on windows and doors (HUD, 1993 and Minor, 1994). In nearly all cases, failures of roof elements initiate at the connections (Reardon et al., 1999) and, in many cases, these connections are made by nails (Keith and Rose, 1994).

Failures of structural roof components dramatically increase losses because of water infiltration (Sparks et al., 1994), which makes keeping the roof connected to the house critical in reducing financial losses during extreme wind events. Moreover, with all or part of the roof missing, the walls are more susceptible to collapse, especially in modern wood-frame construction, which is a significant life safety issue. Following Hurricane Andrew, improvements were made to the South Florida Building Code regarding single family homes, which were adopted in 1994 in Broward and Dade Counties and later adopted by the entire state of Florida in 2001 (Gurley et al., 2006). Gurley et al. (2006) have shown the newer homes built to this new standard have measurably less damage than those built to the previous standard.

Figure 1.1 to Figure 1.3 show some recent examples of failures of roof-to-wall connections (RTWC) in timber frame construction under high wind loads. Toe-nails are the most common type of RTWC in North America. While it is now common to use hurricane straps in hurricane prone regions such as South Florida and the Gulf Coast, other regions can still be susceptible to extreme wind events, such as tornadoes and downbursts, which are capable of causing failures to toe-nailed RTWC connections, examples of which are discussed by Kopp et al. (2009) and Morrison et al. (2010). Furthermore, there still exist a large number of residential houses in hurricane prone areas that use toe-nails as RTWC, making the development of mitigation strategies important. One major challenge is that mitigation strategies need to be cost effective in order to be widely implemented; a point which has proven difficult for retro-fitting existing structures. This is where realistic analysis of performance, leading to optimal solutions,

is critical. However, understanding the real performance of a wood frame structure can be extremely difficult, for several reasons:

- Wind loads on low rise buildings are complex, with high spatial and temporal variations on the roof of the building.
- Structural analysis of wood frame structures is challenging, due to ill-defined load paths, redundant structural members, as well as many non-structural or architectural features that can take significant load (Reardon 1996).
- Significant variability in many aspects of construction, not only due to construction errors and variability in wood strength, but also differences in construction practices from region to region.

Figure 1.1 Global roof failure of a house due to a tornado that struck Vaughan, Ontario on August 20, 2009.

Figure 1.2 Failure of windward windows, shingles and roof trusses during Hurricane Katrina in August, 2005.


Figure 1.3  Failure of a group of trusses during a tornado in Midland Ontario, June, 2010.

To illustrate these effects, Figure 1.4 presents a flow diagram linking the wind field to the actual response of the connections. While Figure 1.4 could apply to any structural wind force resisting system, the following discussion will concentrate specifically on toe-nail RTWC connections. The blue arrows in Figure 1.4 represent actual physical interaction and behaviour that engineers need to understand in order to obtain the engineering values required for design. These three interactions are:

1. The interaction between the incoming wind field and the structure
2. The transfer of loads through the structure
3. The behaviour of the structure and connections to the load

There are also two feedback mechanisms as indicated by the red and yellow arrows. The first feedback mechanism (red arrow) represents a change in the shape or configuration of the structure caused by the wind loads that will effect the wind loads at a later time. Related to this, a change in the relative wind speed and direction can occur due to the movement of the structure. This latter effect can be significant for high rise buildings that tend to sway in the wind, as well as for long span bridges. However, for low rise buildings, both of these effects are minimal, and if the structure were to displace sufficiently for them to have an effect, the structure would have already sustained significant damage. Consequently these effects will not be considered herein as they are not considered relevant to the onset and mechanisms of failure. The second feedback relates to the performance of the structural elements and connections. As the structure displaces this could affect the future response. An example of this effect is performance of pierced metal fasteners under wind loads, where failures due to low cycle fatigue occur

(Henderson et al., 2009). Moreover, it is possible that as the connections or elements displace, this will cause a change in distribution of the loads, thereby changing the structural system. The following sections will discuss these four aspects of Figure 1.4 in further detail.

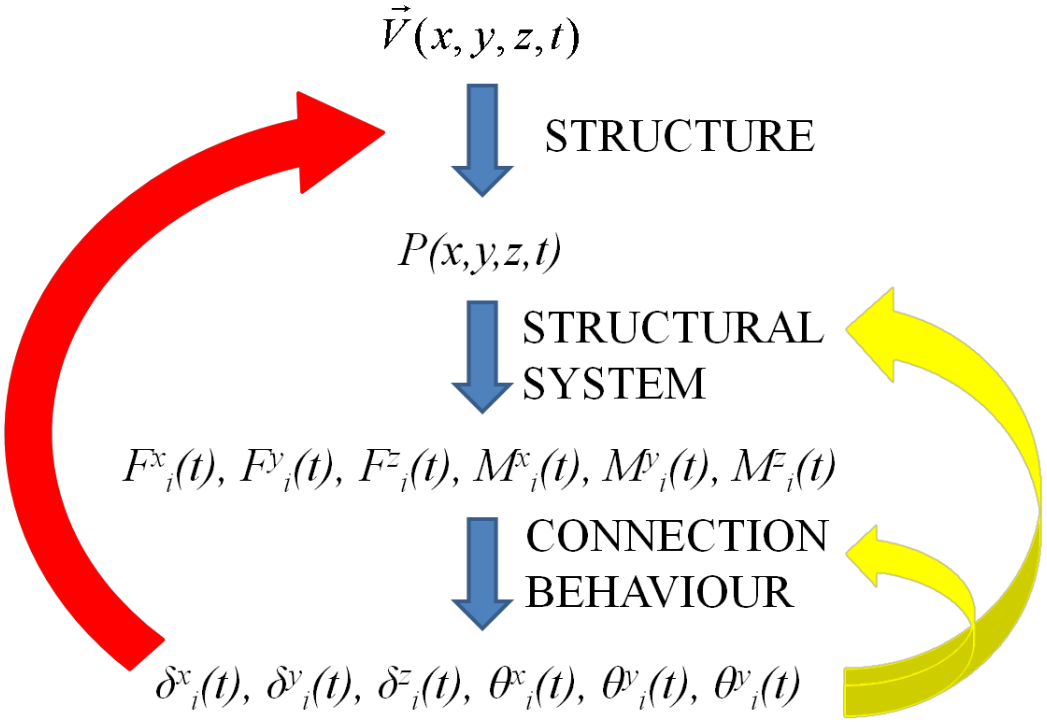


Figure 1.4 Flow diagram of wind action on a building and the structural response

## 1.1 Obtaining wind loads on a low-rise building

Our understanding of synoptic wind loads on low rise buildings ("STRUCTURE" in Figure 1.4) has increased significantly over the past 35 years because of wind tunnel testing as well as full-scale, field studies. The work of Stathopoulos (1979) allowed for the codification of wind loads for low-rise buildings and is included in design standards for both Canada and the United States (ASCE7-05, 2006 and NBCC, 2005). Conducting wind tunnel studies on low-rise buildings involves significant challenges, since nearly all

boundary layer wind tunnels (BLWT) naturally develop wind profiles that have typical geometric scaling in the range of 1:300 to 1:500. However, as discussed by Tieleman (2003) and Kopp et al. (2005), models of this scale are so small they offer minimal practical value due to low measurement resolution and low Reynolds numbers. However, the requirement of matching the full scale Reynolds number is also a challenge for high rise buildings and can generally be relaxed for sharp edged buildings so long as it remains above ~50,000 (Tieleman, 2003). As such, for low rise buildings, a more appropriate model scale of 1:100, or even 1:50, is commonly adopted. However, in order to match the wind velocity and turbulence intensity profiles at this scale, there is usually a mismatch in the turbulence integral scales, as discussed by Kopp et al. (2005). Generally a mismatch of the integral scale is allowed, Stathopoulos (1983) suggested that the integral scales can be relaxed by a factor of 2 while more recently Tieleman (2003), has said that the deviation should be less than 20%. In any case matching the integral scale more precisely is at the expense of matching the turbulence intensities, which are critical in achieving a proper flow simulation (Tieleman, 2003).

Full scale experiments such as those conducted at Texas Tech University (Levitan and Mehta 1992a, 1992b) have provided wind loading pressure data to compare with wind tunnel experiments. Despite all the challenges in achieving a proper flow simulation in the wind tunnel, numerous comparisons conducted by Cochran and Cermak (1992), Xu and Reardon (1996) and Surry (1991) have shown that the match between full scale and wind tunnel data is very good with the exception of highest peak pressures over small areas. Lin and Surry (1998) have shown that this discrepancy between model and full-

scale peak pressures can be explained in part by scale mismatches between the full and model scale pressure tap diameters. For this reason, Surry (1999), summarizing the state-of-the-art a decade ago, came to the conclusion that:

> "we know enough about the wind loads on low buildings now, so that disastrous failures (such as seen during Hurricane Andrew) to storms other than severe tornadoes, are much more likely to be due to faults in codes, or construction and inspection practices, than due to lack of basic wind engineering knowledge." (Surry 1999).

More recently, questions have arisen on the wind loads on structures in more localized and less stationary wind events due to hurricanes and thunderstorms. Liu et al. (2009) compared pressure data obtained from a full scale instrumented house during Hurricane Ivan in 2004, to pressure coefficients obtained from a wind tunnel test. Similar to previous comparisons between full and model scale, for synoptic winds, mean and RMS pressures match well.

For thunderstorms, high winds near the ground can be caused by tornados, downbursts or gust fronts, all of which likely have significantly different flow characteristics than synoptic winds. Determining the effect these flow fields have on the wind loading has been the subject of several recent studies. In the case of tornados, Haan et al. (2010) have shown that wind loads generated by tornadoes on a low-rise building are dominated by the suction pressure in the core of the vortex, in contrast to typical boundary layer winds, where the highest loads are the results of vortices generated by the roll up of the separated shear layer at leading edge of the building (Saathoff and Melbourne 1997). As

such, pressure coefficients derived from typical boundary layer wind tunnels may not be applicable for tornados. Preliminary work using a downburst simulator Chay and Letchford (2002), indicate that typical boundary layer wind tunnel measurements may underestimate the wind loads. In contrast, Lombardo (2009) has shown that pressure coefficients from several non-stationary thunderstorm wind events are within the range of pressure coefficients obtained from typical boundary layer winds on the same building, based on his analysis of several non-stationary wind events on the full-scale Texas Tech Building. This suggests the current use of wind tunnel boundary layer pressure coefficients may be appropriate, for these types of events. Although, the true wind loads caused by severe thunderstorm winds is still the subject of significant research.

Wind loads on low-rise buildings are best characterized by their fluctuations, both in time and spatially across building surfaces, because of turbulence in the atmospheric boundary layer and turbulence generated by the building (and the interaction of the two). An example of the spatial variations of wind loads on a gable roof of a house is shown in the colour contours in Figure 1.5, while the temporal variations at a single point are shown in inset "A" (blue line). Because of the large spatial gradients, it is well known that averaging over larger areas yields significantly smaller aerodynamic force coefficients than those at a single point (Surry et al., 2007). This is illustrated in inset A of Figure 1.5 by comparing the time history for the 3 $m^2$ area (green line) with that of a single point (blue line) within that area. This has significant ramifications for residential construction with its many redundant members, variability of materials and connections, and ill-defined load paths. Figure 1.5 also indicates that, even for spatially-averaged loads, the

largest fluctuations occur intermittently such that loads can double in magnitude, or more, in less than a second, and then drop again just as quickly. Thus, the duration of the storm is an important parameter, since, on average, longer durations will lead to larger peak values (for the same mean wind speed), and also to more of them. Current design standards, such as the ASCE 7-05 (2006), do not consider this since only single peak values are used. To illustrate the temporal variations further a video of the temporal variation of the pressure coefficient is provided in APPENDIX A.

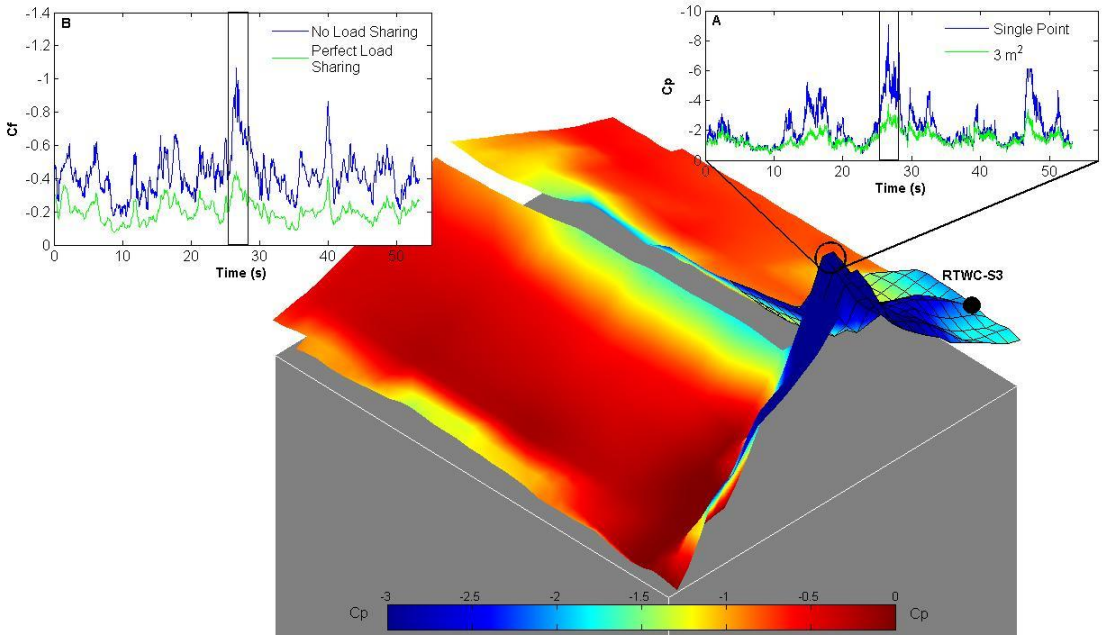


Figure 1.5 Contours of the spatial gradients of external wind pressures on the roof of the test house. Inset A: wind tunnel pressure coefficients at a single point and averaged over a $3m^2$ area. Inset B: Applied force coefficients for a single roof to wall connection (RTWC), considering no load sharing and perfect load sharing.

While wind tunnels are able to provide a good representation of the true wind loads that act on a building, they are not able to explain how the building will respond to these loads. The use of failure models in wind tunnel investigations such as those conducted by

Visscher and Kopp (2007) and Kordi et al. (2010), have been used to predict failure wind speeds, provided the structural details along with the mode of failure are assumed explicitly, and thus, may not be a true reflection of how failures occur in reality.

## 1.2 Connection Behaviour and Response

As mentioned above, a key issue for timber-framed houses is the load and response of the connections between the roof and the wall. In general, the uplift load at a connection, $F_U$, can be obtained via:

$$C_f(t) = \int_A Cp(x,y,z,t) I(x,y,z,\delta) \frac{dA}{A} = \frac{F_U(t)}{\frac{1}{2}\rho V_{H,zo,3600s}^2 A} \qquad (1.1)$$

where $Cp\ (x,y,z,t)$ is the pressure coefficient at location $(x,y,z)$ on the building surface at time, $t$, $I(x,y,z,\delta)$ is the structural influence function, $A$ is the area where $I(x,y,z,\delta) \neq 0$ for the connection under consideration, $C_f$ is the force coefficient, and $V_{H,zo,3600s}$ is the hourly mean wind speed at mid-roof height (assuming that $Cp$ has been normalised to the hourly mean wind speed at mid-roof height). The structural influence function is non-zero in regions where loads are being transferred to the connection. However, in order to obtain $I(x,y,z,\delta)$, knowledge of how the wind loads interact with the structure, before and during failure is required. This is indicated by the parameter, $\delta$, which represents these effects, including changing stiffness and load sharing as the connection, and the adjacent ones, displace and are damaged. Influence functions for wood frame structures are generally not known, even for the simple case of $\delta$=0 (i.e., no displacements), let alone when there has been damage. Consequently, the approach usually taken for design is to assign each

connection a geometric tributary area where $I = 1$. This standard design approach, which is inherently conservative, essentially assumes that there is no load sharing between adjacent connections. An alternative is to assume "perfect" load sharing between all connections, so that the applied load at each connection is the same, resulting in a reduction of the worst aerodynamic coefficient by a factor of approximately 3, in the present case. These two cases represent the bounds for the true load at a particular connection; in reality the true reaction must lie between these two cases. Load coefficients using these two approaches are shown in inset B of Figure 1.5, for a single connection RTWC "S3".

The capacity of toe-nail connections to uplift loads has been the subject of several studies, such as Cheng (2004), Reed et al. (1997), Riley and Sadek (2003) and Shanmugam et al. (2009). These experiments apply loads at a constant displacement rate (typically 2.54 to 6.35 mm/min) and measure the required force to keep the connection moving. These tests are nominally static and quite different from the highly fluctuating loads generated by real winds. Experiments conducted by Shanmugam et al. (2009) on in-situ connections did apply a form of cyclical loading, although a maximum of only three loading cycles were used. The cycles were applied at a low displacement rate of 2.54 mm/min and the end of a cycle was based on a displacement threshold. The loading from these tests are significantly different than that induced by real wind where there are a large number of cycles and the loads can double or even triple in less than a second and decrease just as quickly. The mean maximum withdrawal capacity from these studies is in the range from 1130N to 2840N, depending on the type and number of

nails (for the capacities above the nails ranged from 8d to 16d), age of the connection, type of wood, and the wood moisture content. To date there has been no study to document the effects, if any, that cyclical or realistic wind loads have on the withdrawal performance of toe-nailed RTWC. The hysteretic behaviour and reduction of the failure capacity when subjected to cyclical shear loads, has been tested and implemented in finite element models of entire structures, e.g., He et. al. (2001), primarily for studies involving earthquake loading.

While these standard tests for toe-nail connections provide valuable information on the ultimate hold down capacity, they are unable to answer whether the behaviour of the connection will be similar under a highly fluctuating load, such as that shown in Figure 1.5. Moreover, it assumes that there is no change in the connection response after repeated loading, this effect is represented by the yellow feedback arrow between the connection response and "CONNECTION BEHAVIOUR" shown in Figure 1.4. Finally, in order to use these capacities to obtain failure winds speeds requires an assumption of the load sharing behaviour in the structure. For the example shown in Figure 1.5, depending on the assumption, the failure wind speed can change by a factor of 1.7.

## 1.3 Full-Scale Structural Testing and Load Redistribution

Testing of entire full-scale structures is both extremely challenging and expensive. For this reason, structural tests are often conducted on portions of the structural system, as a compromise. These experiments attempt to capture the effects of the structural system, which is missing from individual component tests, while keeping the test to a reasonable

size and cost. Numerous standard airbox tests have been developed to test roof coverings, such as the ASTM E1592-01 (2001) to test standing seam metal roofing (SSMR), the SIDGERS test method developed at National Research Council of Canada to test membrane roofs (Baskaran and Chen, 1998), and the Low-High-Low (LHL) (Mahendran, 1995) test method used in Australia to test pierced metal fasteners, to name a few. These standard tests normally apply spatially uniform loads that are either constant in time, as in the case of the ASTM E1592-01, or sinusoidal loading, as is the case of SIDGERS and LHL test protocols. Structural testing using more realistic wind loading has been achieved using a loading system named BRERWULF developed at the British Research Establishment by Cook et al. (1988). This system was able to apply spatially uniform, but temporally varying pressures to a cladding specimen provided it was nominally sealed. Experiments conducted at Mississippi State University (MSU), reported by Surry et al. (2007), have used magnetic actuators to apply spatially and temporally varying loads to SSMR. These tests showed that the ASTM E1592-01 (2001) test used in conjunction with the wind loading provision ASCE7-05(2006) standard was conservative. Morrison and Kopp (2010) were able to explain that this apparent conservatism was mostly due to load sharing between the highest loaded connections and the edge of the roof. This illustrates the importance that the boundary conditions have on the outcome of structural testing. In the case of wood frame structures this problem is even more apparent since the structural system itself is poorly defined as compared with commercial and industrial buildings, having many redundant load paths and non-structural members which can contribute substantially to the overall structural system. Other researchers, such as He et al. (2001), have attempted to create finite element

models of entire three-dimensional wood frame structures, to predict the response, to earthquake and wind loading. In order for these models to be effective they need to be validated against benchmark data from experiments. Historically, these models have been mainly used and validated for earthquake loads, where the loading to the structure is temporally varying but spatially uniform as applied at the foundation, resulting in mainly shear loading at the RTWC. In contrast, as previously discussed, wind loads cause significant uplift loading on the structure that not only has significant temporal variations but spatial variations as well. To date, it is unclear if these models accurately predict the behaviour of the structure to realistic wind loads. Investigations by Wolfe and McCarthy (1989) and Wolfe and LaBissoniere (1991) on several full scale roof truss assemblies have used static point loads on different trusses within the assembly to determine the influence function, $I(x,y,z)$ at these loading points for all RTWC in the assembly. Wolfe and LaBissoniere (1991) found that the RTWC of the truss that was actually loaded experienced between 40% and 60% of the applied load, with the remaining load being transferred to adjacent RTWC up to 4 trusses away. Mani (1997) conducted a similar series of tests on a 1/8 scale model using point loads at different loads on the roof, obtaining similar results to Wolfe and LaBissoniere (1991). While these measurements provide a good indication of the load sharing behaviour between adjacent RTWC, in order to use these results to predict the reactions at specific roof-to-wall connections, two key assumptions must be made. The first assumption is that these influence functions are valid for loads that vary significantly in time, or in other words, that the time scale of the structure to transfer the loads to the connections is essentially zero. The second assumption comes from the behaviour of the RTWC and the testing method used. In

order to measure the reactions, load cells were installed in place of the RTWC, as a result there was no displacement at the connection. This implicitly implies that the failures of the RTWC are brittle, meaning that the failures occur suddenly with minimal displacements prior to failure, or that the displacement of the RTWC does not significantly affect the influence function. During the tests conducted by Wolfe and McCarthy (1989), it was found during in initial setup that the dead loads at the RTWC varied significantly, and that adjusting the heights of the load cell supports resulted in a more even distribution of the dead load between connections. For this reason it is unclear if the influence functions developed through the test methods can be applied directly to realistic fluctuating wind loads, or if the failure behaviour of the connections plays a role in changing the influence functions.

### 1.3.1 Structural Testing of Full Scale Wood Frame Structures

Instrumented residential timber and steel framed houses were tested at the Cyclone Testing Station (CTS) at James Cook University in Australia using load spreaders and hydraulic rams. With such a system, they were able to apply static loads with limited spatial variations, similar to those in building codes. Boughton (1988) and Reardon (1996), provide a detailed summary of the full scale house tests that have been conducted at CTS. These tests have shown that non-structural elements have a significant influence on the structural system in wood frame construction, in addition to identifying weaknesses in the hold down chain. However, the experiments were not able to identify the effects that temporally varying wind loads have on the structure. The temporal variations of the force coefficient even for large tributary areas can vary significantly in

time, as shown in Figure 1.5. These effects can be significant and may change the structural system over time, as represented by the feedback arrow in Figure 1.4 between the connection response and the "STRUCTURAL SYSTEM". Moreover, the spatial gradients of the wind loading used were not fine enough to capture the true spatial variation of the wind, especially for cornering winds. Consequently, it is unknown if the structure will respond to loading of all frequencies or if there is a certain required duration of the peak wind load required to induce a response in the structure. This implicitly implies that the structure has a time scale of response, which may have significant implication since the magnitude of the wind loads increase with the square of the wind speed while the duration decreases linearly. This could mean that lower amplitude longer duration loads would produce a larger response than higher amplitude shorter duration loads. Finally, since construction techniques and methods differ between Australian and North American homes, the interpretation of the results obtained at CTS for North American houses is difficult.

## 1.4 Objectives

Sections 1.1 to 1.3 outlined the key aspects, shown in Figure 1.4, which influence how a structure responds under wind load. Wind tunnel testing can give us very detailed information on the actual wind loads but cannot predict how the structure will respond to these wind loads. Damage investigations conducted following severe wind events provide valuable information on both what has failed and what has remained intact, however; these investigations can rarely indentify how the failures initiated, at what wind speed (failure load), or how the failures progressed. Testing on individual toe-nail

connections has provided the hold down capacity of the connection, but has not taken into account the effects that realistic fluctuating wind loads may have on the response, the effect of loading duration, or the effect of load sharing on the connections. Ultimately, the objective of the current work is to attempt to link the aerodynamic loading of the building to the response and ultimately the initiation of failure of the structure. Specifically, the performance of toe-nailed RTWC connections will be examined in detail, through testing of individual toe-nail connections using realistic fluctuating wind loading. The tests will examine the differences, if any, in the response of toe-nail connections to realistic loads rather than the static testing that has previously been conducted.

In addition, since the individual toe-nail connection tests are unable to account for structural system effects, such as load sharing between adjacent connections or overall structural response time to high frequency loads, full scale testing of a complete structure is required. These full scale tests on a complete structure will provide an improved understanding of the structural system and connection behaviour during real wind storm events, and ultimately a better understanding of how failures occur. The loading system developed as part of the 'Three Little Pigs' (3LP) Project at the University of Western Ontario (UWO) allows the application of realistic fluctuating wind loads to full scale structures. The objective of the current work is to evaluate the performance of toe-nail RTWC in a typical two-story, wood frame residential house, built as part of the 3LP project.

# 2.0 EXPERIMENTAL SETUP

In order to conduct the experiments outlined in Chapter 1.0 three different experiments setups are required: the full-scale structural experiments, the individual toe-nail RTWC experiment and finally the wind tunnel tests that are required to obtain the realistic wind loads. The following chapter will outline these three experimental setups in detail.

## 2.1 Full-Scale Structural Experiment

The full scale structural tests were conducted as part of the 3LP project at the Insurance Research Lab for Better Homes (IRLBH). The following sections describe the first test house, as well as the loading system used to apply wind loads to the structure and the measurement equipment used.

### 2.1.1 Test Specimen and Instrumentation

A typical 2-story wood frame, brick veneer house shown in Figure 2.1, was built at the Insurance Research Lab for Better Homes following the Ontario building code, by Building Science Students from Fanshawe College in London Ontario. The house plan dimensions are 9.0 m by 8.9m with an eaves height of 8.0 m and a gable ended roof with a roof slope of 4:12 ($\varphi$= 18°). The roof overhangs the external wall of the house on all sides by approximately 0.61m. The prefabricated roof trusses are spaced 0.61m on center and connected to the wall top plate using standard toe-nail connections. The roof is sheathed with 9mm plywood, and asphalt shingles. The walls were built with standard 2 x 4's at 0.41 m centers and the exterior walls are covered with 25mm foam insulation which was then covered by a brick veneer. Figure 2.3 shows a picture of the house under construction prior to the installation of the roof sheathing and brick veneer. The construction of the house was intended to approximate typical construction in the region.

As such, no attempt was made to enforce any particular quality control measures that would not be implemented in standard construction, although construction errors and structural details were documented during and after construction.

Figure 2.1 Photograph of the test house surrounded by the steel reaction frame used to mount the air bags and PLAs.

Through this documentation of the structure it was observed that 2 different types of twisted shank nails had been used for the toe-nail RTWC, either 12d (length: 82.6mm, shank diameter: 2.87 mm) or 16d (length: 88.9 mm, diameter: 3.33 mm) nails. Overall, the use of each nail appeared to be equal. The use of 2 nails likely occurred because different students having different sized nails available. While the number of nails per connection varied from connection to connection, the average number of nails per

connection is three, however, it should be pointed out that this is a simple count of the number of nails and not a reflection of the quality of the nailed connection. Chapter 9 of the National Building Code of Canada NBCC (2005), prescribes that the roof trusses should be held down with three 82mm nails. So, the current test appears to meet the prescriptive requirement for RTWC of the NBCC (2005). Figure 2.2 provides a side by side photograph of each of these nails. The documentation of the RTWC also included photographs of each connection from both sides so that errors in construction or construction defects are noted and to provide a basis of comparison once testing had commenced and damage occurred to the house.

Figure 2.2 Photograph of the two types of nails used for the toe-nail RTWC on the test House. The grid shown is 6mm by 6mm, above is the 12d nail, below is the 16d nail.

Figure 2.4 shows a photograph of one toe-nail connection prior to testing. From the photograph it is observed that one nail has been nailed at too shallow an angle, likely reducing the hold down capacity of the connection compared with a "perfect" connection. APPENDIX B provides further photographs for the other RTWC prior to testing. The house was inspected by 30 building inspectors from across southern Ontario who, on average, found it to be typical of construction within the region. The documentation of the structural details of the house also revealed that there were additional RTWC between the roof trusses and the internal walls. While these additional connections may be present in typical construction, it is not guaranteed. Moreover, the number and location of these connections are dependent on the internal floor plan of the house. Since the connections may not exist in typical construction, or may even be removed during renovations it was decided to remove these internal connections after construction had been completed. While an attempt was made remove all of these connections, it was discovered upon removal of the roof that some connections had been missed, although an exact count and location of the extra connections to the internal walls is not available.

Prior to testing of the roof the shingles were removed and the roof sheathing was screwed to the roof trusses to prevent failures of these elements and to allow the attachment of the air-bags to the roof (the air-bags will be discussed in Chapter 2.1.2). This reduces the dead load of the roof, but does not significantly alter the overall structural system. Moreover, since the dead load is evenly distributed over the entire roof, the effect on each individual connection is the same. As a result the results can be re-interpreted in post processing to account for the missing weight.


Figure 2.3 Photograph of the test house under construction. Photograph shows the house prior to the installation of the brick veneer and roof trusses.

The test house has a total of 16 roof trusses, for a total of 32 RTWC. Figure 2.5 provides a schematic drawing of the truss layout, the naming convention, along with cardinal directions, which will be used through the remainder of the thesis.

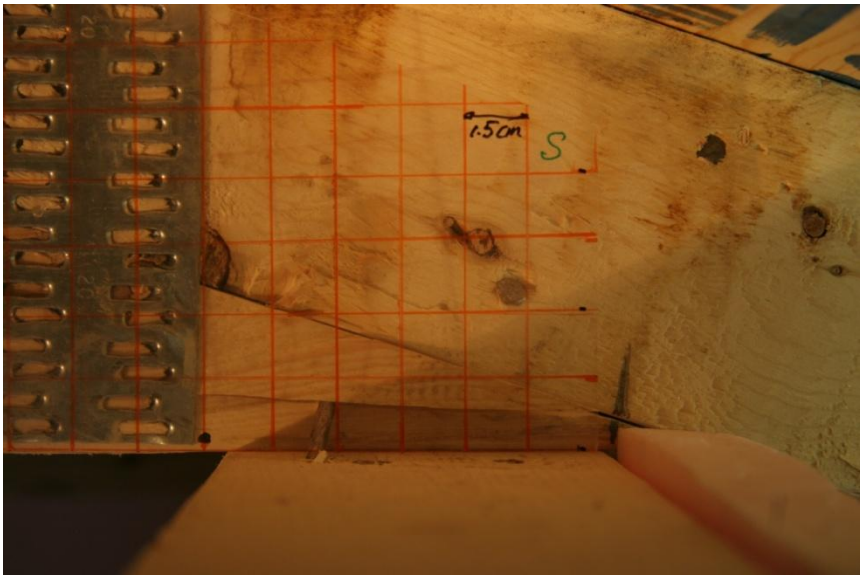


Figure 2.4 Photograph of toe-nail RTWC "S3" taken with the camera facing East

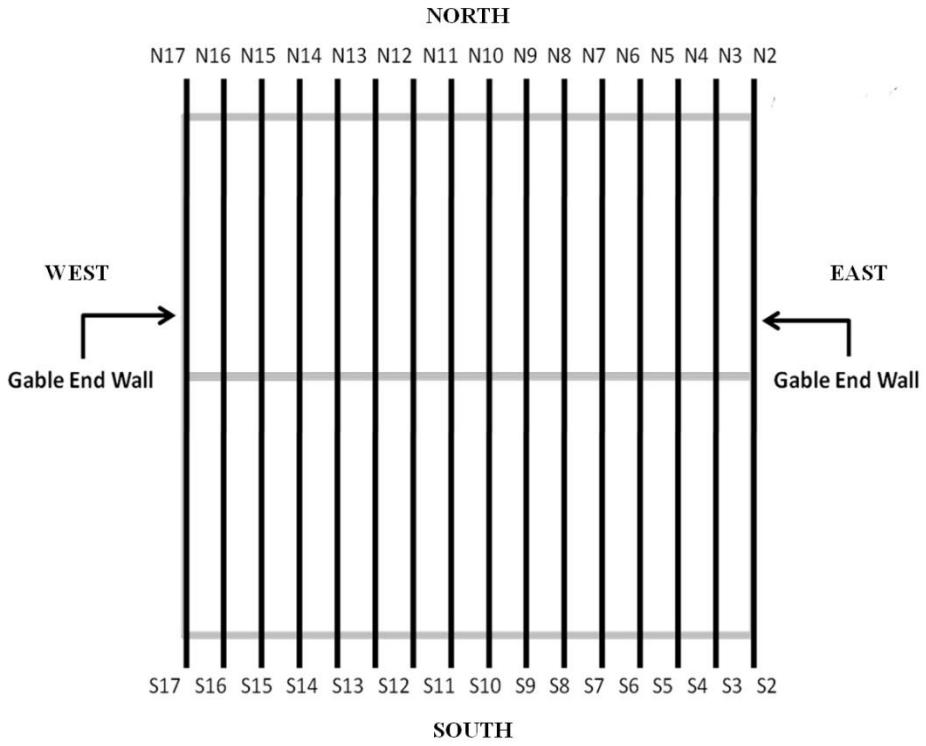


Figure 2.5Truss layout and naming conventions, with laboratory cardinal directions

The goal of the current experiments is to monitor the response of the 'as built' house under realistic wind loads. As such, an effort was made to make as few modifications to the house as possible. In order to monitor the movement of the house during the experiment, displacement transducers were mounted on the brick veneer shown in Figure 2.6, to measure the displacement of every roof to wall connection, with the exception of the north and south connections on truss 17. Truss 17 was the gable end wall on the Western side of the house and during construction the truss was cut so that the truss did not overhang the North or South walls; as a result, it was not possible to measure the displacement of this truss. Independent measurements from the ground ensured that the brick veneer remained stationary throughout all of the tests. In addition, 16 video

cameras as shown in Figure 2.6, were placed at various positions around the house and were also used to monitor the response.

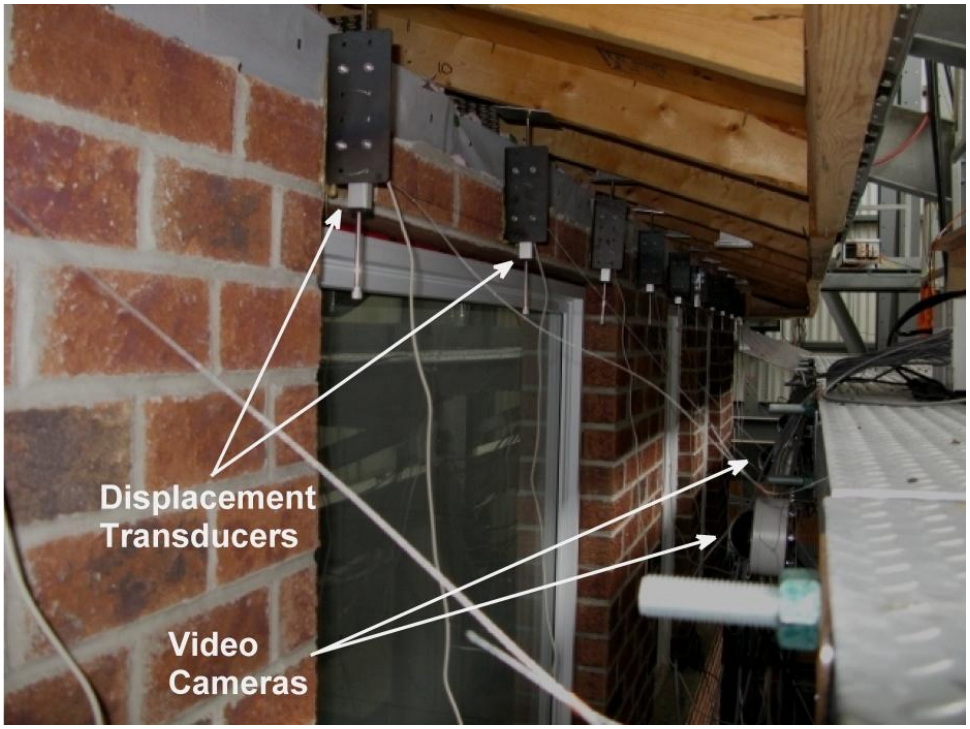


Figure 2.6 Photograph of the displacement transducers mounted on the brick veneer to measure the displacement of the roof to wall connections

### 2.1.2 Structural Loading

Rather than constructing an enormous wind tunnel to load the structure, like the new full scale wind tunnel under construction by the Institute for Business and Home Safety in South Carolina, the current approach is based on reproducing the surface pressure distribution that is created when the wind flows over the structure. A key element of this approach is the ability to replicate the full spectrum of the temporal variations of surface pressures on buildings, which lead to the development of the "Pressure Loading Actuators" (PLAs). By using many PLAs, the spatial variations can also be captured.

Since this is a pressure-based tool, a flexible air-bag system is required to apply these pressures to the specimen. This idea essentially combines the BRERWULF loading system and the multiple magnetic actuators used at MSU into a single system. The major differences with the previous experiments are that every building surface can be covered (except small areas such as fascia) and that the large leakage flows through typical cladding materials, such as bricks and siding, can be accommodated. Note that both the metal roofs tested at MSU and the metal panels tested with BRERWULF were nominally sealed in contrast to the typical porosities of brick, siding and other building materials typical of residential construction. The new system is also much more compact in order to allow for high spatial resolution for building locations where the pressures have high gradients, such as windward corners of the roof. Each PLA has one input pressure trace to replicate, the pressure traces coming from wind tunnel measurements, full-scale field measurements (e.g., Levitan and Mehta 1992, Liu et al. 2009), databases (Ho et al. 2005), or simple time histories such as ramps or sinusoids. This approach leads to an efficient system in terms of power usage and initial capital cost, which are both about a factor of 10 lower than for a full-scale wind tunnel. However, because the current system replicates the surface pressures on a building these surface pressures need to be known prior to testing. As a result, when failures initiate and cause significant motion of the structure, the aerodynamic loading will change due to the change in the shape of the structure i.e. the red arrow shown in Figure 1.4. Since the current system requires the aerodynamic loading prior to testing, the loads cannot be adjusted to account for significant movements of the structure. Moreover, because of the need for physical connections to the surface of the building due to the airbag concept, the failures can only

progress to a certain point until the system cannot accommodate further displacements. Consequently, the current system links the aerodynamic loading to the observations of failures from damage surveys by determining where and at what load the failure initiated.

### 2.1.3 Description of the Pressure Loading Actuators

Figure 2.7 shows an isometric view from the computer-aided design (CAD) model of a single PLA unit, and its major components. A blower (fan) is used to generate the required pressure rise and flow rates, while a rotating disk inside the valve, controlled by a servo motor is used to regulate the pressure applied to the specimen. The pressure inside each air-bag is monitored by a pressure transducer connected to each PLA. The PLAs are controlled either individually or in a group over an Ethernet (CAT-5) network using a PC-based control program, which updates the position of the valve approximately 100 times per second. From a practical perspective this limits the maximum frequency that the PLA can accurately reproduce to approximately 10 Hz. Ultimately the performance of the PLA is governed by the fan curve of the blower, minus the minor losses through the connecting hoses and valve which defines the maximum possible pressure as a function of leakage flow rate. The current blower can generate maximum and minimum pressures of 23 kPa and -20 kPa, respectively, and has a free air flow rate of 0.24 $m^3/s$. The frequency response of the system depends upon the fan curve and leakage flow rates so that tracking the most extreme temporal pressure gradients is limited by these factors.

Each PLA is calibrated statically so that the pressure as a function of valve position is known for the range of airbag volumes and leakage rates. In fact, the valve was designed

so that the functional dependence is linear, making control easier. The effective leakage rate (i.e., the system response characteristics) is continuously monitored during testing so that the pressure-valve relationship which most accurately describes the airbag volume and leakage is adaptively chosen. Because of this, the pressure continues to track accurately even as the building characteristics alter during testing, for example, as a crack opens up on the surface or as a component begins to "let go".

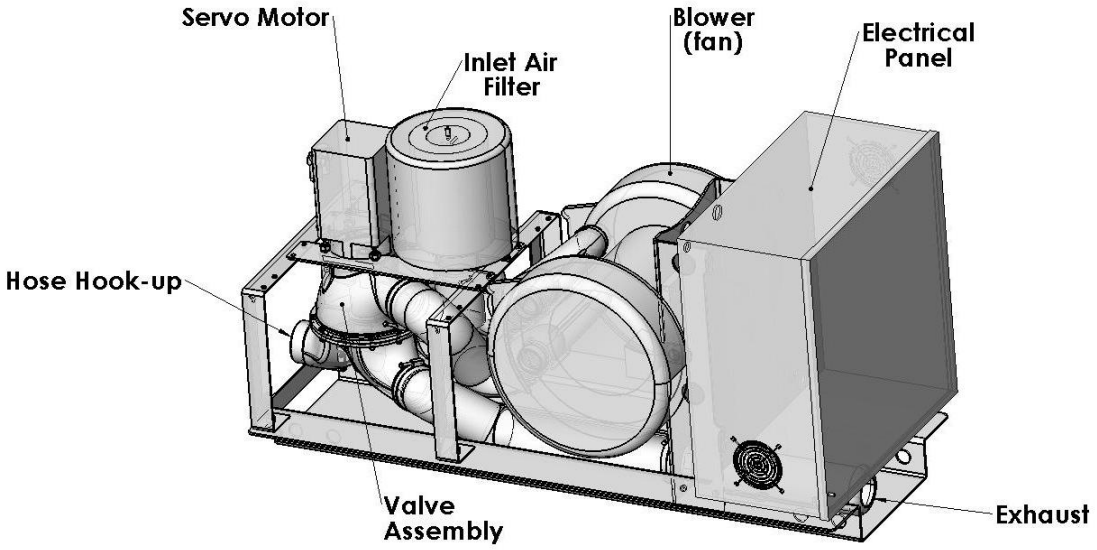


Figure 2.7 Three-dimensional assembly drawing of the Pressure Loading Actuator (PLA)

### 2.1.4 PLA Performance

Figure 2.8 presents the performance of a single PLA connected to a 1.22 x 1.22 m airbag for a portion of the total time trace. The match between demand and achieved pressure is good, with correlation coefficients between typical target signals and actual achieved signals are typically greater than 0.95. Perhaps more importantly, the correlations between two separate achieved time histories are also within 5% of the actual values so

that overall structural loads can be accurately simulated and repeated. Thus, the overall fidelity of the traces is acceptable, with minor deviations during extremely short duration peaks.

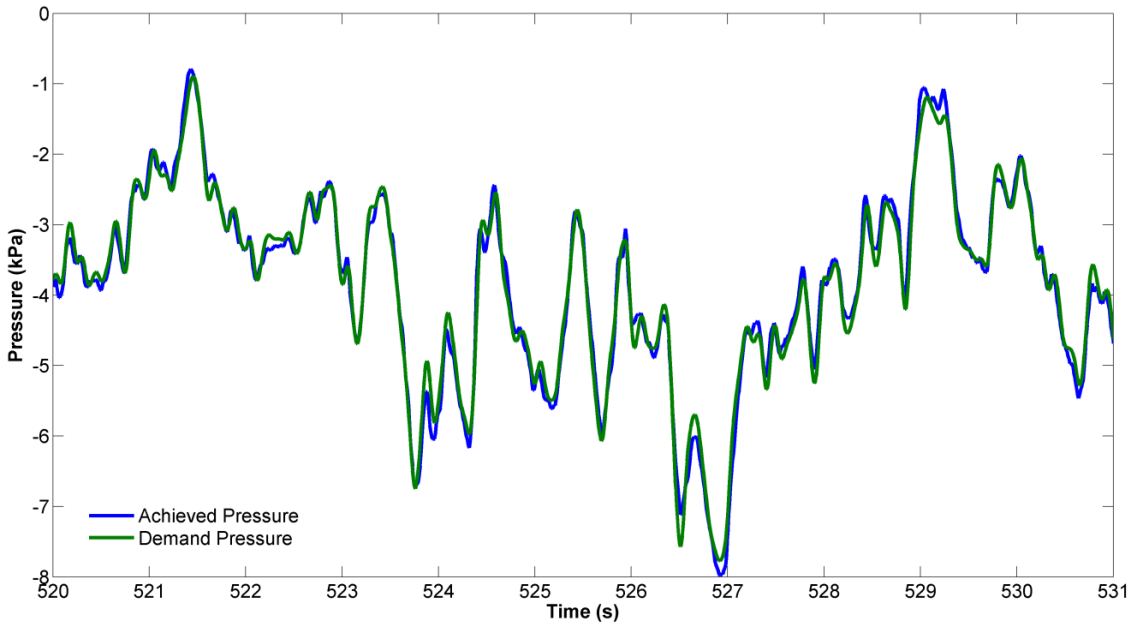


Figure 2.8 A typical example of the match between a wind tunnel demand pressure time history and the actual achieved pressures, using a single PLA applied to an area of 1.5 $m^2$.

Load tests on a 3.66 m high by 6.71 m long timber framed and lined wall were conducted with 10 PLAs operating simultaneously. Loads transmitted through the wall to supports were measured using an array of load cells. Figure 2.9 provides a comparison between the time varying load applied by the 10 PLAs and the reaction measured by the load cells. The agreement between the PLAs and the load cells is good with an average error of approximately 7%, which is within the measurement uncertainty. To provide an example of what a typical test setup would look like, Figure 2.10 shows the windward corner of the test house with the air bags and PLAs installed.

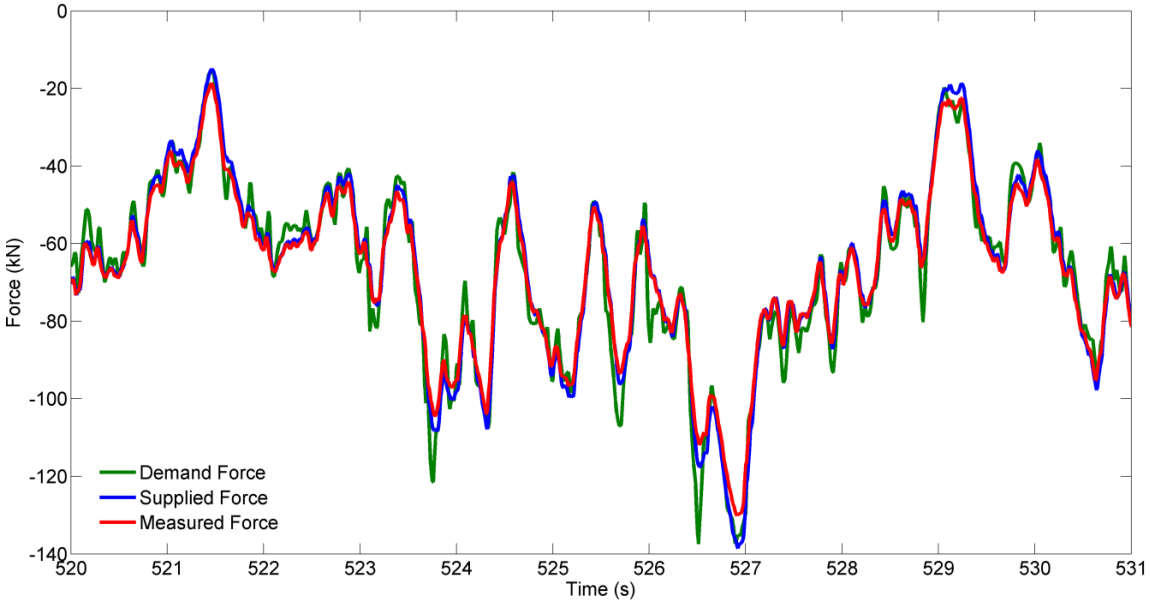


Figure 2.9 The applied time varying force on a 3.66m by 6.71 m test wall using 10 PLAs compared to the demand force obtained from the wind tunnel and the actual measured reactions on the wall.

### 2.1.5 Loading of Full Scale Test House

In order to apply the wind loads to the test house, airbags needed to be installed on the roof of the house. The airbags make use of steel frames that are mounted to the steel reaction frame shown in Figure 2.1, while the installation of the airbags and PLAs for the North East corner of the test house is shown in Figure 2.10. A flexible vinyl membrane (blue material in Figure 2.10) is glued to both the steel airbag frame and the plywood sheathing on the roof of the house. For the current test setup the membrane allows for movement of the roof either towards or away from the air bag lid of up to 100 mm. The PLAs are then mounted to the steel reaction frame and attached to a plywood lid, which is installed on the top of the airbag as shown in Figure 2.10. The number and layout of the airbags will be discussed further in Chapter 3.1.

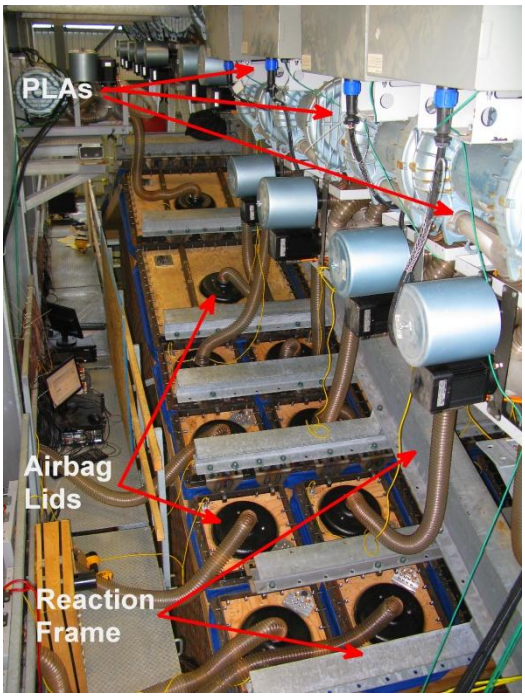


Figure 2.10 Photograph of the windward corner of the test house with the PLAs and air bags installed

## 2.2 Wind Tunnel Experimental Setup

In order to apply realistic wind loads to the full scale house using the PLAs the pressure distribution must be known first. A wind tunnel study was conducted on a 1:50 scale model of the test house in Boundary Layer Wind Tunnel II at UWO. The flow simulation approximates a typical open country atmospheric boundary layer at a scale of 1:50 with an aerodynamic roughness length, $z_o$, of approximately 0.03m (equivalent full-scale). Figure 2.11 shows the measured mean velocity and turbulence intensity profiles along with the target profiles (ESDU 1982) for an open country terrain ($z_o$=0.03m). The mean wind velocity has been normalised to eaves height and both the mean and turbulence intensity show reasonable agreement with the target profiles. Figure 2.12 presents the longitudinal wind tunnel spectra at roof height along with the target ESDU (1982)

spectra. While the match between measured and target spectra is good, it is not perfect with too much fine scale turbulence, which is not unusual for wind tunnel simulations at this scale. The terrain simulation used in the current study is identical to that of (Kopp et al. 2005, 2008), where a detailed discussion of the flow simulation and modeling approaches can be found.

Figure 2.13 depicts the building geometry and tap layout for the current model. The model had a total of 432 pressure taps. The tests were conducted at a reference speed of 13.7 m/s and approximately 37 minutes of full scale data was collected assuming a velocity scale of 1:4. The pressure taps were connected to PSI pressure transducers using a tubing system presented in Ho et al. (2005), which has a frequency response which is flat up to approximately 200 Hz. The pressures were sampled nearly simultaneously (maximum lag of 0.0025s) at a frequency of 400 Hz for a total of 180s. In total 18 wind angles were tested ranging from 0° to 90° at a mean roof height wind speed of 9.6 m/s and Reynolds number, $Re = VH/\nu = 1.0 \times 10^5$. The raw wind tunnel pressure data for all wind angles is available in APPENDIX C in the HDF format of Ho et al. (2005).

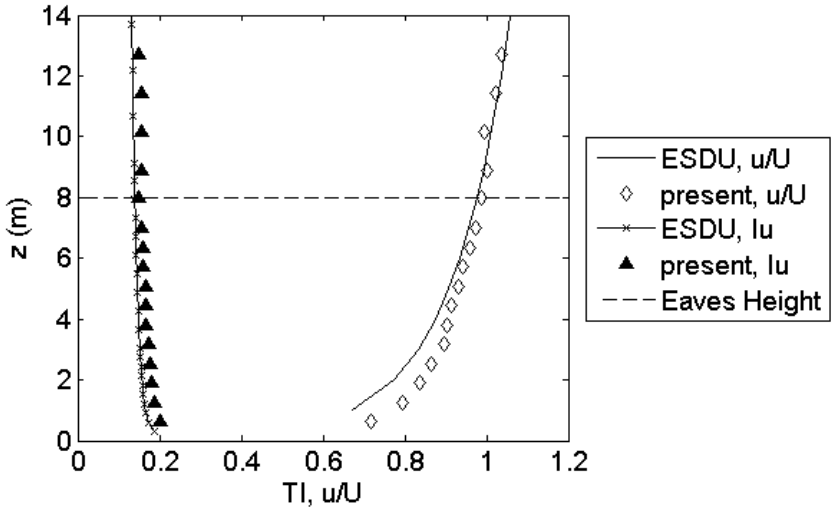


Figure 2.11 Comparison of measured and ESDU mean normalized wind speed and turbulence intensity profiles for open country, $z_0$=0.03m

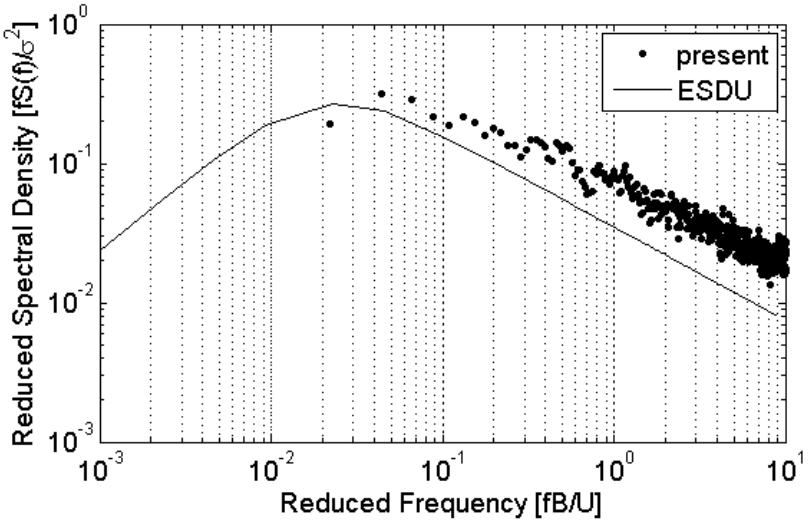


Figure 2.12 Comparison of measured and ESDU mean normalized wind speed and turbulence intensity profiles for open country, $z_0$=0.03m

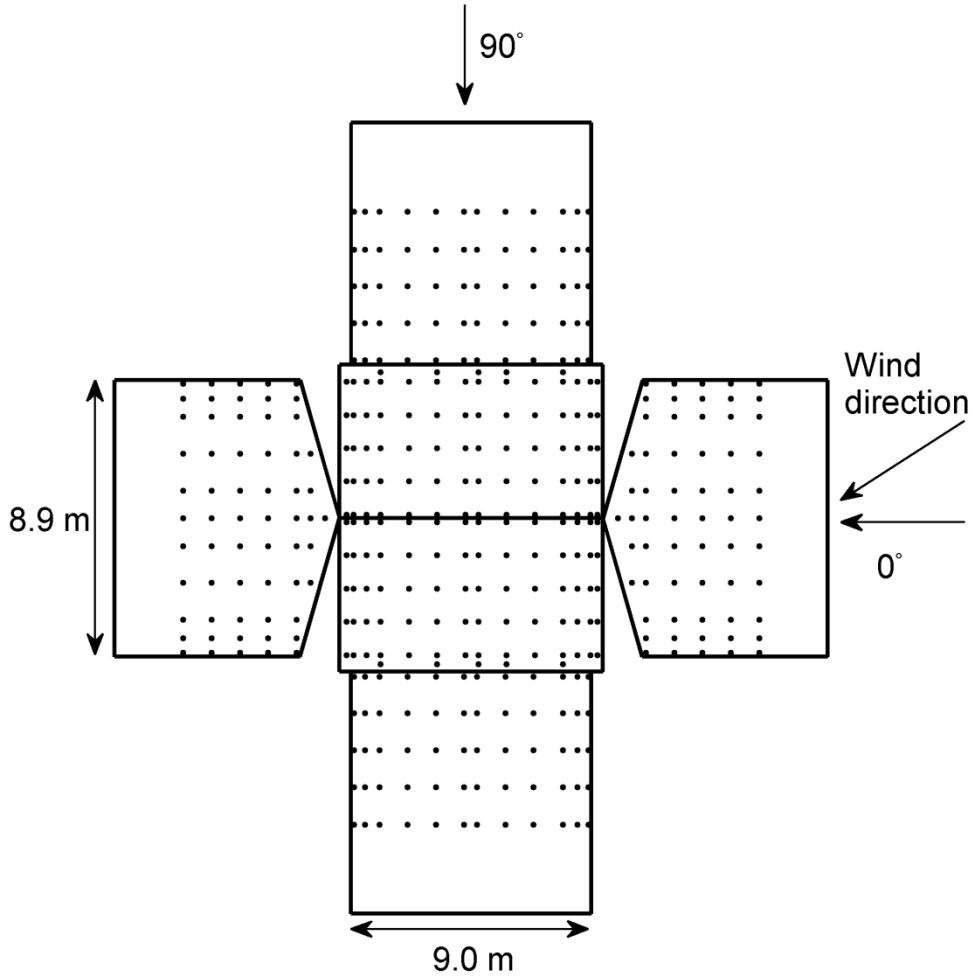


Figure 2.13 Pressure tap layout for the 1:50 scale model of the full scale test house

## 2.3 Individual Toe-nail Withdrawal Experiments

Individual toe-nail connections were tested using a load control approach with the test setup shown in Figure 2.14. Static, ramp or fluctuating loads can be applied to the specimen and are controlled using a PLA attached to an airbag. The top of the airbag is attached to the steel frame and the bottom to the toe-nail specimen. The toe-nail specimen shown in inset A of Figure 2.14 consists of two 0.61m long 2x4's representing a typical portion of the top plate mounted at either end to load cells, as indicated, to

measure the reaction of the connection. A 0.3 m long 2 x 6, connected to the bottom of the airbag, is toe-nailed to the top-plate using three 12-d twisted shank nails and a pneumatic nail gun. As previously discussed in Chapter 2.1.1, two different sized nails were used, along with a different number of nails per connection. Since it would not be feasible to conduct tests for every nail configuration that exists on the current roof, it was decided that a single connection type would be used, that being 3 air-gun driven nails per connection, driven at an angle of 45 degrees. Of the two types of nails used in the test house, the 12d nails were selected for the individual toe-nail experiments. The 12d nails were selected based on availability; while 16d gun nails are available, it was found that they were not commercially available locally and would have to ordered specially. This indicates that contractors in the area would likely use 12d nails rather than 16d nails in construction when using pneumatically driven nails. For the present document the term ‘d-nails’ will refer to the side of the rafter with 2 nails, while ‘s-nails’ will refer to the side of the rafter with just a single nail. The displacement of the connection is measured, relative to a rigid location, using a displacement transducer connected to the specimen.

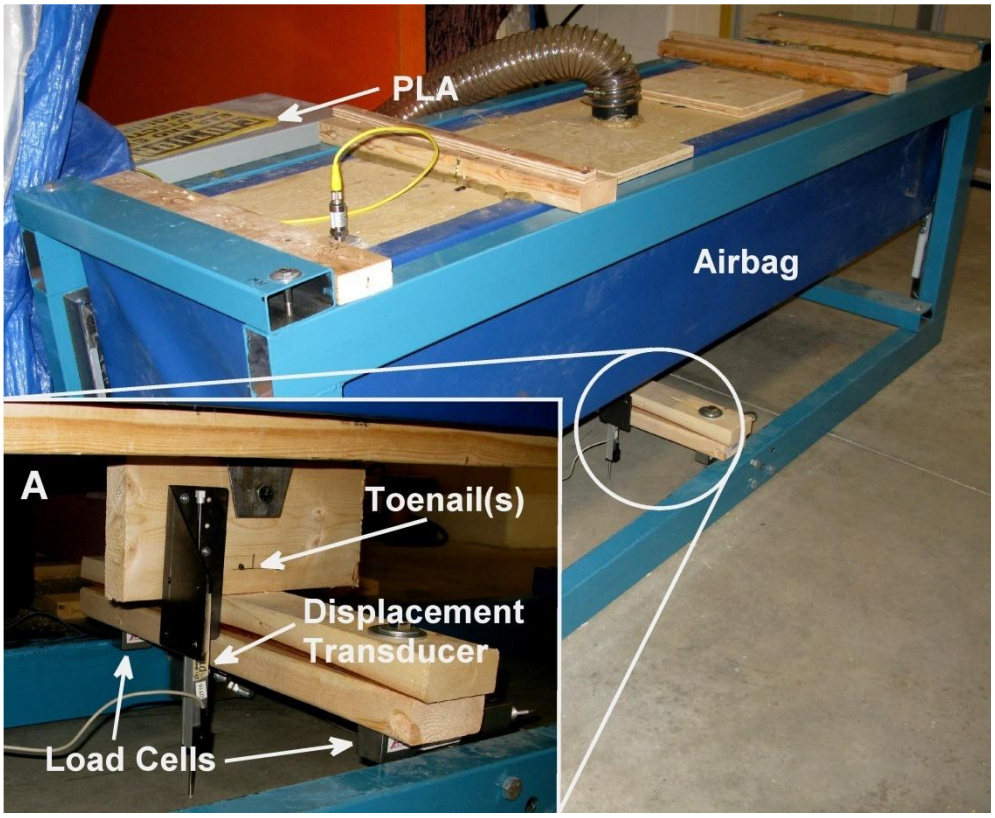


Figure 2.14 Photograph of the nail pull out rig. Loads are controlled by altering the pressure in the blue air bag while load cells and a displacement transducer measure the response of the toe-nail connection.

# 3.0 WIND LOADING ON THE ROOF OF THE TEST HOUSE AND TEST PROTOCOLS

The following chapter will provide an analysis of the wind tunnel pressure data which provides the basis for the full scale structural testing. First a brief comparison of the wind tunnel data will be made with the ASCE 7-05 (2006), for uplift forces and overturning moments for numerous tributary areas. Next a description of how the wind tunnel data was used to generate the wind loads for the full scale structure tests will be provided. Finally, the testing protocol and how it relates to the realistic fluctuating wind loading will be described.

## 3.1 Wind Loads Obtained From Wind Tunnel Testing

The following section will outline a brief analysis of the wind tunnel pressure data. The data will be compared with data from the ASCE 7-05 (2006) building code. In order to make this comparison the wind tunnel data time series for each pressure tap shown in Figure 2.13 is converted to a $GCp_{eq}$ value following the procedure outlined by St. Pierre et al. (2005) and described by:

$$GCp_{eq} = \frac{0.5\rho V_{h,zo,3600s}^2 Cp}{0.5\rho V_{10m,o.c.,3s}^2 K_{zt} K_h K_d I} = F_{WT} Cp \qquad (3.1)$$

where $GCp_{eq}$ is the pressure coefficient normalised to a 3s gust wind speed, $V_{10m,O.C,3s}$ is the 3s gust wind speed at 10m, $K_{zt}$ is the topographic factor, $K_d$ is the wind directionality factor, $K_h$ is the velocity pressure exposure factor at mean roof height, $I$ is the importance factor (not to be confused with $I(x,y,z,\delta)$). In the current study, $K_{zt}$, $K_d$, and $I$ will be taken to be 1, resulting in a factor, $F_{WT}$, of 0.48. Using a tributary area analysis for all of the

pressure taps, uplift coefficients are calculated for rectangular areas of any shape on the roof ranging from 1 $m^2$ to 115 $m^2$ which represents the entire area of the roof (i.e., global uplift). Figure 3.1 presents the worst uplift coefficient for each area size for 7 of the tested wind angles on the house. Also included in Figure 3.1 are the *GCp* coefficients for components and cladding (C&C) loads for the three zones on the roof provided by the ASCE7-05 (2006). For small tributary areas, less than 5 $m^2$, the $GCp_{eq}$ coefficient exceeds the *GCp* coefficients provided for the Corner Zone by ASCE 7-05(2006) for two wind angles (40° and 65°). A clear reduction in the $GCp_{eq}$ values is observed for all wind angles as the averaging area is increased. For areas larger than 85 $m^2$, all three zones for C&C load coefficients in the ASCE 7-05 (2006) are conservative as compared to the wind tunnel data for this particular house, indicating that the ASCE 7-05 (2006) will be conservative for global roof uplift loads.

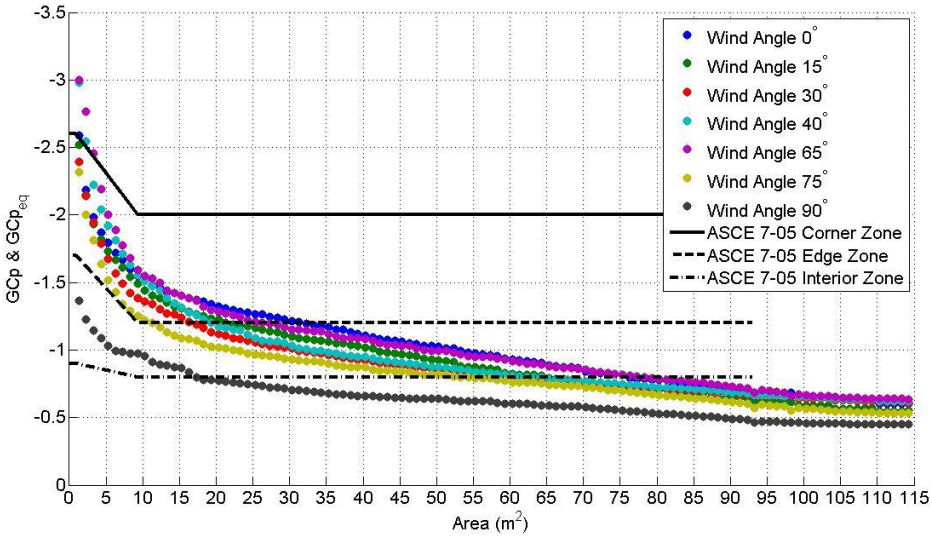


Figure 3.1 The worst *GCp* vs. area generated from the wind tunnel data of the test house for several wind angles.

To compare the results to the Main Wind Force Resisting System (MWFRS) coefficients

provided in the ASCE7-05(2006) the coefficients for zones 2, 3, 2E and 3E shown in Figure 6-10 in the ASCE 7-05(2006) are calculated for each wind angle for the current test house and are shown in Table 3.1. For all wind angles the MWFRS coefficients in the ASCE7-05 are unconservative for the current test house in zones 3E and 3, while being conservative in zone 2. For Zone 2E the ASCE7-05 (2006) coefficients are conservative for wind angles between 65° and 90° and unconservative for wind angles ranging from 0° to 40°. For all wind angles the uplift for the entire roof is less than that calculated using the ASCE7-05 (2006), similar to when C&C coefficients are used.

Table 3.1 Summary of *GCp* and $GCp_{eq}$ coefficients for the current test house for MWFRS roof zones at different wind angles

| | *GCp* or $GCp_{eq}$ | | | | Global Roof Uplift |
|---|---|---|---|---|---|
| ASCE 7-05 Roof Zone | 2E | 3E | 2 | 3 | |
| ASCE | -1.07 | -0.69 | -0.69 | -0.48 | -0.64 |
| Wind Angle 0° | -1.49 | -1.44 | -0.51 | -0.54 | -0.48 |
| Wind Angle 15° | -1.42 | -1.18 | -0.40 | -0.58 | -0.43 |
| Wind Angle 30° | -1.25 | -1.17 | -0.40 | -0.66 | -0.51 |
| Wind Angle 40° | -1.14 | -1.39 | -0.43 | -0.69 | -0.55 |
| Wind Angle 65° | -0.69 | -1.41 | -0.49 | -0.78 | -0.60 |
| Wind Angle 75° | -0.50 | -1.10 | -0.41 | -0.70 | -0.51 |
| Wind Angle 90° | -0.38 | -0.72 | -0.40 | -0.60 | -0.45 |

### 3.1.1 Realistic Wind loads for the Full Scale House Experiment

As explained in Chapter 2.1.1, the objective of the current experiments is to examine the response of the house "as is," meaning as few modifications as possible were made to the test house so as not to alter the structural system. A key disadvantage of this decision is that while the exact loads applied to the structure are known, the reactions at the RTWC are not. As such, in order to estimate the loads at each connection, an assumption for the structural influence function $I(x,y,z,\delta)$ had to be made. Assuming a geometric tributary

area approach the reaction loads at each RTWC are calculated from the applied wind loads. In addition, to calculate the net loads an estimate for the weight of the entire roof needed to be obtained. There is some uncertainty with the estimate of the weight, however, similar to the shingles, the weight is evenly distributed over the entire roof, with the exception of the end walls. As a result different assumptions for the weight can be used in post processing. Details pertaining to the estimate of the weight of the roof can be found in APPENDIX D. The reactions for each RTWC were calculated using both the sum of moments (SOM) about the Northern wall and the uplift for each truss, taking into account the estimates for the weight of the roof; details of the SOM calculations can be found in APPENDIX D. As shown in Figure 3.1, a wind angle of 65° generates the largest uplift coefficients for small tributary areas for all the wind angles shown. However, these area averages are for areas of any shape and location and as such may not reflect the tributary areas for the actual roof trusses. In fact, a wind angle of 40° was found to produce the largest reactions at a single RTWC connection. As a result it was decided that a wind angle of 40° would be used for the full scale house scale experiment, since this would likely result in the highest loads on individual RTWC. Moreover, the global uplift at 40° is only 2% lower than the worst global roof uplift at any angle. Table 3.2 provides a summary of the statistics of the net reaction forces of all 32 RTWC using both loading methods for a wind angle of 40° and assuming an hourly roof height wind speed of 45 m/s. With the exception of truss number 2, the reactions at the connections on the South side of the roof are larger than those on the North side for this wind angle, with the highest loaded connections located on the Eastern side of the house. For the remainder of the thesis, the tributary area loads will be those calculated by the SOM

method described in APPENDIX D unless otherwise stated.

Table 3.2 Statistics for the net reactions at all RTWC assuming a geometric tributary for each connection and using an hourly roof height scaling wind speed of 45 m/s.

| RTWC | $R_z$ max, min, mean (kN) | | RTWC | $R_z$ max, min, mean (kN) | |
|---|---|---|---|---|---|
| | SOM | Uplift | | SOM | Uplift |
| | | | | | |
| "S2" | 1.3, -10.5, -3.6 | 1.4, -11.4, -3.7 | "N2" | 0.8, -11.0, -3.4 | 0.8, -11.8, -3.3 |
| "S3" | 0.7, -8.0, -2.9 | 0.8, -9.0, -3.1 | "N3" | 0.5, -6.4, -2.1 | 0.4, -7.0, -1.8 |
| "S4" | 0.8, -5.5, -2.3 | 1.0, -6.2, -3.0 | "N4" | 0.3, -4.0, -1.4 | 0.2, -3.5, -0.8 |
| "S5" | 0.8, -5.6, -2.4 | 1.0, -6.3, -3.0 | "N5" | 0.3, -4.3, -1.5 | 0.3, -3.7, -0.9 |
| "S6" | 0.6, -3.8, -1.6 | 0.5, -4.9, -2.1 | "N6" | 0.2, -2.8, -1.2 | 0.4, -2.1, -0.8 |
| "S7" | 0.6, -4.0, -1.7 | 0.4, -5.2, -2.2 | "N7" | 0.2, -3.1, -1.3 | 0.4, -2.4, -0.9 |
| "S8" | 0.8, -3.8, -1.5 | 0.7, -4.6, -1.9 | "N8" | 0.9, -2.9, -1.2 | 1.0, -2.3, -0.8 |
| "S9" | 0.9, -4.1, -1.6 | 0.8, -5.0, -2.0 | "N9" | 1.2, -3.4, -1.4 | 1.2, -2.7, -1.0 |
| "S10" | 1.0, -2.9, -1.3 | 0.9, -3.5, -1.6 | "N10" | 1.2, -2.8, -1.1 | 1.3, -2.4, -0.8 |
| "S11" | 1.2, -2.9, -1.2 | 1.1, -3.6, -1.5 | "N11" | 1.3, -3.0, -1.2 | 1.4, -2.6, -0.9 |
| "S12" | 1.1, -2.7, -1.2 | 1.1, -3.4, -1.5 | "N12" | 1.2, -2.7, -1.1 | 1.2, -2.4, -0.8 |
| "S13" | 1.1, -2.8, -1.2 | 1.3, -3.4, -1.5 | "N13" | 0.9, -2.9, -1.2 | 0.7, -2.7, -0.9 |
| "S14" | 1.0, -2.4, -1.0 | 1.1, -2.9, -1.3 | "N14" | 0.9, -2.5, -1.0 | 0.7, -2.3, -0.7 |
| "S15" | 0.9, -2.4, -1.0 | 1.0, -3.0, -1.2 | "N15" | 1.0, -2.5, -1.0 | 0.8, -2.3, -0.7 |
| "S16" | 0.8, -2.2, -0.9 | 0.9, -2.7, -1.1 | "N16" | 0.9, -2.2, -0.9 | 0.8, -2.1, -0.7 |
| "S17" | 1.3, -2.2, -0.7 | 1.5, -2.8, -0.9 | "N17" | 1.4, -2.3, -0.7 | 1.3, -2.2, -0.4 |

### 3.1.2 Testing protocol

To test the uplift capacity of the roof-to-wall connections the entire roof needed to be covered with air-bags. The correct number, size, and location of each air-bag on the house is a balance between adequately capturing the spatial gradients of the wind pressures and the physical and technical constraints inherent to the system. For example the foot print of a PLA is approximately 0.6m by 0.6m which essentially limits the minimum bag size. Through careful analysis of the wind pressure distribution, the final airbag layout of the roof is shown in Figure 3.2. In total 58 bags were used to cover the entire roof, with the highest density of bags located at the windward corner of the roof.

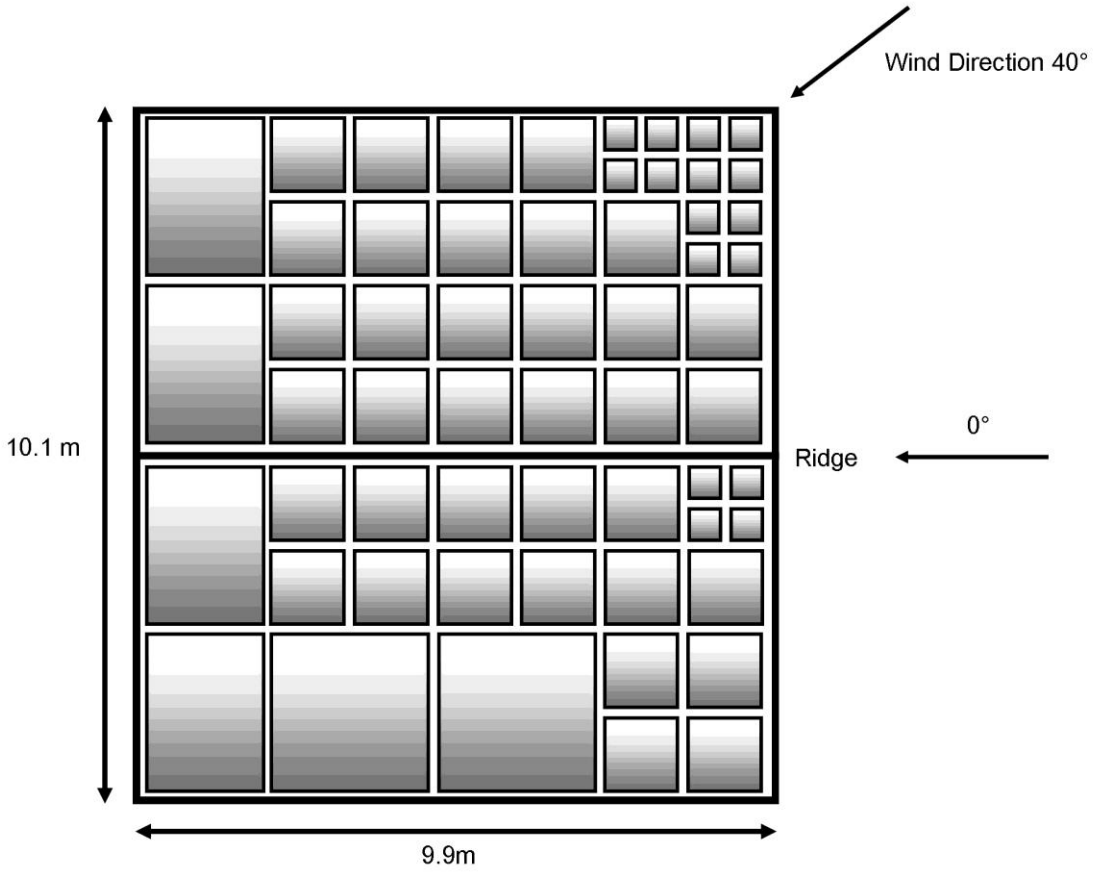


Figure 3.2 Air bag layout on the roof of the full scale test house, the smallest bags are 0.61m by 0.61 m, the medium bags are 1.22m by 1.22m and the largest bags are 2.6m by 2.6m.

The test protocol used in the current experiment is similar to that used by Surry et al. (2007). A representative portion of the wind tunnel pressure coefficient (*Cp*) time series was selected and scaled to full scale pressures using a mean roof height wind speed of 20 m/s using:

$$P = 0.5\rho V^2 Cp \qquad (3.2)$$

where $P$ is the surface pressure, ρ is the density of air and $V$ is the scaling wind speed.

These pressures were then applied to the roof of the test house. After the completion of the test, the house was inspected and any damage was documented. The wind loads were then increased by increasing the wind speed in 5 m/s increments, the full scale wind pressures were re-calculated using the same representative portion of wind tunnel data and then applied to the house. This process was repeated to a maximum wind speed of 45 m/s. These wind speeds were applied considering external pressures only (so that the house was nominally sealed) but could be reinterpreted taking into account dominant openings and internal pressures. However, this must be done on a case by case basis since the location and size of the dominant opening has a significant effect (Kopp et al. 2008). It was decided that the same segment of wind tunnel data would be used so that an identical number of peaks occur for each scaled wind speed, however, it is noted that because of the scaling laws shown in Eq. 3.3 the actual duration is shortened.

$$\left(\frac{VT}{L}\right)_{model-scale} = \left(\frac{VT}{L}\right)_{Full-scale} \tag{3.3}$$

where, $T$ is total duration time, $v$ is the velocity and $L$ is a representative length. Table 3.3 provides a summary of the 6 tests performed on the house.

Table 3.3 Summary of the 6 full-scale tests conducted on the house

| Test #1 | Scaling Wind Speed $V$ (m/s) | Test Duration (s) | Peak Net load* on the entire Roof (kN) | Mean Net load* on the entire Roof (kN) |
|---|---|---|---|---|
| 1 | 20 | 900 | -7.2 | +5.3† |
| 2 | 25 | 720 | -21.4 | -2.1 |
| 3 | 30 | 600 | -38.3 | -11.1 |
| 4 | 35 | 514 | -59.5 | -21.7 |
| 5 | 40 | 450 | -81.1 | -34.2 |
| 6 | 45 | 400 | -107 | -47.8 |

† Mean load is downward towards the house.

* This includes both wind loads and gravity loads.

## 3.2 Loads for the individual toe-nail connection experiment

### 3.2.1 Ramp Loading Experiments

As discussed in Chapter 1.2, the capacity of toe-nail connections varies substantially in the literature based on the type of nails, grade of lumber, moisture content and age of the connection. The goal of the individual toe-nail RTWC tests are to determine the behaviour and capacity of toe-nail connections under realistic wind loading, and less emphasis on a direct comparison with connections found in the literature. As such, the static capacity of the connections used in the current study must be determined using a method similar to that of previous studies. These capacities will provide a baseline static withdrawal capacity for the toe-nail connections used in the current study, and will be used as a basis of comparison, for the realistic wind loading tests. To obtain the static capacity, various ramp loads are applied to the specimen until failure. To assess the effect of loading rate on the response of the connections, three different loading rates are used, viz., 1, 8, and 32 kN/min, resulting in expected failure times ranging from 5 to 200 seconds. These loading rates were selected so that the slowest rate would result in a failure time similar to those of previous experiments using a constant displacement rate, while the highest loading rate would approximate a loading rate closer to that found in actual wind loads. A total of 21 toe-nail specimens were tested at each ramp loading rate in order to account for variability in wood properties and construction.

As shown in Chapter 2.1.1, toe-nail connections in actual construction can have significant variability due to defects and construction errors. To attempt to quantify the

effect of these errors in a controlled way, experiments were conducted using a ramp loading rate of 8kN/min using toe-nail connections that were missing a single nail, which results in two types of defect cases. Defect #1 will refer to tests where the 's-nail' is missing, while defect #2, will refer to tests where one of the 'd-nails' is missing.

### 3.2.2 Realistic Wind Loading Experiment

Using the reaction loads at each RTWC calculated in APPENDIX D, the RTWC that contain the largest peak *Cf* in its time series was then chosen to be the realistic loading case for the individual toe-nail connection experiments. The connection that contained the highest force coefficients, that was not a gable end wall was RTWC "S3". Using the same representative portion of the wind tunnel time series and the same scaling wind speeds that were used for the full house experiment, a force time history was generated and is shown in Figure 3.3. This force time history would be the same force time history applied to RTWC "S3" in the full roof experiment provided that the assumption holds that the influence function is equal to the geometric tributary area for this connection. This assumption is almost certainly incorrect, however, these results combined with the full scale experiment results, should give us an indication of how different the true influence function is from the geometrical tributary area assumption. Table 3.4 provides a summary of the uplift force applied to the individual toe-nail connections for each scaling wind speed. Similar to the ramp loading rate experiments, a total of 25 specimens were tested using the realistic wind loading time series to account for variations in connections.

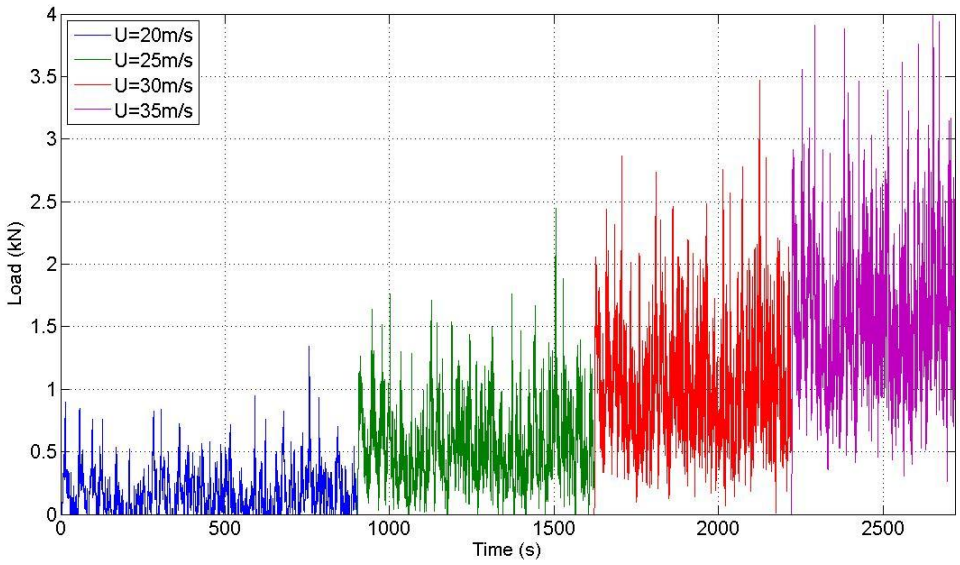


Figure 3.3 Realistic Wind Loading Trace used for testing individual toe-nail connections

Table 3.4 Summary of the real wind load traces applied to the toe-nail connection

| **Scaling Wind Speed (m/s)** | **Peak Force (kN)** | **Trace Duration (s)** |
|---|---|---|
| 20 | 1.35 | 900 |
| 25 | 2.45 | 720 |
| 30 | 3.47 | 600 |
| 35 | 4.91 | 514 |

# 4.0 INDIVIDUAL TOE-NAIL RESULTS

The current section presents the results of the ramp loading and realistic wind loading experiments described in Chapters 2.3 and 3.2.

## 4.1 Ramp Loading

Figure 4.1 shows a typical load displacement relationship for one of the 8 kN/min ramp tests. The failure capacity of the connection is defined as the maximum measured reaction, as indicated in Figure 4.1. After this point, the measured reaction drops as the nails pull-out. Since the current study uses a load control approach, when failure begins to occur it proceeds in an uncontrolled manner; therefore, the data beyond the failure capacity are not used in the analysis.

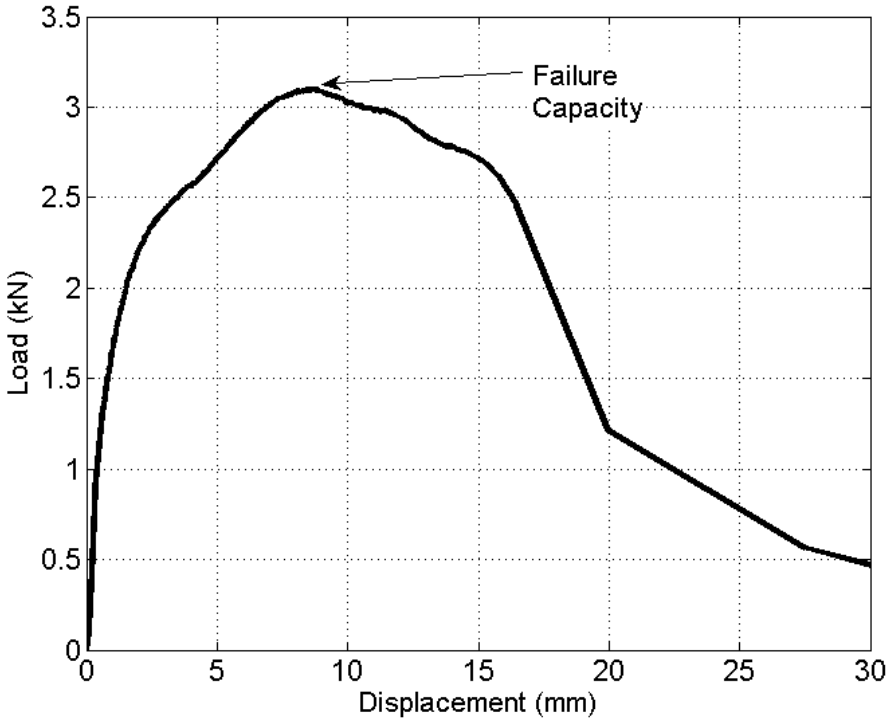


Figure 4.1 Load vs. Displacement relationship for a ramp rate of 8 kN/min

As discussed in Chapter 3.2.1 a total of 21 tests were conducted at each loading rate. Similar to Shanmugam et al. (2009), the log-normal distribution was found to best fit the maximum capacities when considering normal, Weibull or Gumbel distributions. The cumulative distribution for all three ramp loading rates is shown in Figure 4.2. The distributions for the ramp rates of 8 and 32 kN/min are nearly identical, while the 1 kN/min test has less variability in the failure capacity. The mean failure capacity for each ramp rate is nearly the same ranging from 2.7 kN at 1kN/min to 2.9 at 32 kN/min. The difference in mean failure capacity based on loading rate is insignificant as compared to the range of failure capacities observed which ranged from 1.2 to 4.7 kN from all ramp rates. Using a Kolmogorov-Smirnov test the null hypothesis cannot be rejected between the three ramp loading rates using a 95% confidence interval. This indicates that with the current data, the failure capacity of the nails is independent of the loading rate within this range, which encompasses nearly all loading rates of the realistic wind loading trace shown in Figure 3.3. This finding is consistent with that of Rosowsky and Reinhold (1999) who found no loading rate dependence in the capacity of nailed connections (although toe-nails were not examined). Figure 4.3 presents the probability distribution for the same ramp rate data used for Figure 4.2, and shows that distributions become broader with increasing loading rate suggesting that there is an increased variability of the failure capacity. In addition, the inset of Figure 4.3 shows that the distributions vary significantly in the tail regions of the distribution, which is likely the result of an imperfect fit of the log-normal distribution to the experimental data. Although, there is no statistical difference in the distributions for different ramp loading rates with the data currently available, additional samples at the current loading rates, along with

investigating more loading rates between 1 and 8 kN/min would be needed to determine if the reduced variability of the failure capacity observed for the 1 kN/min is a true loading rate effect.

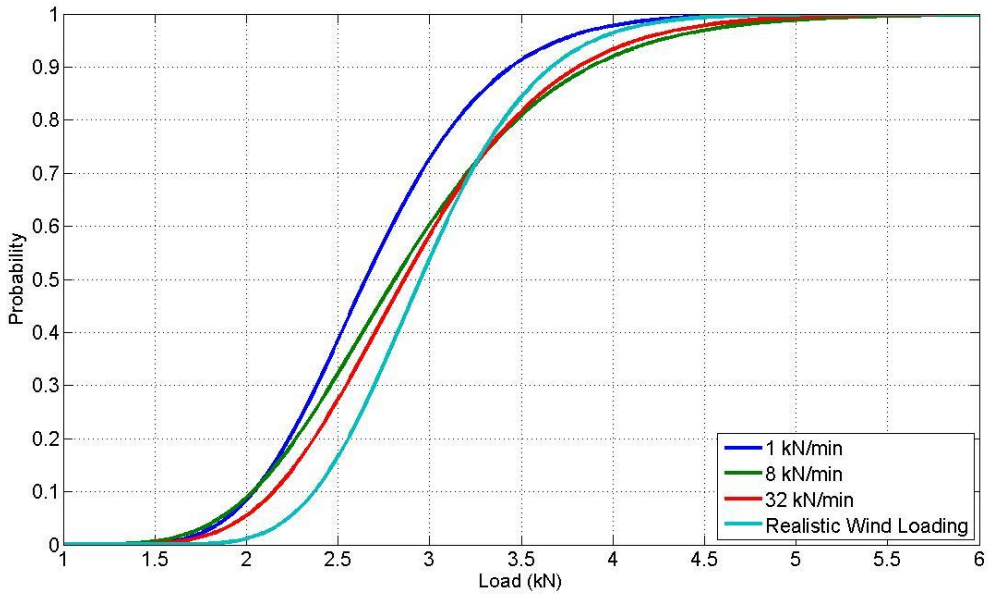


Figure 4.2 Cumulative distribution of the mean failure capacity for all 3 ramp loading rates and the realistic wind load

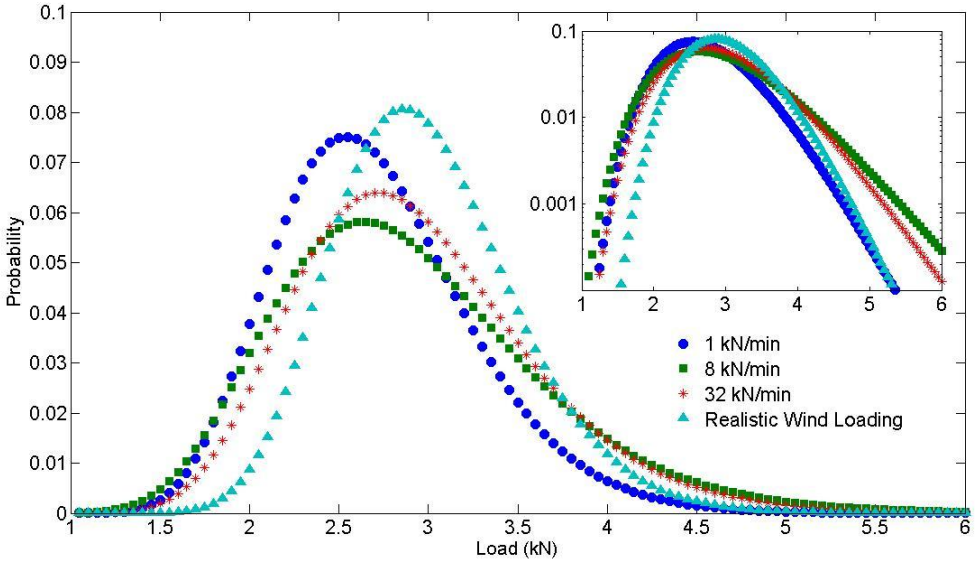


Figure 4.3 Probability distribution for the same data as presented in Figure 4.2. The inset in the top right of the figure presents the probabilities on a logarithmic scale

During the ramp loading experiments the nails were observed to fail in two different ways: either "pullout," where the nails pulled out of the top-plate; or "splitting," where the wood of the rafter splits with the nails remaining attached to the top-plate. As a result of these two types of failures, four different failure modes were observed, the wood around all of the nails split (all nails remained in the top-plate), the wood around the 'd-nails' split, the wood around the 's-nails' splits, or all of the nails pulled out of the top-plate. The ramp test results sorted by failure type are shown in Table 4.1. Since the loading rate was found to have a minimal effect on the capacity of the toe-nail connections, all test results have been put together. These results show that the predominant failure mode is when all nails pull out together. This failure mode has a lower failure capacity than when splitting failures occur, which is consistent with the results of Shanmugam et al. (2009). However, there does not seem to be any significant

difference in capacity between types of splitting failures, although the d-nails splits were more common than the other two types of splitting failures indicating that the proximity of the two nails on one side may cause that side to be more prone to splitting.

Table 4.1 Summary of the types of failures from the ramp loading tests and there average failure capacity

| Failure Type | Average Failure Capacity (kN) | Standard Deviation (kN) | % of Failures |
|---|---|---|---|
| all nails split | 3.3 | 0.58 | 8 |
| d-nails split | 3.2 | 0.41 | 21 |
| s-nail split | 3.2 | 0.87 | 6 |
| all nails pull out | 2.6 | 0.54 | 65 |

## 4.2 Effect of Missing Nails

In order to quantify the possible effects of construction defects in a controlled way, tests were conducted on toe-nail connections where a single nail was missing. This results in two types of defects: defect #1 will refer to tests where the 's-nail' is missing, while defect #2, will refer to tests where one of the 'd-nails' is missing. In total 16 tests were conducted for each defect condition and the loading rate used for all tests was 8 kN/min. The mean and standard deviation of the failure capacity along with the type of failure observed are given in Table 4.2. For both defect cases, the failure capacity per nail is higher than that of the no defect case. The mean failure capacity for defect #1 is lower than that of defect #2 while the predominant failure mode of defect #1 is splitting. Only pull out failures are observed for defect #2. This is opposite to the observations for the no defect case, where splitting failures are generally associated with a higher mean failure capacity, although it is likely the result of the extreme asymmetry of the connection in the case of defect #1.

Table 4.2 Summary of failure capacity and failure modes of connections with defects for ramp tests

| | Mean Failure Capacity (kN) | Standard Deviation (kN) | #Split / #pull outs |
|---|---|---|---|
| No Defect | 2.8 | 0.6 | 22/41 |
| Defect #1 | 1.9 | 0.46 | 11/5 |
| Defect #2 | 2.2 | 0.48 | 0/16 |

## 4.3 Fluctuating Wind Loading

A displacement time series for a single toe-nail specimen subjected to realistic wind loading is shown in Figure 4.4. Rather than the connection gradually being withdrawn from the top-plate as in the ramp loading experiments, the majority of the withdrawal of the nails occurs at a handful of damaging peak loads as indicated in Figure 4.4. Figure 4.5 shows the load vs. displacement relationship for the same test as shown in Figure 4.4. Over the first portion of the test where the loads are relatively small (20 m/s), the load displacement behaviour is nearly linear; however, following the first damaging peak (as indicated in the figure), the connection is permanently displaced by approximately 0.4 mm. This is observed by the load-displacement curve shifting upwards. Each subsequent damaging peak increases the permanent displacement of the connection until ultimate failure occurs. However, between these damaging peaks, the load-displacement behaviour remains similar to the undamaged case, following the same slope. This indicates that the stiffness of the connection remains unchanged despite having been partially removed from the top-plate.

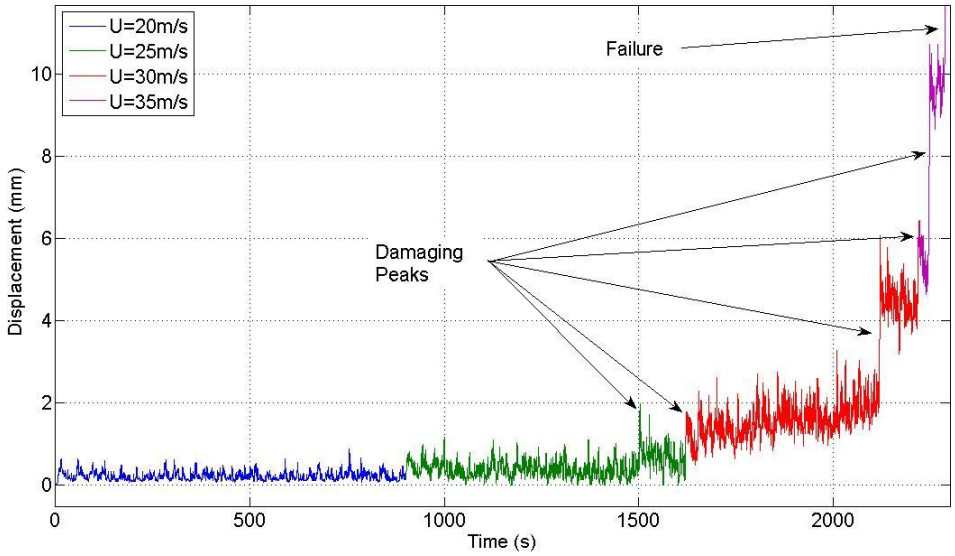


Figure 4.4 Displacement time series of a typical realistic wind loading trace applied to a toe-nail connection. The damaging peaks are indicated in the figure.

Furthermore, because of this incremental removal of the nails, the connection no longer fails at the maximum load applied to the connection as shown in Figure 4.5, where the failure load was 3.3 kN as compared to a maximum applied load of 3.4kN. While this difference is not substantial, the ratio of the failure load to the maximum load applied was observed to range from 87% to 100%. The overall mean failure capacity was found to be the same as the ramp loading rates, being 2.8 kN. The probability distribution for the fluctuating loads is shown in Figure 4.2 and is similar to that of the ramp loading experiments. Pullouts are the most common mode of failure, similar to the ramp rate experiments, representing 76% of the failures. This is slightly higher than that of the ramp loading tests. However, unlike the ramp loading, there is no observed change in the mean failure capacity between these two failure modes under the realistic, fluctuating wind load.

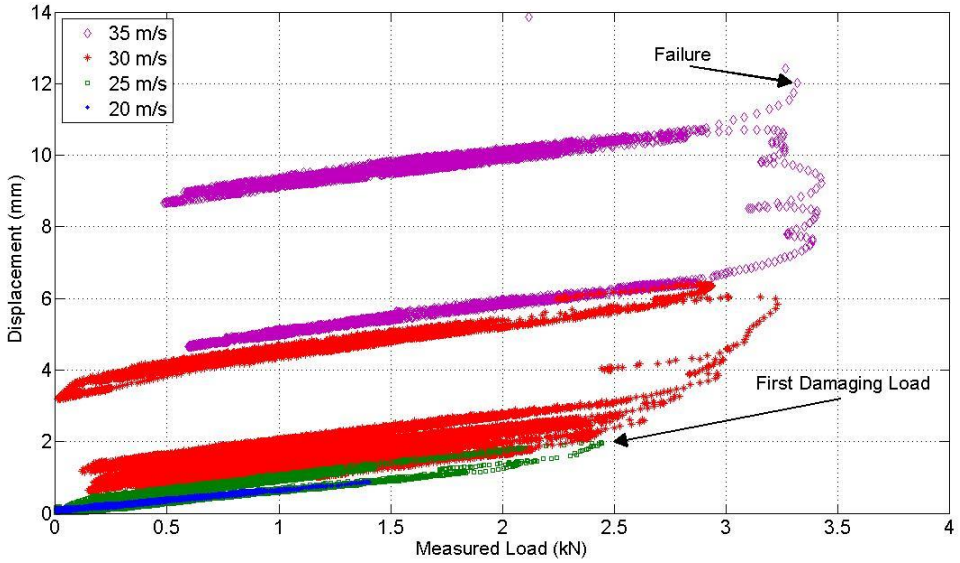


Figure 4.5 Load vs. Displacement for the realistic wind loading trace shown in Figure 4.4

# 5.0 DISCUSSION OF INDIVIDUAL TOE-NAIL RESULTS

While the failure of toe-nail connections due to ramp loads was a gradual withdrawal of nails, the nails subjected to dynamic loading are incrementally removed from the top-plate during the peak pressures in the applied trace. Despite the difference in observed behaviour between the ramp and realistic wind loading, the average failure capacity is remarkably similar. The following discussion will examine the realistic loading time history in detail and discusses the peak loads that cause damage to the connection.

## 5.1 First Damaging Peak

In order to consider damage to the connection, a definition for what actually constitutes a damaging peak is required. For the purpose of this study, a "damaging peak" is a peak load that causes a permanent partial withdrawal of the nail from the top-plate. For all 25 specimens, damage initiated at one of the 3 peaks that are summarized in Table 5.1. It would be expected that the load required to cause the first damaging peak for a particular specimen would be a random variable that would follow a certain distribution, similar to the failure capacities shown in Figure 4.2. However, under a single, repeated, fluctuating time series not all load levels are applied (as they are in a ramp). Consequently, the peak values may be significantly larger than any previous peak value applied, as shown in column 4 in Table 5.1. As a result, while the load required to cause initial damage may follow a distribution, the loads that actually cause the initial damage will cluster around specific peaks as observed for the particular chosen load time history. For example, for the first damaging peak, which occurs at 755.6 s, the true initial damaging threshold of the specimens could range from 1.09 to 1.47 kN. It would also be expected that, the lower the initial damaging peak, the lower the maximum load that the specimen can take.

This has been found to be generally true (although the exception to this trend is the strongest specimen between the peaks at 755.6 s and 999.3 s; however, this discrepancy is likely the result of having insufficient specimens to account for the complete variability in strength of the connections). Furthermore, it is important to point out that none of the specimens failed during the first peak indicating that toe-nails subjected to hurricane wind loads will always have some form of damage prior to the wind loading that actually causes the failure of the connection. The average load that causes the initial damage to the connection (damage threshold) as a function of the mean maximum load applied to the connection ranges from 56% to 77%.

Table 5.1 Summary of the First Damaging Peaks under Realistic Wind Loading

| Trace Time (s) | Number of Specimens | Load at the Peak (kN) | Largest load prior to damaging peak (kN) | Maximum magnitude Load Applied for tests with this as a first damaging peak (kN) Max, Mean, Min |
|---|---|---|---|---|
| 755.6 | 6 | 1.47 | 1.09 | 1.99, 2.63,3.73 |
| 999.3 | 10 | 1.87 | 1.64 | 2.30, 2.87, 3.58 |
| 1502.5 | 9 | 2.49 | 1.89 | 2.76, 3.24, 4.14 |

## 5.2 Damaging Peaks

Through all 25 fluctuating wind load tests, permanent, incremental damage to the connection due to local peak pressures is observed a total of 187 times or 7.5 peaks per toe-nail specimen, including the peak loads that caused failure. However, since the same loading time history was applied to each specimen, of the 187 damaging peaks, there were only 22 unique peaks. These 22 damaging peaks are shown in Figure 5.1, out of these 22 peaks, 5 were found to damage 100% of the connections that saw that particular peak. The later on in the time series the peak occurred the lower the number of specimens that actually saw that particular peak due to failures of specimens. The load of

these 5 peaks was found to always be of a higher magnitude than any previous peak in the load time history. In fact, peak loads that caused damage to greater than 40% of the test specimens where found to always have a larger magnitude than any peak previously applied to that specimen. Of those peaks that had a lower magnitude than the previous peak load, the average load difference was approximately 0.15 kN with a maximum of 0.57 kN. The incremental pullout of the nails for these peaks was always less than 1 mm. This suggests that the threshold load where damage occurs to the connection can be reduced following a damaging peak, the level to which it is reduced varies, as one would expect, for each specimen. However, it is in the order of 5%.

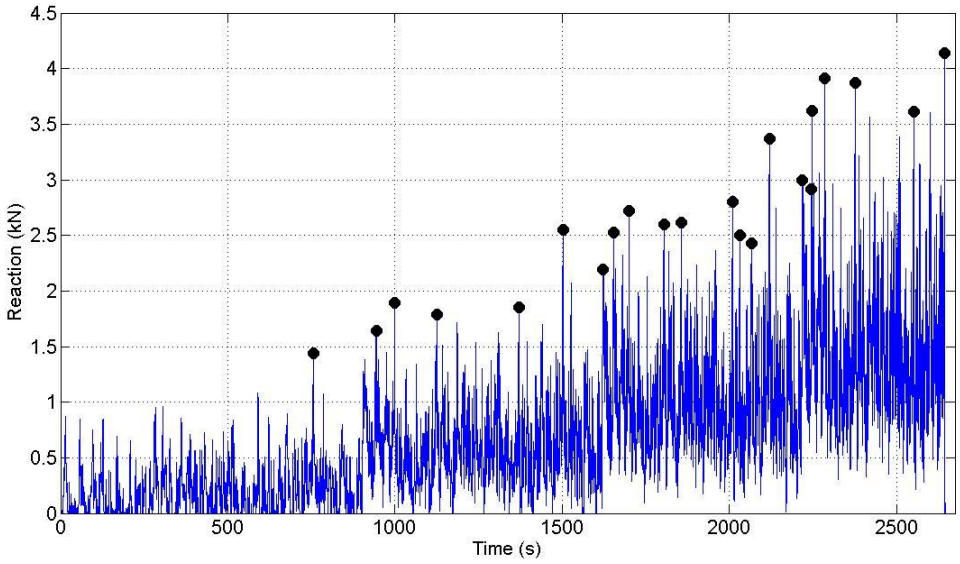


Figure 5.1 Time series of the realistic wind trace used in the nail test rig. The 22 damaging peaks are marked by the black circles.

Figure 4.2 shows the statistical distributions of the ramp loading experiments along with the distribution of the maximum load applied during the fluctuating loading tests. The distribution for the maximum load applied to the specimen during the fluctuating wind

load tests is shifted slightly to the right of the ramp load distributions indicating that, at least in a static sense, the current ramp loading tests are slightly conservative. That being said the results from the realistic wind load experiments have shown that the connections will suffer permanent partial withdrawal at loads as little as 56% of the maximum applied load. Furthermore, during the realistic wind loading experiments the connection does not necessarily fail once the peak load has been applied, but may fail at a latter point in time, and at a lower load. This raises the question of duration effects and reduced capacity of the connection. The current study cannot answer this question completely since only one particular loading sequence was considered and was designed to, on average, increase the wind load until failure. It is possible that a trace with lower amplitudes, but with a much longer duration, could induce a fatigue failure of the connection, as it has been shown that following certain peak loads there can be a reduction in the capacity of the nailed connections. However, the longer the duration of the wind event, the higher the probability that a larger peak will occur, even at the same wind speed. Furthermore, the failure loads were on average only 0.2kN less than the peak capacity of the connection. This is significantly less than the reduction of capacity that can occur due to errors in construction such as a missing nail which, on average, reduces the capacity of the connection by 0.65 kN.

## 5.3 Comparison to ASCE 7-05

A comparison of test results to the ASCE7-05 (2006), was carried out to determine the design wind speeds based on the strength of the toe-nail connections. Due to the significant variability in toe-nail capacity, a factor of safety (FOS) must be selected in

order to make a useful comparison to a design standard. Studies by Reed et al. (1997) used FOS of 2 to 3 along with the 5 and 10 percentile values from the failure capacity distributions, while Cheng (2004) used a factor of safety of 2.5.

The full scale test house described in Chapter 2.1.1 was used to obtain the design wind forces from ASCE 7-05 (2006). It is unclear whether toe-nail connections should be treated as Main Wind Force Resisting Systems (MWFRS) or as a Components and Cladding (C&C) element in the ASCE 7-05 (2006). Consequently, the design forces at RTWC "S3" were obtained by treating toe-nail connections as both a Main Wind Force Resisting System (MWFRS) and a Components and Cladding (C&C) element. The design terrain was assumed to be category C, with wind directionality factor ($K_d$), topographic factor ($K_{zt}$), and importance factor ($I$) all equal to 1. The ASCE7-05 (2006) wind speeds are then calculated and presented in Table 5.2, using the toe-nail capacity for each assumed factor of safety and a dead load due to the weight of the roof of 250 N, for both MWFRS and C&C loads using the FOS of Reed et. al. (1997). It is noted that the $5^{th}$ and $10^{th}$ percentile peaks correspond well with the failure capacities found for toe-nail connections with missing nails reported in Table 4.2. In addition, since the wind tunnel data for the building under consideration is available, $GCp_{eq}$ values are calculated from this data, using the procedure outlined by St. Pierre et al. (2005) and presented in Eq. (3.1). For the current test house the value '*a*' in the ASCE 7-05 that defines the different regions of the roof is 1.0m and is defined by 10% of the least horizontal dimension. This means that using a tributary area approach to calculate the loads on connection "S3" using MWFRS the tributary area (3.2 $m^2$) is within Zone 3E, with a *GCp* value of -0.69.

However, when using the C&C portion of the code, the tributary area for connection "S3", is spread over 3 zones: Zone 1 44%, Zone 2 45% and Zone 3 11%. This results in an area average *GCp* of -1.47. The wind speeds shown in Table 5.2 show that the MWFRS loads calculated for this particular connection are unconservative compared to that obtained from the wind tunnel data. In contrast the C&C loads are shown to be conservative compared to the wind tunnel data. Considering the wind speeds calculated using the C&C loads and the wind tunnel pressure data, the toe-nail connections tested do not have sufficient hold down capacity for the highest loaded region of the test house, in any wind region given by the ASCE7-05 (2006). It is noted that the wind tunnel wind speeds meet the 90 mph wind speed region, provided no factor of safety is assumed. Wind speeds calculated using the MWFRS coefficients from the ASCE7-05 (2006) show that toe-nail connections can be used in several wind regions, when using the $5^{th}$ and $10^{th}$ percentile toe-nail strength. Caution should be taken however, since these results are significantly unconservative as compared to the wind tunnel data.

Table 5.2 ASCE 7-05 Design Wind speed calculated using both the MWFRS and C&C coefficients from the code as well as from wind tunnel pressure data

| FOS | Toe-nail Design Capacity (kN) | ASCE7-05 Design Wind Speed (mph) | | |
|---|---|---|---|---|
| | | MWFRS | C&C | Wind Tunnel |
| 0 | 2.8 | 108 | 64 | 92 |
| 2 | 1.4 | 80 | 47 | 65 |
| 3 | 0.93 | 67 | 40 | 65 |
| $5^{th}$ Percentile | 1.9 | 91 | 53 | 76 |
| $10^{th}$ Percentile | 2.2 | 97 | 57 | 82 |

Other factors, such as internal pressure and load sharing were not considered in the present analysis and both can have a significant effect on the calculated failure wind speed. In the case of internal pressures, dominant openings in the windward wall can

significantly lower the failure wind speed (Kopp et al. 2008). At the present time the amount of load sharing that occurs for wood frame structures is unknown, although this is examined to some extent in chapter 7.0. The results presented in Table 5.2 assume that there is no load sharing between connections, which is a conservative assumption. The wind speeds presented in Table 5.3, have been calculated assuming perfect load sharing between all connections on the roof. Or, in other words, that the load at every connection is the same. As discussed in Chapter 1.1, this assumption is likely unconservative for the worst loaded connections. In contrast, to the no load sharing case, by assuming perfect load sharing both the MWFRS and C&C loads from the ASCE7-05 (2006) are conservative compared with the wind tunnel data for RTWC "S3". This is likely the result of the ASCE7-05 (2006) over-predicting the pressure coefficients in the field of the roof for this particular structure. The wind speeds for the MWFRS and C&C loads have increased in comparison to the worst loaded connection case shown in Table 5.2, however the changes are small. In the case of the wind tunnel data, the wind speeds are substantially higher. This result is not surprising since the low spatial correlation of the wind loads on the roof are well known and have been shown earlier in Inset B of Figure 1.5. However, the added benefit of significant load sharing between connections is that the FOS can be reduced from that used when considering a single connection.

Table 5.3 ASCE 7-05 Design Wind speed calculated using both the MWFRS and C&C coefficients from the code as well as from wind tunnel pressure data, assuming perfect load sharing between toe-nail connections on the roof

| FOS | Toe-nail Design Capacity (kN) | ASCE7-05 Design Wind Speed (mph) | | |
|---|---|---|---|---|
| | | MWFRS | C&C | Wind Tunnel |
| 0 | 2.8 | 112 | 84 | 124 |
| 2 | 1.4 | 82 | 61 | 91 |
| 3 | 0.93 | 70 | 52 | 77 |
| $5^{th}$ Percentile | 1.9 | 94 | 70 | 104 |
| $10^{th}$ Percentile | 2.2 | 100 | 75 | 111 |

# 6.0 RESPONSE OF THE ROOF OF FULL SCALE HOUSE TO REAL WIND LOADING

As discussed in Chapter 1.0 individual connection tests do not account for effects that the structural system has on the response at any particular connection. Chapters 4.0 and 5.0 detailed the response of single toe-nail connections to realistic fluctuating wind loads. However, due to the spatial variation of winds loads over the roof of a structure, as well as the load sharing, it is not clear how the failure will progress in an actual structure or the required wind speed to cause failure even if the hold down at every connection is known perfectly. Moreover, the response of a toe-nail connection to a fluctuating realistic load as it fails has been found to be far more complex than that observed during simple static pullout. In order to understand and predict failures of wood frame structures, an understanding of the relationship between the response of the toe-nail connections and the overall structural system of the house is required. In order to fully capture these effects, testing of the entire structural system is needed to determine the true performance. This chapter presents the data obtained during the full scale house test(s) described in Chapter 2.1.5, with a brief description of the observations made during testing. A detailed discussion of the results and implications will be made in Chapter 7.

## 6.1 Displacements

Figure 6.1 is a repeat of Figure 1.5, but with the displacements from RTWC "S3" for test #6 (45 m/s) now shown in inset C for the same short segment of time as the load time histories depicted in insets A and B. As previously discussed in Chapter 1.0, inset A shows that, due to the high spatial gradients on the roof of the house, the area-averaged pressure coefficients (*Cp*) for a $3m^2$ area are substantially lower than the worst

coefficients at a single point within that same area. Similarly, the calculated applied load to RTWC "S3" can vary by a factor of 3 by assuming no load sharing between adjacent connections or with perfect loading sharing as shown in inset B of Figure 6.1. It is noted that the no load sharing curve shown in inset B represents a portion of the force coefficient, *Cf*, used for the individual toe-nail connection testing discussed in chapters 4.0 and 5.0. Comparing the load and displacement curves at the time increment of 26-28 sec (indicated by the box in the figures), it is apparent that the displacement rises immediately with the increasing load, and the load on the connection remains large for a relatively short period of time before dropping off just as quickly. However, the displacement of the connection remains elevated for a substantial period of time and reduces more gradually than the load. This phenomenon, which is examined further later in this chapter, was not observed during the individual toe-nail connection tests and must be the result of the structural system.

Figure 6.2 to Figure 6.11present the complete displacement time series for RTWC "S2" through "S6" and RTWC "N2" through "N6" for all 6 tests, the displacements for the remaining connections can be found in APPENDIX E. Positive displacements represent the roof moving upward away from the wall, while negative displacements represent movement towards the floor (foundation). Although, a clear upward trend in the displacements can be observed as the load increases (increasing scaling wind speed), the damaging peaks are not as apparent as they were during the individual toe-nail connections experiments. The RTWC with the highest displacement is "S3", which is consistent with what was expected prior to testing since the loads calculated in Chapter

3.1.1 using a tributary area SOM approach indicate that the highest loaded connections are located on truss #2. Since truss #2 is a gable end wall that has additional hold downs along the length of the wall, it could be anticipated that the net effect is to reduce the reactions "S2" and "N2". Consequently, the next highest loaded RTWC is "S3" which has been found to have the highest displacements of any RTWC on the roof.

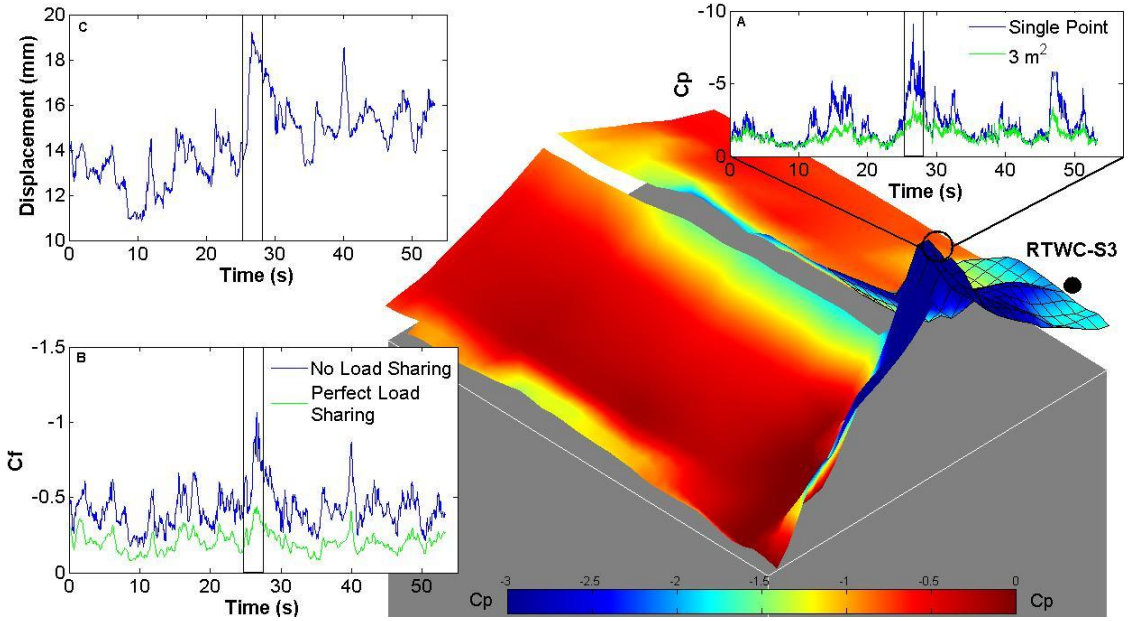


Figure 6.1 Contours of the spatial gradients of external wind pressures on the roof of the test house. Inset A: wind tunnel pressure coefficients at a single point and averaged over a $3m^2$ area. Inset B: Applied force coefficients for a single roof to wall connection (RTWC), considering no load sharing and perfect load sharing. Inset C: the displacement of the RTWC-S3 under the loading shown in Inset B.

Examining the displacements on the North side of the house during tests #1 and #2 (20 m/s and 25 m/s), it can be seen that the displacements are negative. Since the displacement transducers are mounted on the brick veneer on the outside of the house, the negative displacements along with the positive displacements observed on the South side of the house indicate that the roof is overturning about the Northern wall. This is not

surprising since, as discussed in Chapter 3.1.1, the highest loads at a wind angle of 40° for this building occur on the leeward side (South) of the roof. However, it is important to note that the roof would not "fly" off in this configuration, since as the roof begins to lift a significant amount the aerodynamic pressure coefficients on the roof of the house will be altered and counteract this rotation.

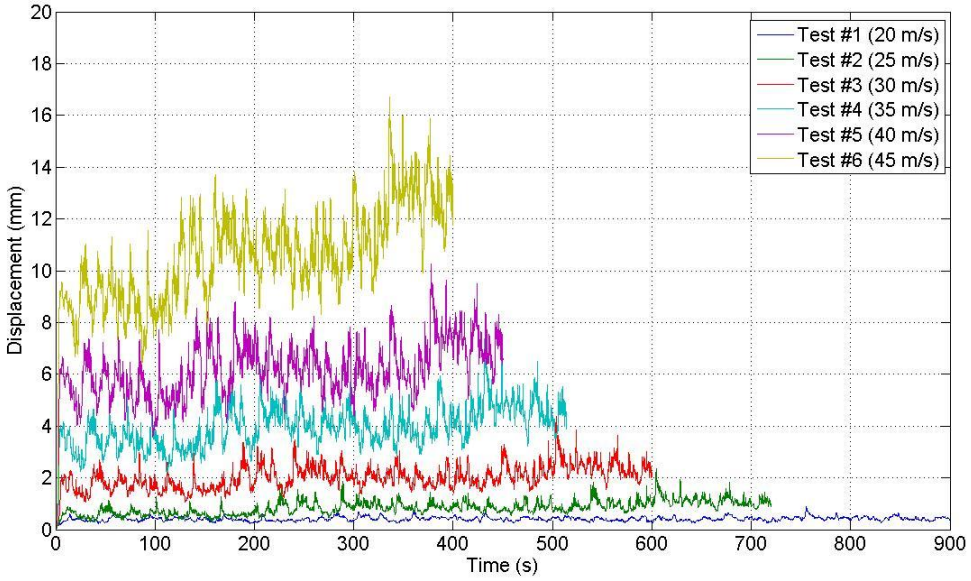


Figure 6.2 Displacement Time Series for all 6 tests for RTWC "S2"

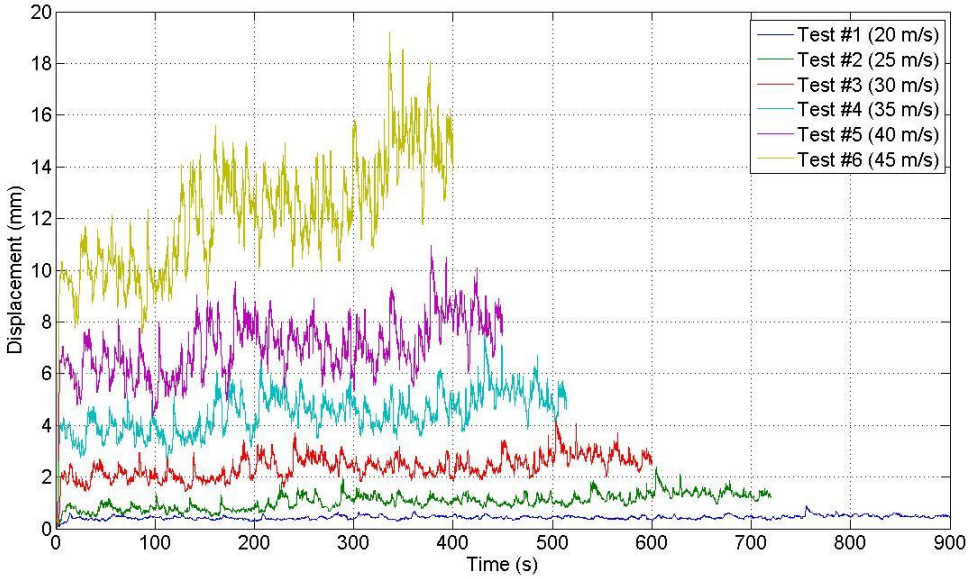


Figure 6.3 Displacement Time Series for all 6 tests for RTWC "S3"

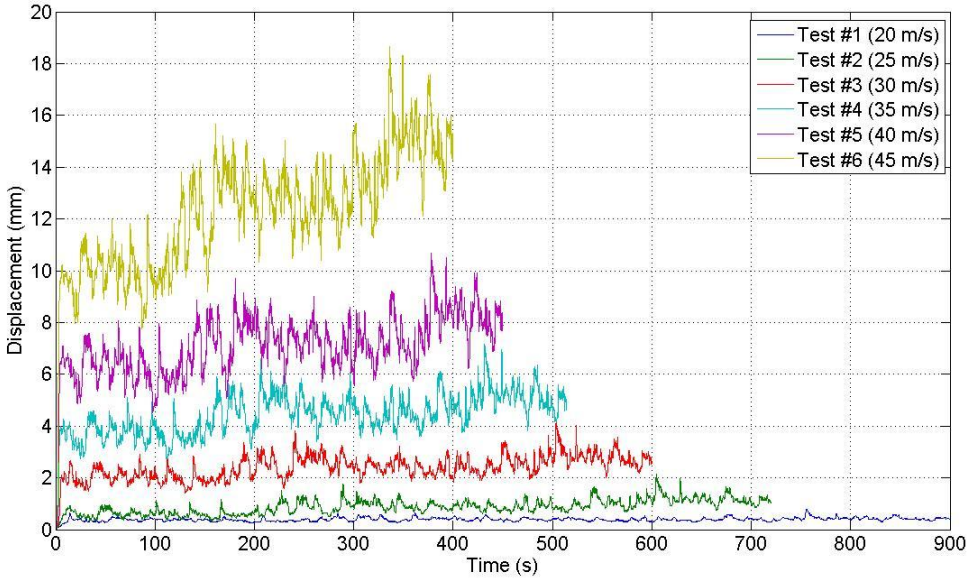


Figure 6.4 Displacement Time Series for all 6 tests for RTWC "S4"

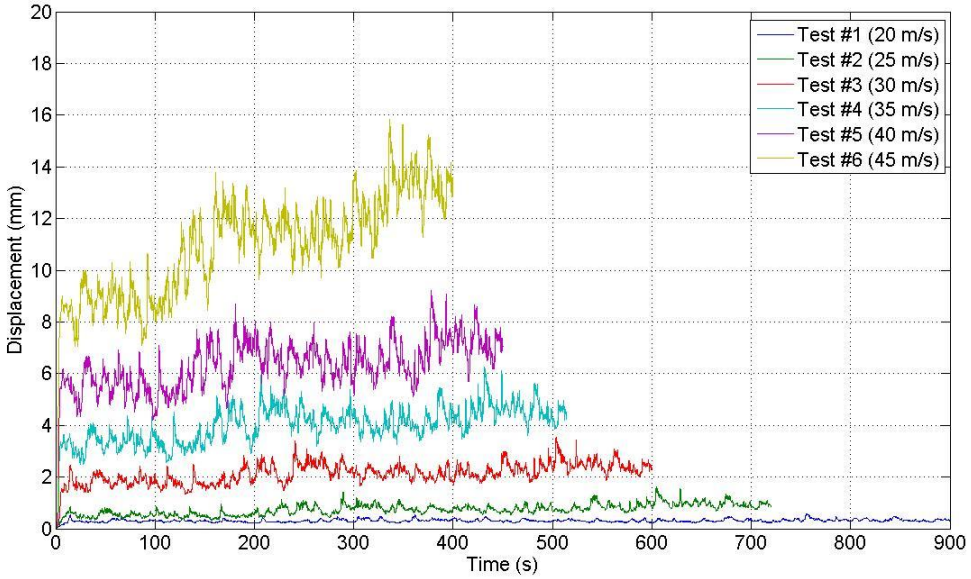


Figure 6.5 Displacement Time Series for all 6 tests for RTWC "S5"

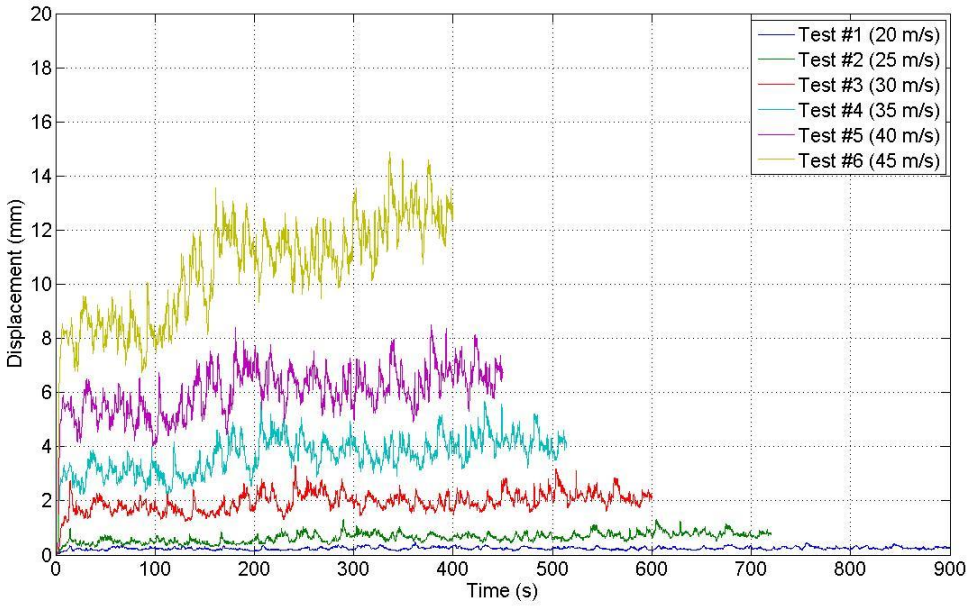


Figure 6.6 Displacement Time Series for all 6 tests for RTWC "S6"

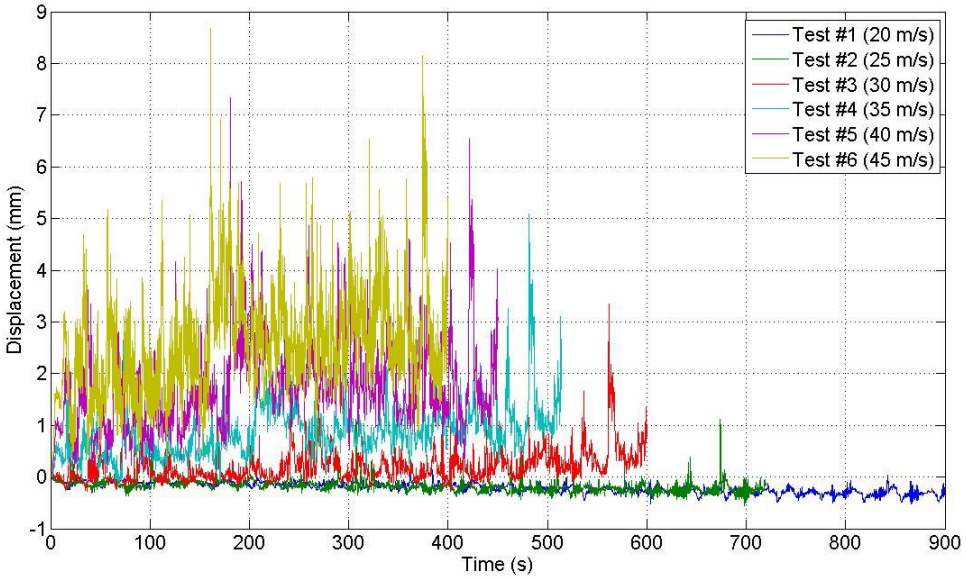


Figure 6.7 Displacement Time Series for all 6 tests for RTWC "N2"

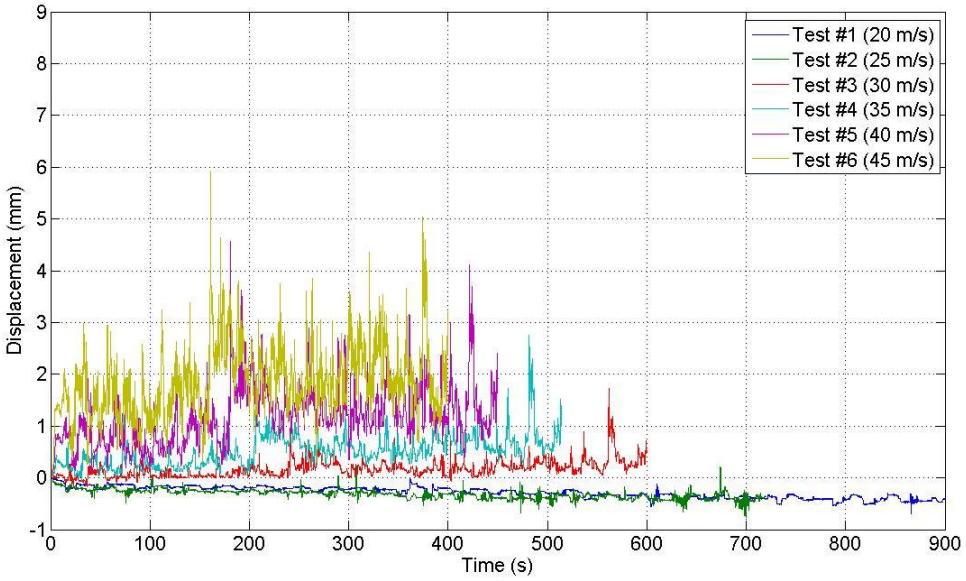


Figure 6.8 Displacement Time Series for all 6 tests for RTWC "N3"

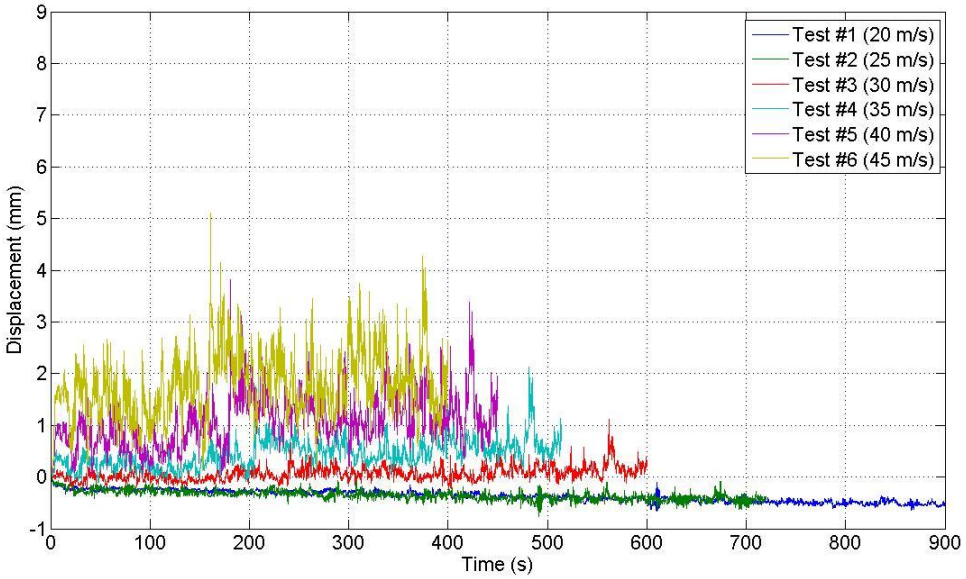


Figure 6.9 Displacement Time Series for all 6 tests for RTWC "N4"

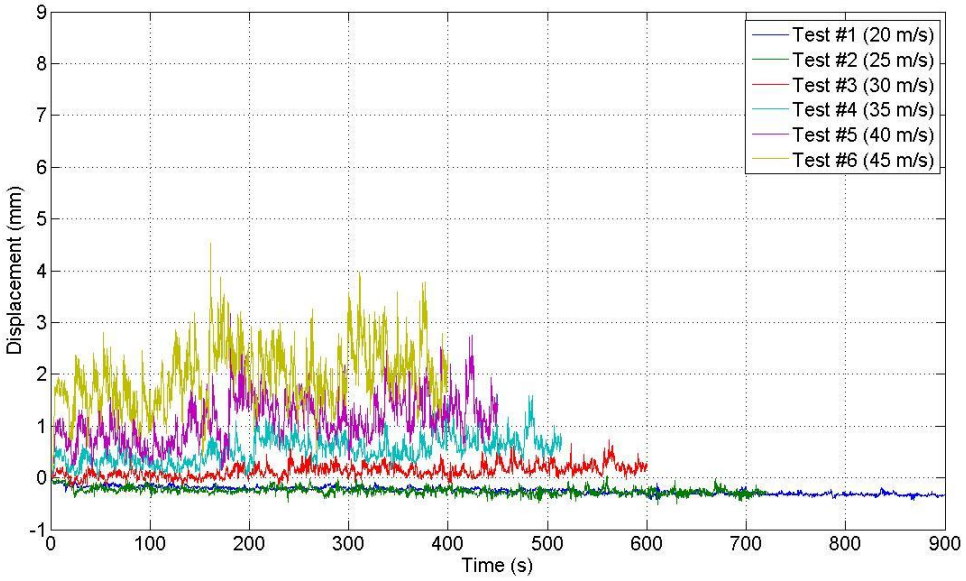


Figure 6.10 Displacement Time Series for all 6 tests for RTWC "N5"

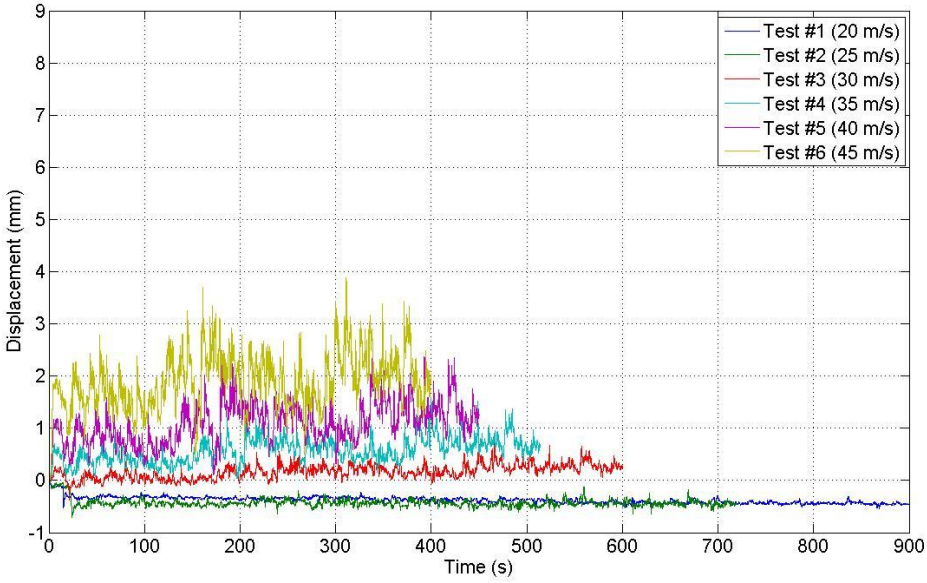


Figure 6.11 Displacement Time Series for all 6 tests for RTWC "N6"

As previously discussed in Chapter 3.1.1, the same portion of wind tunnel data is used for each test; however, the duration of each test reduces with increasing scaling wind speed as the result of the scaling law given in Eq. 3.3. However, the number of peaks in each test is the same, meaning that a peak in a given test has a corresponding peak in all of the other tests. It should be noted that the peak pressures increase with the square of the scaling wind speed, while the duration of the test is reduced linearly with increasing wind speed. To compare corresponding peaks between tests, the displacement time series for connections "S3" and "N3" have been artificially stretched for all tests to correspond to the time series duration of test #1 (20 m/s). The stretched time series are shown in Figure 6.12 and Figure 6.13, although the displacements during tests with larger scaling wind speeds and thus higher loads are larger than previous tests the trends in the displacements are remarkably similar.

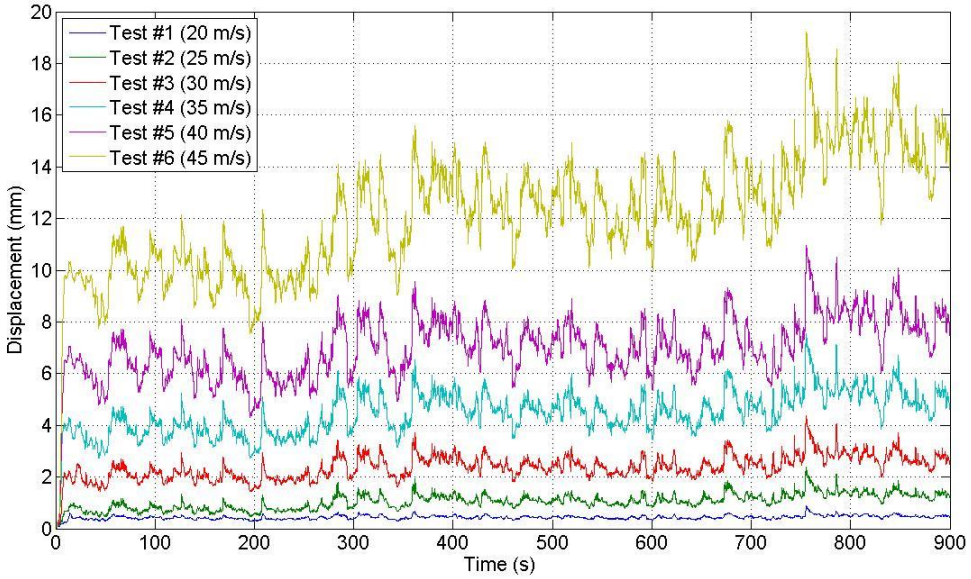


Figure 6.12 Stretched Displacement Time Series for all 6 tests for RTWC "S3"

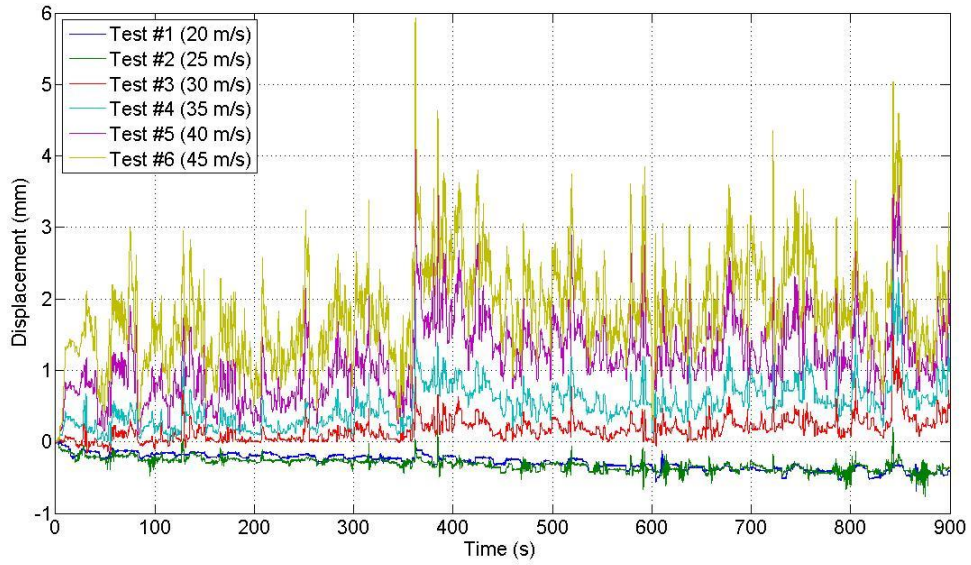


Figure 6.13 Stretched Displacement Time Series for all 6 tests for RTWC "N3"

## 6.2 Load Displacement Curves

The displacements shown for RTWC "S3" in Figure 6.3 are plotted versus the SOM geometric tributary area load for connection "S3" calculated in APPENDIX D and is shown in Figure 6.14. Similar to the displacement time series an overall shift in the displacements is observed. However, unlike the load displacement curve for the individual toe-nail connection tests presented in Figure 4.5, incremental damage of the connection cannot be attributed to a single individual peak. The scatter of the data is likely the result of load sharing between adjacent connections as the connections are being displaced relative to one another. Figure 6.15 presents a similar figure to that of Figure 6.14 for connection "N3", there appears to be only a slight incremental permanent displacement throughout all of the 6 tests. Since the calculated applied loads are similar to those applied to "S3" it is likely that the loads on the connections on the South side of the house are significantly larger than those on the North side. APPENDIX F provides the load displacement curves for all other RTWC.

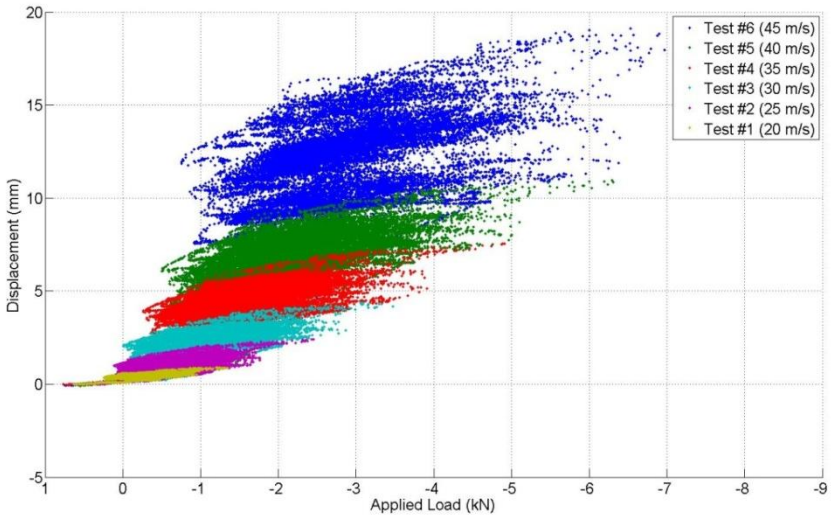


Figure 6.14 Load Displacement data for connection "S3" for all 6 tests.

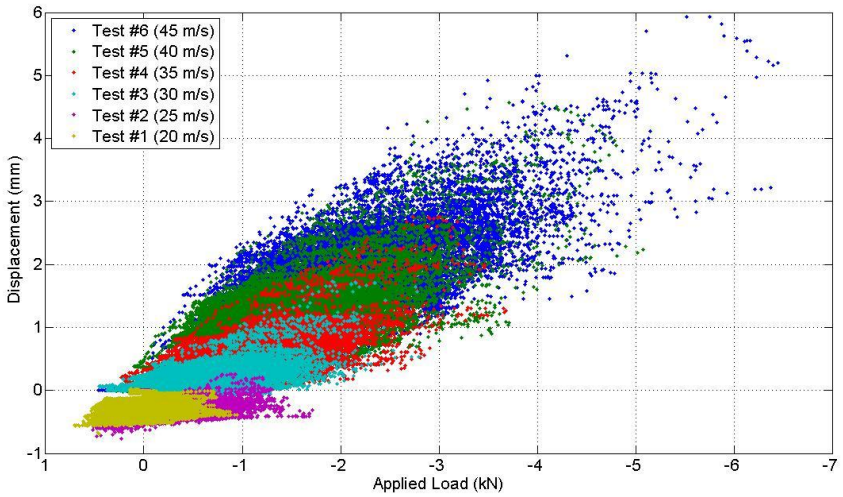


Figure 6.15 Load Displacement data for connection "N3" for all 6 tests.

In order to illustrate the effect of peaks more effectively, Figure 6.16 presents the load deflection data for a single peak in the time history for test 3, 5, 6 ($V$ = 30, 40, 45 m/s) centred around 504, 378, 336 seconds for the three wind speeds, respectively. Hysteretic behaviour of the displacements between loading (blue) and unloading (green) segments of the peak is clearly observed for each test. This phenomenon was not observed during the individual connection tests and must be caused by the stiffness of the roof and the load sharing between connections. For each subsequent test, the displacement-load curves shift upwards, indicating that the connections are becoming increasingly damaged. The net permanent accumulation of damage is observed by comparing the curves prior to (magenta) and after (red) the peak curves for a single peak load. In the case of the Test #6 data (for V = 45 m/s) this represents the single largest peak load applied to the structure; however, the incremental permanent displacement, or damage to the connection

due to this peak, is only 2 mm or about 10% of the total nail withdrawal observed, while the net displacement from the base of the peak load to the peak itself was only 5 mm. This means that, while the magnitude and duration of the peak load is important, the number of large damaging peaks also plays a vital role in the ultimate failure. Comparing the results with those in Chapter 4 indicates that many more peaks are required to fail any given connection in the roof.

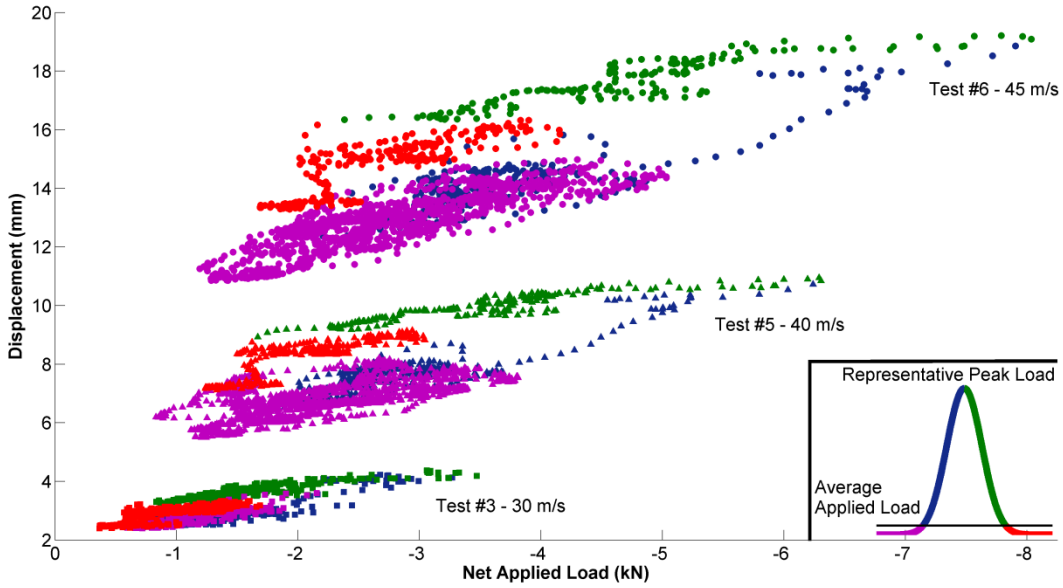


Figure 6.16 Load displacement curves for the same peak load over 3 tests. The different colours represent different potions of the peak load, as sketched: magenta is before the peak occurs, blue is during the loading portion of the peak, green is the unloading portion of the peak and red is the after the peak.

Figure 6.17 to Figure 6.19 present the load displacement curves for RTWC "S3" through "S8" assuming different load sharing arrangements for test #5 (40 m/s). Figure 6.17 uses the SOM tributary area loads for each connection calculated in APPENDIX D, Figure 6.18 assumes that the tributary loads for RTWC "S3" through "S8" are shared equally among these connections. Finally, Figure 6.19 plots the displacements vs. global roof

uplift. Examining Figure 6.18 and Figure 6.19 connections, the displacements at a given load level seem to shift upwards from connection "S8" through connection "S3". This indicates that provided that there is no difference in physical properties of the connections that the loads on the connections with the highest displacements are underestimated, while the load on the connections with the lowest displacements are over estimated. Assuming a tributary area approach to the loading as shown in Figure 6.17, provides the best collapse of the displacement data of the 3 loading cases considered, suggesting that the reactions at each connection are close to the tributary area SOM loads. However, caution should be taken since this assumes that the behaviour of the nails is linear elastic which, as shown in Figure 6.16, is not true. In addition, as discussed in chapter 2.1.1, there are additional connections between the trusses and the internal walls which, are likely not evenly distributed among the different trusses and as a result alter the reactions at each connection differently, which will artificially skew the collapse of the data.

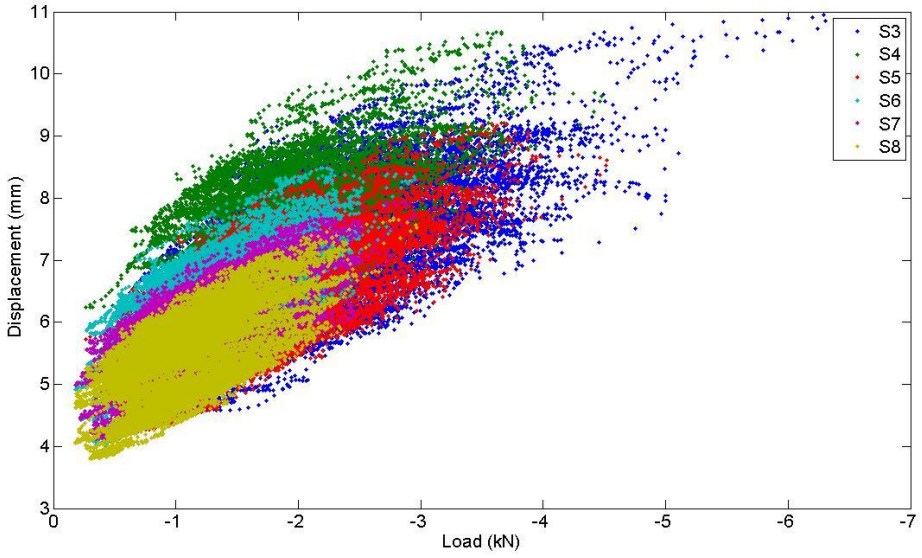


Figure 6.17 Load vs. Displacements curves for test #5 (40 m/s) for RTWC "S3" through "S8" using a tributary area assumption for the applied load.

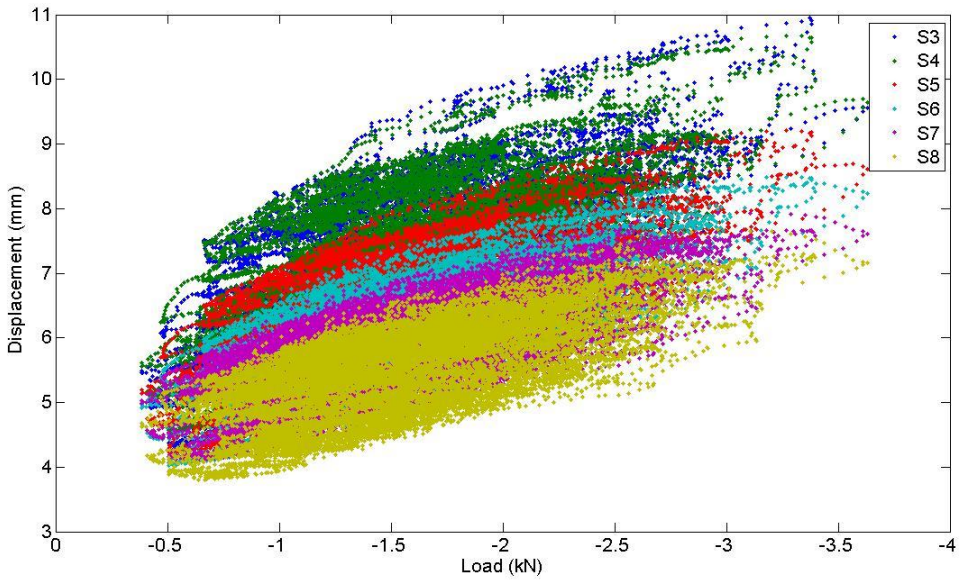


Figure 6.18 Load vs. Displacements curves for test #5 (40 m/s) for RTWC "S3" through "S8" using an averaged load over all 6 trusses.

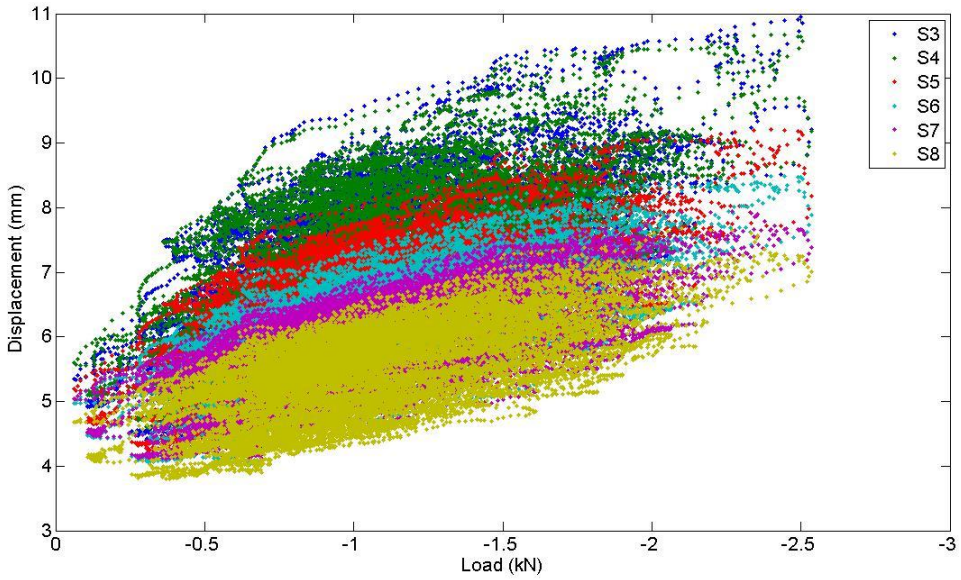


Figure 6.19 Load vs. Displacements curves for test #5 (40 m/s) for RTWC "S3" through "S8" using the global uplift load for each connection.

As discussed in chapter 1.0, the time scale at which the roof responds to the wind loading is unknown. The Normalised Power Spectrum Density (PSD) for the displacements and tributary area SOM loads for RTWC "S3" and "N3" are shown in Figure 6.20 along with the PSD for the global roof uplift load for test #5 (40m/s). Although the wind loads are stationary the displacement time history is not due to the incremental withdrawal of the nails. As a result, it should be noted that this may result in an artificial increase of amplitude of the displacement PSD at lower frequencies that are not present in the loading PSD. While stationary is an important issue when discussing wind loading, especially for short duration wind events, the goal of the current comparison is to examine the cut off frequency along with any amplification or attenuation of the response at specific frequencies. Consequently, the effects of the non-stationary displacement signal have been ignored for the current discussion. The PSD of the tributary area SOM loads for RTWC "S3" and "N3" are nearly the same and match the global uplift spectra up until a frequency of approximately 1 Hz at which point the global uplift spectra drops below the spectra of the tributary area loads. The reduction of energy at higher frequencies for the global roof uplift is not surprising due to the low spatial correlation of the wind loads on the roof. The spectrum of the displacements drops below those of the tributary area loads at approximately 0.1 Hz. It has been shown in Figure 6.16 that there is hysteresis in the displacement time series immediately following a damaging peak, where the displacement reduces more gradually than the loading, which could partially explain the drop off of the displacements at higher frequencies. Figure 6.21 shows the transfer function between the displacements at RTWC "S3" and "N3" and either the tributary area SOM or the global uplift loads. For both loading assumptions the transfer

function drops with increasing frequency, however in the case of the tributary area SOM loads the transfer function remain at or above 1 until a frequency of approximately 0.4 Hz and drops only to 0.6 at 10 Hz. In contrast, the transfer function using the global uplift loading is approximately an order of magnitude lower than that using the tributary area SOM loads. This indicates that there is little correlation between the global uplift loads and the response of these connections, while the correlation between the tributary area SOM loads and the displacements is much better. That being said, it is clear that without the true reactions at the RTWC it is not possible to know for certain if there is an attenuation of the response of the roof at higher frequencies. Moreover, as shown in Figure 6.16 there is clear hysteresis between the loading and unloading portions of the load displacement curve for damaging peaks, which may also cause an attenuation of the transfer function at higher frequencies. However, overall there does not appear to be significant amplification or attenuation in the response of the roof to the fluctuating wind loads.

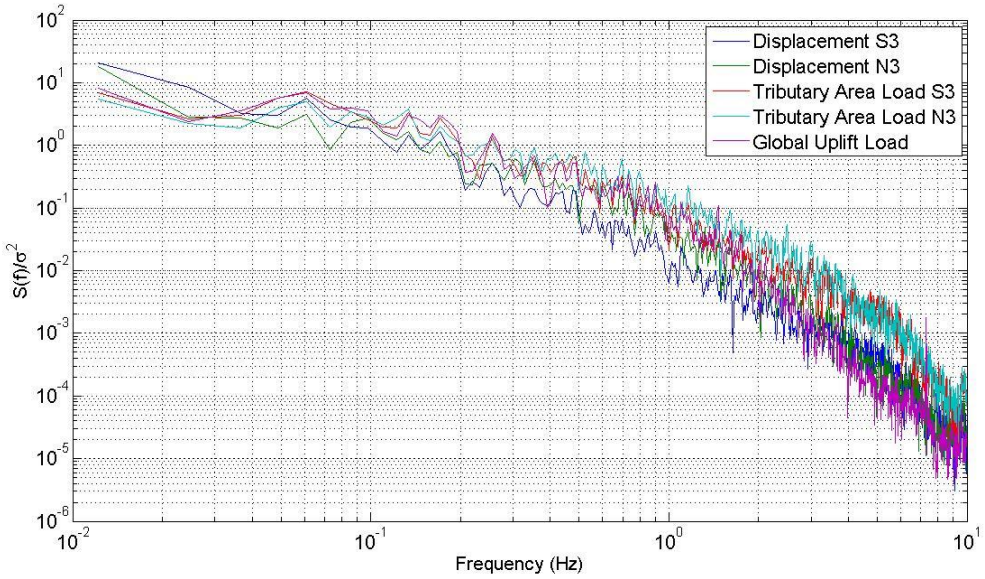


Figure 6.20 Normalised power spectrum density plot for tributary area loads and displacements at RTWC "S3" and "N3". In addition the power spectrum density for the global roof uplift is also included.

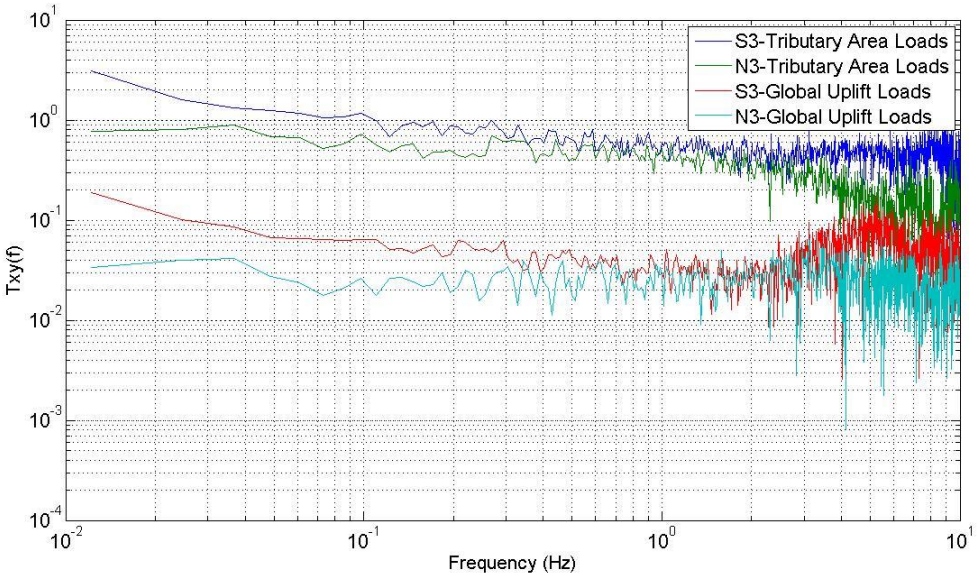


Figure 6.21 Transfer function between the displacements at RTWC "S3" and "N3" and the applied loads.

## 6.3 Visual Documentation of Damage

A photographic comparison of RTWC "S3" from prior to testing and after the application of the wind loads is shown in Figure 6.22. From the photographs, clear withdrawal of both nails is observed, resulting in an air gap between the roof truss and the top plate. Despite the damage that has occurred to the toe-nail connection, the damage to the interior of the house is minimal as shown by Figure 6.23 where only hairline crack(s) can be seen. The size of this crack is not abnormal for a house under normal conditions (not subjected to significant wind loads). For example the crack shown in Figure 6.24, located on the first floor of the house was observed prior to any testing being conducted. This crack remains the largest crack in the entire house, even after testing. As a result, it is likely that following significant wind events, houses could have accumulated a significant amount of damage to the RTWC that is not apparent from the interior of the house. It is not clear if greater interior damage would have been observed had wall loads been applied at the same time.

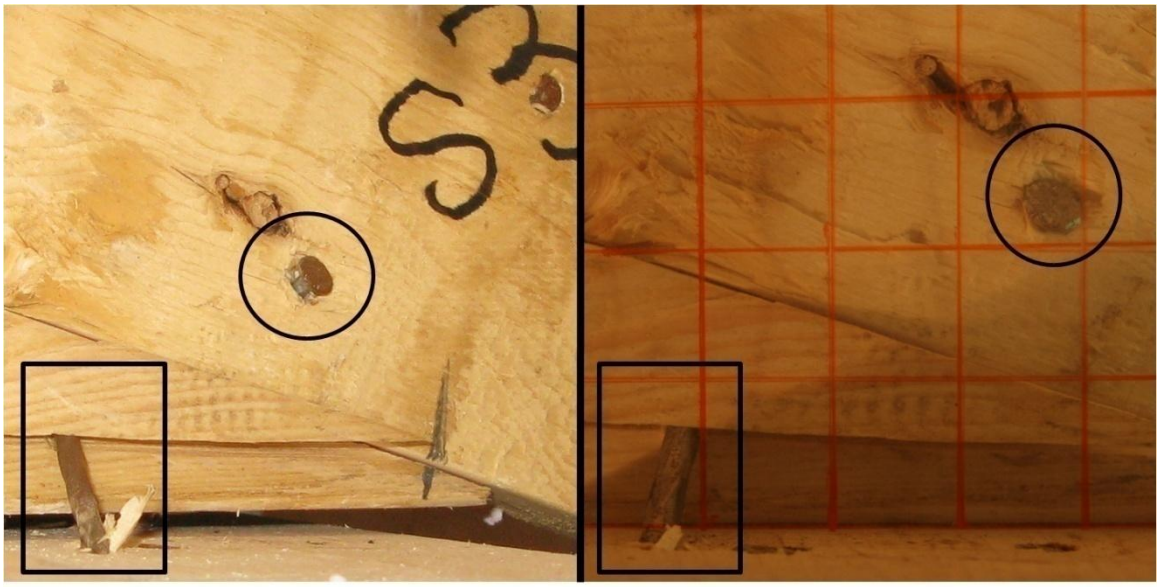


Figure 6.22 Side by Side comparison of RTWC "S3" prior to testing and after Test #5 (40 m/s/)

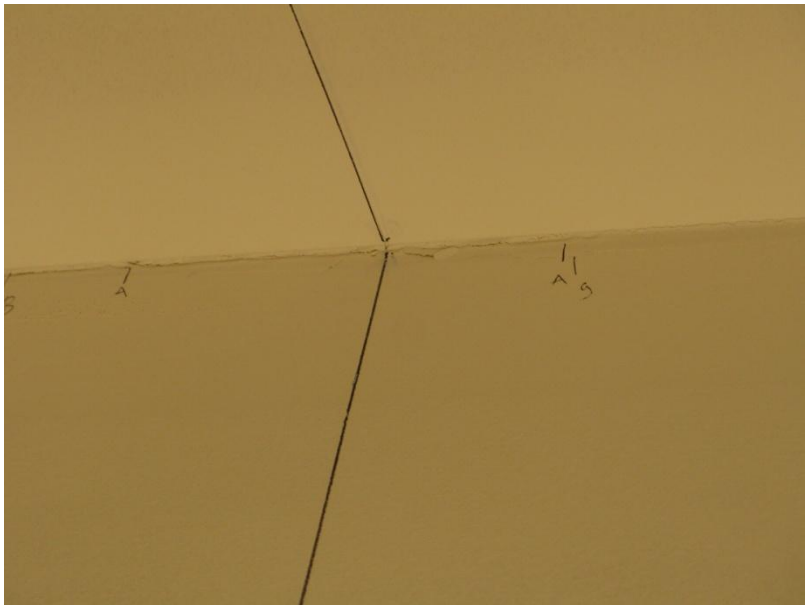

Figure 6.23 Cracks in the drywall below RTWC "S3". Only minor hairline cracks are observed despite the damage that has occurred to the toe-nail connection directly above it.


Figure 6.24 Largest crack documented in the test house, which was not the result of structural testing. Distance between vertical black lines is 0.3 m.

# 7.0 ANALYSIS OF LOAD SHARING

In Chapter 6.0 detailed results from the full scale house experiments were presented and brief observations regarding the results were made. The current chapter will discuss these results in greater detail. Figure 6.16 showed that, similar to the individual toe-nail connection test results, the connections are being incrementally withdrawn from the top-plate for the same peak in several tests. However, this phenomenon is not as clear in the full house test as it is for the individual connection tests, i.e., comparing Figure 4.1 and Figure 6.14, with the structure making the analysis of connection loads more complicated. The most notable difference between the individual connection tests and the full house experiment is that, assuming a typical tributary area approach, the loads applied to the full scale house far exceed the failure capacities found for the individual toe-nail connections in Chapter 4.0, indicating very significant load sharing. The nails used in the toe-nail connection are not identical between the full house and the individual toe-nail connection experiments, and as such the strength of the RTWC on the full house may be different than those tested individually. However, from the inspection of construction quality prior to testing, the quality of the connections used in the full house appear to be lower, on average, than those constructed for the individual toe-nail connection. As a result, it is unlikely that all connections on the roof of the house are significantly stronger than those used for the individual toe-nail tests. Consequently the significantly higher (tributary) loads must be attributed to load sharing between adjacent connections. This Chapter will examine the failures of the connections in greater detail and discuss the role that load sharing plays in the response of the house to wind loads and, ultimately, roof failure(s).

## 7.1 First Damaging Peak

Due to the spatially-varying loading and complex load sharing between adjacent connections, determining the first damaging peak for connections in the full house experiment is more complex than in the case of the individual toe-nail experiments. This is further complicated by the fact that only the loads applied to the roof are known and not the reactions at each particular connection. These factors result in load displacement curves, as shown in Figure 6.14, that are more variable than those of the individual toe-nail connections shown in Figure 4.5. This makes it nearly impossible to determine the precise time where first damage occurred to a connection on the roof. However, Figure 7.1 shows the displacement time series for connection "S4" for Tests #1 (20 m/s) and #2 (25 m/s). The deflections have been normalised by the scaling dynamic pressure $q$ used to determine the full scale loads applied for each scaling wind speed. As such, if the connection behaviour were purely elastic and there are no duration effects, then the two displacement time series should fall on top of each other. (Note that the time series for test #2, 25 m/s, has been artificially stretched by 25% so that similar peaks can be compared directly.) While a perfect match is not expected due to the complexity and variability of the system, this trend seems to follow fairly closely up until the peak that occurs at 280 seconds, at which point the test #2 (25 m/s) curve shifts upwards. This is due to a damaging displacement to the connection having occurred. This does not mean that connection "S4" was the first damaged connection, nor does it mean that no damage to any connection had occurred prior to 224 seconds (note removal of time normalization) of test #2 (25 m/s), however it does show that first significant damage occurred at this point in time for this connection. If we continue to assume a tributary area SOM

approach in calculating the reaction loads, the highest load applied to each connection prior to 224 seconds of test #2 (25 m/s) is presented in Table 7.1. Only connections on the South side of the house were considered since, as shown in Chapter 6.0, the roof is rotating about the north wall of the house. The highest load shown in Table 7.1 is -1.97 kN at connection "S2". As previously discussed in Chapter3.2.2 "S2" represents the gable end wall and as such, the reaction at the toe-nail connection is likely over estimated in the current analysis as the result of additional connections between the roof truss and the wall. In any case, this analysis assumes no load sharing between adjacent connections and, as such, over-estimates the load on the highest loaded connections and underestimates the load on the least loaded connections. That being said, the current result shows that damage to a connection on the roof of the house initiated at a load of -1.97 kN or less, which is consistent with the peak load that causes the first damage for the individual toe-nails. Assuming perfect load sharing between connections, the first damaging peak would have occurred at a load of 0.67 kN or less. Since, it has been shown that on average the magnitude of the first damaging peak is related to the mean maximum capacity, it is probable that the connections of the house are likely to have a similar ultimate capacity to those tested individually, although it is noted that there is likely significantly more variability in the strength of connections for the house.

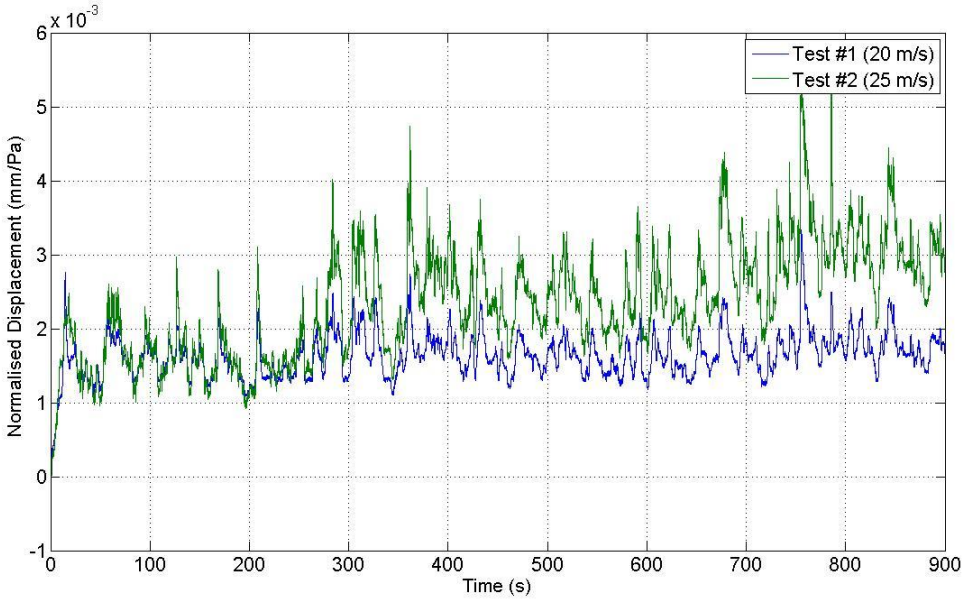


Figure 7.1 Displacement normalised by dynamic pressure versus time for connection "S4" during test #1 and test #2

Table 7.1 Maximum load applied to the connections on the South side of the house prior to 224 seconds of test #2

| Connection | Maximum Load (kN) |
|---|---|
| S2 | -1.97 |
| S3 | -1.76 |
| S4 | -1.09 |
| S5 | -1.10 |
| S6 | -0.98 |
| S7 | -1.15 |
| S8 | -1.03 |
| S9 | -1.08 |
| S10 | -1.00 |
| S11 | -1.35 |
| S12 | -1.34 |
| S13 | -1.36 |
| S14 | -1.07 |
| S15 | -0.99 |
| S16 | -0.88 |
| S17 | -0.70 |

## 7.2 Load Sharing between Adjacent Connections

As discussed above, it is clear that there is significant load sharing. In this section this is examined in greater depth. Table 7.2 provides the peak load applied to all 32 connections, throughout all tests, assuming no load sharing, from the calculations in APPENDIX D. In fact, assuming no load sharing a total of 20 connections, or 63%, would have experienced load greater than the mean maximum capacity found for individual toe-nail connections. Consequently, in order for the roof not to have fully failed during these tests, there must have been considerable load sharing between adjacent connections. Since the current experiment did not measure the reactions it is not possible to know exactly how the peak loads were being shared between adjacent connections. As discussed in Chapter 5, the other limiting case is to assume perfect load sharing between all connections on the roof. Under such an assumption, the peak load per connections is -3.3kN, still exceeding the mean maximum capacity for toe-nail connections found from the individual toe-nail experiments. It is unlikely that perfect load sharing exists for the current test house since this would mean that all connections experience the same load. This implies that the difference between the displacements at different RTWC is the result in variability in connection strength which should be randomly distributed over the entire roof. However, Figure 7.2 clearly shows a clear trend of decreasing displacement from East (highest loaded edge) to West along the South wall, indicating that the reactions at the connections on the East side of the house are higher and are decreasing towards the west side. Moreover, the displacements of the RTWC on the North side of the house are significantly lower than those on the South side of the house, also indicating that the loads on the South side of the roof are higher.

While this may mean that the average toe-nail on the roof may be stronger than those tested individually, there are other significant unknowns regarding the hold downs of the roof. A significant number of connections between the roof trusses and the interior walls were discovered upon removal of the roof. Moreover, the effect of additional hold down connections along the gable end wall has not been fully addressed. The combination of these factors will likely reduce the expected reactions at the RTWC and increase the net capacity of the roof.

Table 7.2 Maximum Load applied to all RTWC assuming no load sharing

| **Connection Name** | **Maximum Load (kN)** | **Connection Name** | **Maximum Load (kN)** |
|---|---|---|---|
| S2 | -10.51 | N2 | -11.03 |
| S3 | -8.03 | N3 | -6.45 |
| S4 | -5.53 | N4 | -4.01 |
| S5 | -5.60 | N5 | -4.29 |
| S6 | -3.82 | N6 | -2.85 |
| S7 | -4.04 | N7 | -3.11 |
| S8 | -3.76 | N8 | -2.94 |
| S9 | -4.11 | N9 | -3.41 |
| S10 | -2.89 | N10 | -2.84 |
| S11 | -2.85 | N11 | -3.03 |
| S12 | -2.70 | N12 | -2.73 |
| S13 | -2.80 | N13 | -2.87 |
| S14 | -2.37 | N14 | -2.46 |
| S15 | -2.39 | N15 | -2.45 |
| S16 | -2.15 | N16 | -2.21 |
| S17 | -2.22 | N17 | -2.28 |

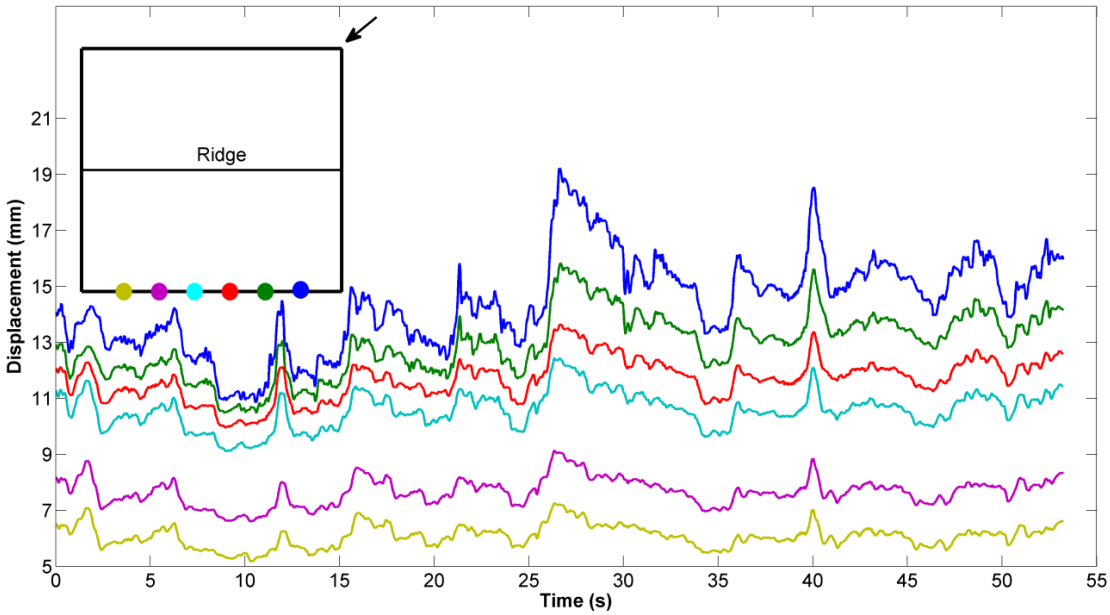


Figure 7.2 Displacement time series for several RTWC's along the South wall of the house during test 6 (V = 45 m/s). The locations of the connections represented by each colour are shown in by the inset diagram of the roof. The blue curve represents RTWC "S3" previously

It is known that along with additional mass, the gable end wall also contains additional connections along the end wall, likely making it significantly stronger than trusses in the interior of the roof. The highest loading in the current experiment occurs adjacent to a gable end wall, which contains both a higher mass and additional hold down connections than interior trusses. Thus, the end walls may take a substantially higher proportion of the load than originally thought. In order to attempt to quantify the loading sharing, the loads per connections were re-calculated by grouping different combinations of trusses together; within each group of trusses, perfect load sharing is assumed. In addition, the truss is assumed to be perfectly rigid, as such, there is perfect load sharing between North and South connections on the same truss. The results of this analysis are shown in Table

7.3, the columns in the table represent the starting truss for the group while the row indicates the last truss from the group, loads before the first truss or after the last truss of the group are not considered. For example, the load presented under the starting column 6 and ending row 10, assumes that the loads applied to trusses 6 to 10 are perfectly shared among these trusses while the loads from trusses 1-5 and 11-17 do not affect this group of trusses. The loads are presented in load per connection, with any load exceeding the global roof uplift load presented in red. Table 7.3, shows that if perfect load sharing was to occur over 6 trusses, and that the gable end walls are strong enough to prevent failure of the first group of 6 trusses then the load per connection could be as low as -2.9 kN. The true load sharing arrangement is not known, however it must lie between the no load sharing case (tributary area approach) and the perfect load sharing case.

Table 7.3 Summary of different load sharing combinations between trusses. Results are presented as load per connection in (kN). The shared load between two adjacent truss is assumed to be perfect. The number at the top of the column indicates at what truss number the load sharing begins, i.e. any load from a lower numbered truss is not considered, resulting in the blank cells on the top right of the table. The number in each row represents where the load sharing is considered to stop. Red numbers indicate where the load per connection exceeds -3.3 kN.

| | | Starting Truss Number | | | | | |
|---|---|---|---|---|---|---|---|
| Ending Truss Number | | 2 | 3 | 4 | 5 | 6 | 7 |
| | 2 | -10.5 | | | | | |
| | 3 | -8.7 | -6.9 | | | | |
| | 4 | -7.0 | -5.4 | -4.8 | | | |
| | 5 | -6.2 | -5.2 | -4.8 | -4.9 | | |
| | 6 | -5.6 | -4.7 | -4.3 | -4.0 | -3.3 | |
| | 7 | -5.2 | -4.4 | -4.0 | -3.8 | -3.4 | -3.5 |
| | 8 | -4.8 | -4.1 | -3.8 | -3.6 | -3.3 | -3.3 |
| | 9 | -4.6 | -4.0 | -3.7 | -3.6 | -3.4 | -3.4 |
| | 10 | -4.3 | -3.8 | -3.6 | -3.4 | -3.2 | -3.2 |
| | 11 | -4.1 | -3.6 | -3.4 | -3.3 | -3.0 | -3.0 |
| | 12 | -4.0 | -3.5 | -3.3 | -3.1 | -2.9 | -2.9 |
| | 13 | -3.8 | -3.3 | -3.1 | -3.0 | -2.8 | |
| | 14 | -3.7 | -3.2 | -3.0 | -2.9 | | |
| | 15 | -3.5 | -3.1 | -2.9 | | | |
| | 16 | -3.4 | -3.0 | | | | |
| | 17 | -3.3 | | | | | |

## 7.3 Stiffness Model

In the case of toe-nail connections, each connection is withdrawn incrementally, resulting in changes to the structural system prior to the next peak or damaging load or possibly even during the peak that causes damage. To attempt to quantify the load sharing between RTWC, Figure 7.3 illustrates a simple example for two identical connections connected by an element with stiffness, *k*. The solid line represents the starting point of two connections *A* and *B*, after a certain amount of loading each connection has been withdrawn a certain amount as shown by the dashed line in Figure 7.3 and represented by

$\Delta z_A$ and $\Delta z_B$. The connections *A* and *B* are then subjected to loads of $F_A$ and $F_B$ respectively, the load sharing between the two connections is represented by the force $F_k$. The amount of load sharing between connections *A* and *B* will be shown to depend on the difference in displacements between connections *A* and *B* and the stiffness (*k*) between them. The implication of this is that as the connections are damaged during the wind storm the load sharing arrangement changes based on the damage occurring to the connections. As highly loaded connections become more damaged, additional load gets transferred outwards to the adjacent connections. As a result, initial damage to the connections are caused by local loads similar to those calculated in APPENDIX D using a simple tributary area approach, and supported by the initial failure loads, while ultimate failures are likely to occur at multiple connections simultaneously and possibly up to the entire roof, depending on the stiffness.

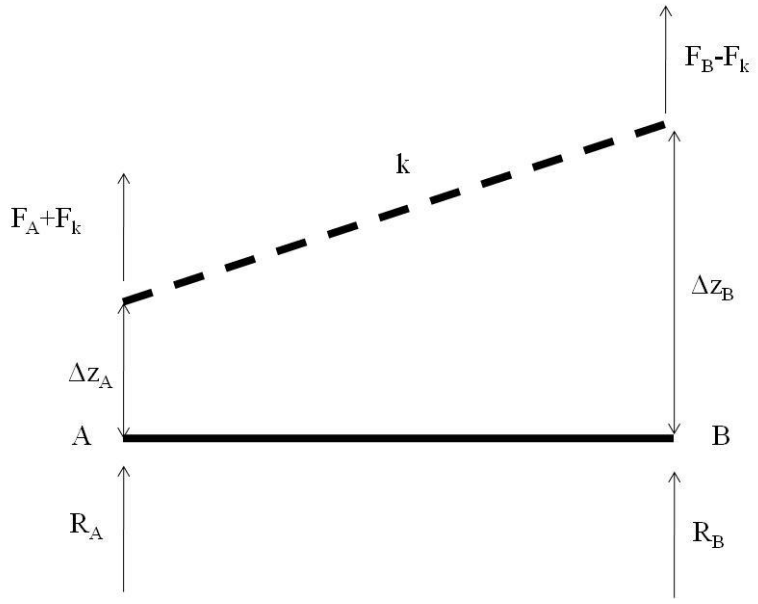


Figure 7.3 Simple model representing the displacement of the two RTWC, subjected to different applied loads, connected by an element with stiffness *k*

The most favourable scenario would be that there is perfect load sharing between all connections on the roof of the house, and failure is the result of global roof uplift. Using the example in Figure 7.3, it is possible to calculate the critical stiffness, $k_{crit}$, required so that there is perfect load sharing across both connections *A* and *B* as:

$$k_{crit} = \frac{F_A - F_B}{2(\Delta z_A - \Delta z_B)} = \frac{2\Delta F}{2\Delta z} \tag{7.1}$$

and is dependent on the differences of applied force and displacement of both connections. Figure 7.4 provides a family of $k_{crit}$ curves generated for different values of $\Delta F$ and $\Delta z$. The values of $\Delta F$ and $\Delta z$ were chosen to encompass the largest and smallest differences in force and displacement between two RTWC observed for the test house examined in Chapters 6.0 and 7.0. The stiffness of the plywood sheathing used on the current test house is also included on the plot, to provide a baseline for the current test house, while the stiffness for 20.5 mm plywood is also included for comparison. Clearly, increasing the stiffness between 2 connections significantly decreases the allowable displacement between them. During the realistic fluctuating loading on individual toe-nail connections experiments discussed in Chapters 4.0 and 5.0 the minimum displacement at failure was 5mm with an average displacement at failures of 10 mm. This suggests that, for this simple case of two connections, failure of the connection(s) can occur without perfect load sharing using the plywood that is currently used on the test house. However, if the 20.5 mm plywood were used instead, then failure of these two connections would likely occur at the same time since perfect load sharing is more probable. Also implied in Figure 7.4 is that initially, prior to any damage occurring to the connection, there is not perfect load sharing between adjacent connections since this

would imply infinite stiffness.

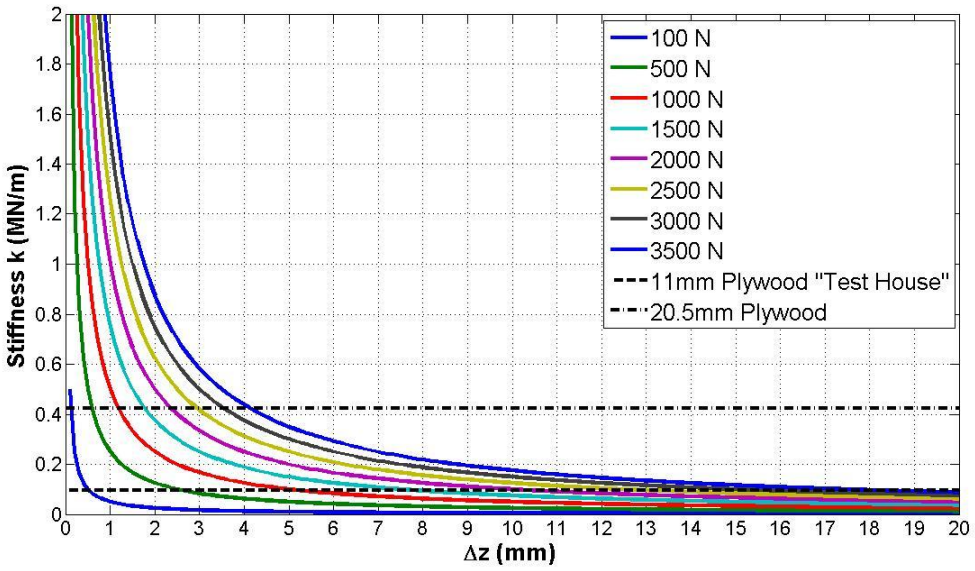


Figure 7.4 Calculated values of $k_{crit}$ based on different $\Delta F$ and $\Delta z$ values

From the results discussed above, there is clearly significant load sharing between adjacent connections on the roof. This suggests that an appropriate retrofitting strategy for existing homes could be to increase the lateral stiffness of the house, thereby increasing the load sharing between adjacent connections and strengthening select connections. As previously discussed, the failure of the roof will likely initiate at multiple RTWC connections up to the entire roof which takes advantage of the poor spatial correlation of the wind loads, reducing the peak load on the highest load connections. In addition, since a number of toe-nail RTWC are acting together due to the lateral stiffness of the roof the factor of safety used for the group of toe-nail connections can be reduced from the value used for an individual design. Finally the results have shown that the load sharing between adjacent connections changes throughout the loading

time history due to the way in which toe-nails are incrementally pulled out of the top plate. As such, static tests that could be conducted to determine the influence function for each RTWC would only be valid until first damage occurs, at which point the influence function will likely change, reducing the reaction at the damaged connection.

## 7.4 Role of Internal Pressures

In Chapter 5.3 the strength from the individual toe-nail connections were examined in conjunction with the ASCE7-05 Standard and it was shown that, if no load sharing or internal pressure were assumed, then the design wind speed for toe-nail connections would be lower than most wind regions defined by the ASCE7-05 (2006). Using the method of St. Pierre et al. (2005), test #6 has a ASCE7-05 (2006) 3s gust wind speed at 10 m of 146 mph. This wind speed is higher than any wind region defined in the ASCE7-05 (2006); however this wind speed assumes no internal pressurization of the house. As shown by Kopp et al. (2008) and Morrison et al. (2010), internal pressures caused by dominant openings can substantially increase the load on the roof of the house and, thus, reduce the wind speed causing failure. Figure 7.5 shows a schematic of the North side of the test house, assuming the same wind angle as the test, the windows and patio door are labelled from A to E and represent different possible breaches in the building envelope that can cause internal pressure. The external pressures at each opening were calculated from the wind tunnel data discussed in Chapter 2.2 and used to determine the internal pressures that would act on the roof of the house. Opening "A" and "B1" were found to have the largest positive external pressures at the tested wind angle of 40°. However, the external pressures at opening "A" had a higher correlation

with the highest external pressures on the roof of the house. As a result the following analysis will use opening "A" to represent a breach in the building envelop since it will represent the highest net load being applied to the RTWC. Opening "A" represents more than 2% of the area of the North Wall, as such it is assumed to be a dominant opening, and for the purposes of this analysis no resonant behaviour is assumed to occur. The load due to the internal pressurization of the house acts uniformly on the ceiling of the 2nd story; therefore, the RTWC which will have the largest response will remain "S3". Figure 7.6 presents the load time series from test #6 (45 m/s) for the external pressure loads only (assuming no load sharing), the internal pressure load only and the resultant load for RTWC "S3". As expected for this opening at this particular wind direction the loading at the RTWC is worse than if no internal pressure was applied. Using the difference in calculated loads between the external and net loads the scaling wind speed of 45 m/s can be re-interpreted using:

$$\frac{F_{ext}}{45^2} = \frac{F_{net}}{V_{net}^2} = \frac{F_{ext} - F_{\text{int}}}{V_{net}^2} \tag{7.2}$$

where $F_{ext}$ is the external load, $F_{int}$ is the internal load, $F_{net}$ is the net load and $V_{net}$ is the re-interpreted wind speed for test #6. $V_{net}$ is a function of time when formulated in this way, as shown in Figure 7.7 and ranges between 21 to 58 m/s depending on the point in time that is examined. The wind speeds that are greater than 45 m/s are due to the internal pressure becoming negative reducing the load applied to the RTWC. However, there is no correlation with load level shown in Figure 7.7, which is important since a low $V_{net}$ may not necessarily correspond to high resultant force. Figure 7.8 plots the calculated $V_{net}$ versus load level for RTWC "S3" at the higher load levels $V_{net}$ is within

the range of 25 and 40 m/s, when converted to an ASCE7-05 (2006) wind speed corresponds to 81 and 130 mph. This result clearly illustrates the importance and effect internal pressures can have on the ultimate failure, which is well known. For the current test house it seems unlikely that the toe-nail RTWC of this house would fail under design conditions unless there was a breach in the building envelope.

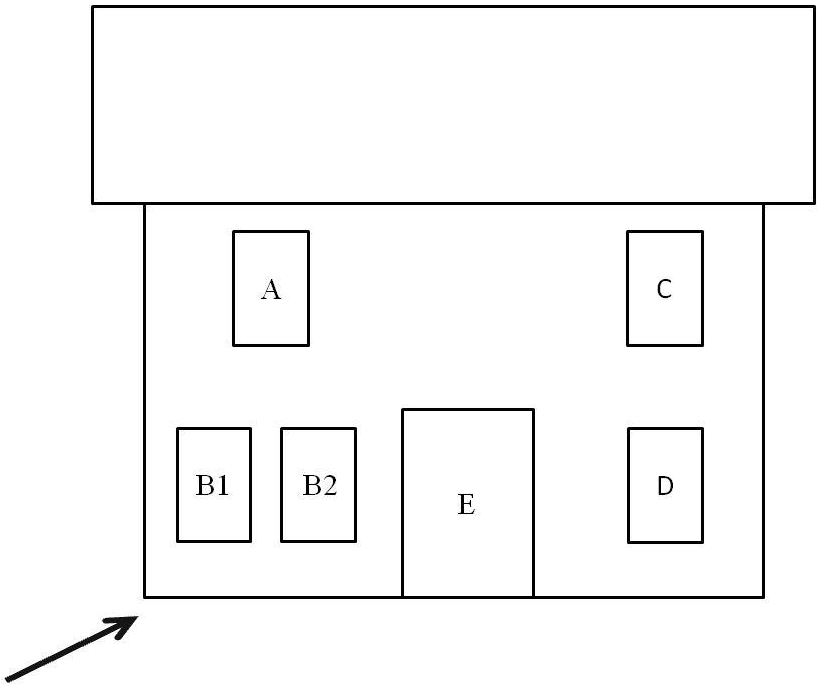


Figure 7.5 Schematic of the windows and doors located on the North side of the test house

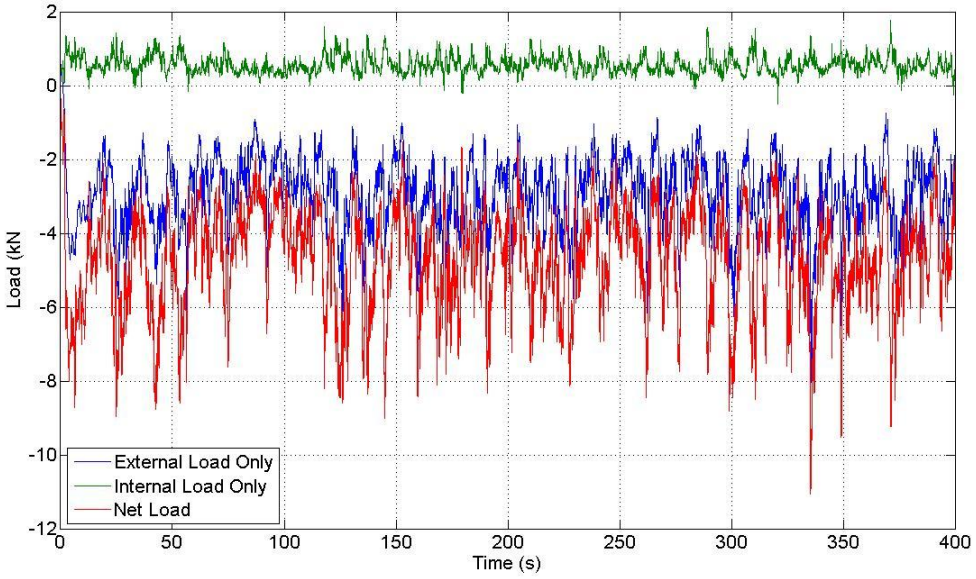


Figure 7.6 Time series of the external, internal and net pressure loads on RTWC "S3" for test #6 assuming a breach of the building envelope at opening "A" in Figure 7.5

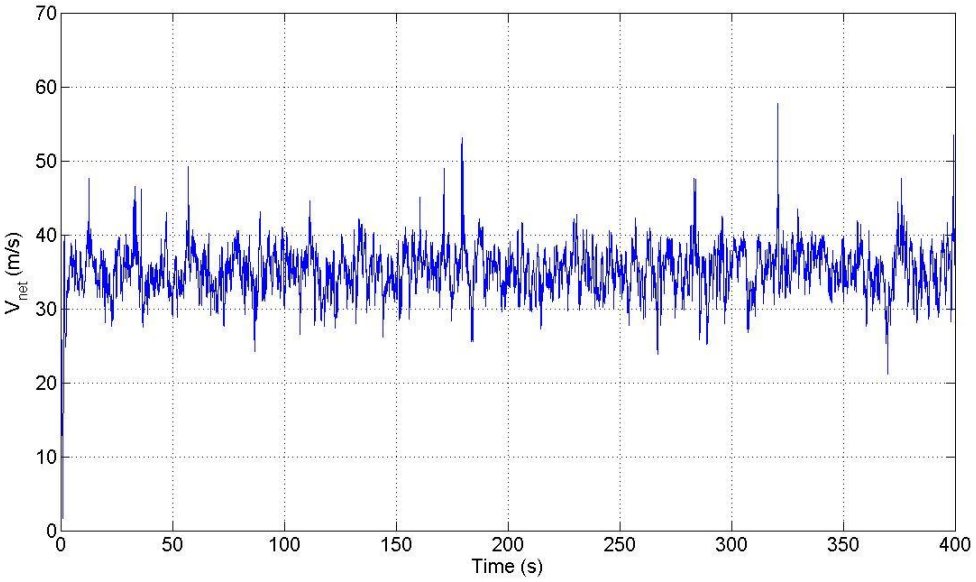


Figure 7.7 Time Series of $V_{net}$ for RTWC "S3" calculated using equation 7.1

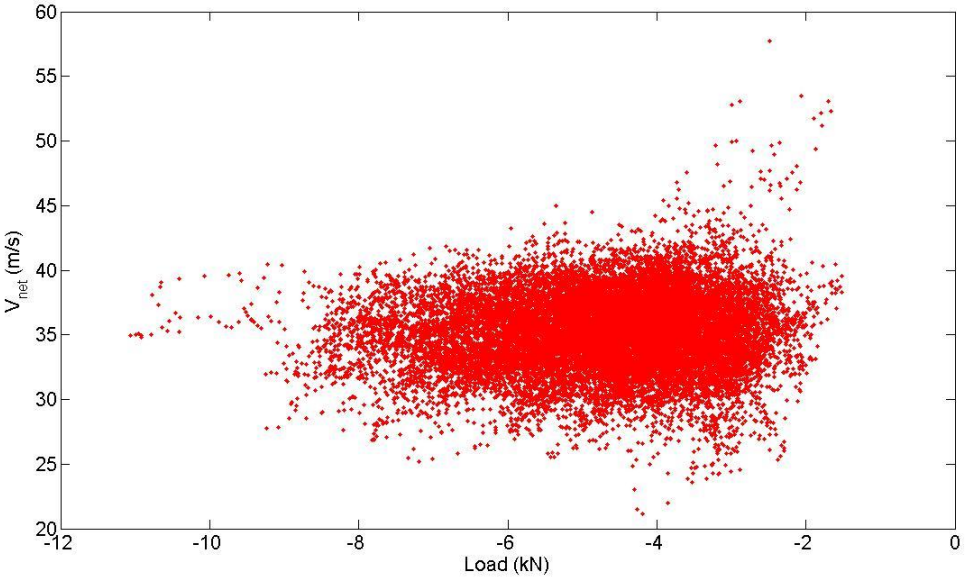


Figure 7.8 $V_{net}$ versus load level for RTWC "S3"

# 8.0 OBSERVATIONS OF A FLEXIBLE ROOF FAILURE IN THE FIELD

The overall motivation for this thesis is to achieve a better understanding of the failures of residential house roofs under extreme wind storms such as hurricanes. Following extreme wind events, damage surveys provide evidence of what has failed; however, determining how and in what order different components failed can be extremely difficult. This chapter examines one specific example where the failure of the roof-to-wall connections was observed by the author.

## 8.1 Tupperville Ontario Gust Front, June 8, 2008

The following case study involves the analysis of a failure of a wood frame structure during a gust front that traveled through Southern Ontario on June 8, 2008. Further analysis and discussion can be found in Kopp et al. (2010).

### 8.1.1 Damage Survey

Following the storm, a damage investigation was undertaken by the author and G.A. Kopp, in partnership with Environment Canada (EC). The majority of the observed damage was due to trees being uprooted and broken branches, with these sometimes causing secondary damage to adjacent structures. The single exception was a commercial storage building which had its roof completely removed during the storm. The state of the structure immediately following the event is shown in Figure 8.1. The North and East walls had collapsed outwards, while the South and West walls remained partially standing. The plan dimensions of the building were 24.38 m by 15.24 m, with an eaves height of 4.88 m and a roof slope of 4 on 12 ($\varphi = 18°$). Two large 4.57 m roller doors were located on the North side of the building and can be seen in the foreground in Figure

8.1. These doors were found closed and in their tracks. The roof was found to the North East of the structure and appeared to have landed upside down, the furthest piece of debris was found 84 m from the East side of the building. Figure 8.2 shows the debris field looking back towards the structure (facing West).

Figure 8.1 Picture of the Building facing South just after failure

Figure 8.2 Picture of the debris field looking west towards the building

The upstream fetch for the estimated wind direction at the time of the investigation is a typical open country terrain and is shown in the photograph in Figure 8.3. A layout of the building debris field along the cardinal directions at the building site are shown in Figure

8.4, the south gable end wall was found closest to the building (location A), while the North gable was found further away (location B) which is consistent with the observation that the roof landed upside down. The narrow debris swath from the building indicates that the damage is due to straight line and not tornadic winds. This is supported by meteorological data which confirms that there was no sign of tornadic activity in the region during this storm.

Examination of the roof debris revealed that the roof truss spacing was 1.22 m on center, with batons at 0.61m centers. Trusses were held down with 2-3 toe-nail connections using 10d twisted shank nails. These truss hold downs are consistent with Chapter 9 of the National Building Code of Canada NBCC (2005), which prescribes that the roof trusses should be held down with three 82mm nails. However, the maximum allowable spacing is 0.61m, with wider spacing allowed for low occupancy buildings, such as farm buildings. So, the building did not appear to be sub-standard, but was built to a lower standard than would be required for houses and other occupied structures.

Thus, from the observations of the debris field, the roof, and the walls, it appears that the failure was of the complete roof (in more-or-less one piece) by overturning about the east wall. From the observations of the walls, in appears highly unlikely that internal pressures played any part in the global roof failure. Following this damage investigation and based on the structural failure discussed above Environment Canada rated this storm to have been a gust front with F1 damage (Note that Environment Canada uses the Fujita Scale to rate all thunderstorm damage.)

Figure 8.3 of the upstream fetch from the West edge of the building.

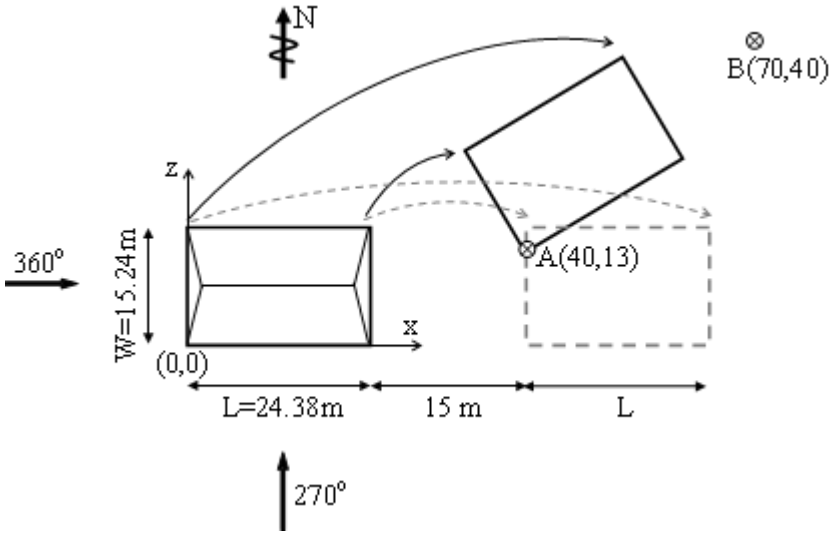


Figure 8.4 Schematic sketch of the plan view of the global roof failure

### 8.1.2 Integrated Pressure Analysis

The current analysis concentrates on the failure of the roof and estimates the wind speed required to produce the observed damage. In addition, effort was placed on putting bounds on the gust wind speed at the time of failure. In order to estimate the wind speed from a wind tunnel pressure test, several assumptions and simplifications are required.

The influence area for each structural (i.e., toe-nail) connection is assumed to be equal to its geometric tributary area. The ultimate capacity of toe-nail connections can vary substantially, depending on the type of wood and moisture content, the angle and location of the nail, in addition to other factors such as age and deterioration. The assumed value for the weight of the roof is given in Table 8.1. Since the nails used in the toe-nail connections are different than those tested in Chapter 4.0 estimates for the ultimate toe-nail capacities are assumed to be equal to be 1850 N/connection, from Visscher and Kopp (2007). A variation of 20% has been assumed for the toe-nail strengths.

Table 8.1 Assumed values for the weight of the roof

| Component | Weight | Variation (%) |
|---|---|---|
| Corrugated Metal Roofing | 51 ($N/m^2$) | 15 |
| Truss (including roof Battens) | 660 (N/truss) | 15 |

The fact that the roof landed upside down indicates that the roof likely failed by overturning of the entire roof about the leeward (East) wall, as discussed above. Perhaps the most significant assumption of this analysis is that pressure coefficients obtained for traditional boundary layer winds are similar to those generated under thunderstorm winds. There is some indication in the literature that this may not be the case (Chay and Letchford 2002), although such a conclusion also involves significant assumptions. Analysis of several non-stationary wind events on the full-scale Texas Tech Building by Lombardo (2009) have shown that pressure coefficients from several non-stationary thunderstorm wind events are within the range of pressure coefficients obtained from stationary wind events (typical boundary layer winds) on the same building. This suggests the current use of wind tunnel boundary layer pressure coefficients may be

appropriate. The current work cannot address this question further, and, in any case, detailed data are not really possible to obtain for buildings of this size with currently available downburst wind tunnels, nor is full scale data available.

In order to estimate the failure wind speeds, pressure data were selected from the NIST aerodynamic database for a building which closely matched the dimensions of the damaged building. The model building selected has full scale plan dimensions of 24.38 m x 38.1 m an eaves height of 4.88 m at the tested length scale of 1:100 and a roof slope of 3 on 12 ($\varphi$ = 14°). The aspect ratio of the model building to the damaged building is nearly identical. In order to match the full scale dimensions, the length scale of the wind tunnel model was reinterpreted using a value of 1:64. However, it is worth noting that the gable slope did not match perfectly. Additional details on the NIST aerodynamic database can be found in Ho et al. (2005), while discussion of scale mismatches can be found in Surry (1982) and St. Pierre et al. (2005). Since the wind direction at failure is not known precisely, the analysis was conducted for wind angles ranging from 315° to 360° which are believed to be the bounding wind angles from the field investigation. (Note that these wind angles are defined in Figure 8.4, and that $360^o$ is due east.)

The individual reaction forces at the connections ($R^i(t)$), the overall roof uplift force ($Fv$), and the overturning moment about the leeward (east) wall ($M_x$) can be calculated from:

$$R(t)^i = qCr^i(t) \tag{8.1}$$

$$Fv(t) = qCf(t) \tag{8.2}$$

$$M_x(t) = qCm_x(t) \tag{8.3}$$

where $q$ is the dynamic pressure and $Cr^i(t)$, $Cf(t)$, $Cm_x(t)$ are force and moment coefficients for the individual connection(s), overall roof uplift and overturning moment, respectively. These coefficient time series are calculated from the wind tunnel pressure coefficient ($Cp$) time series and have an overall length of approximately 1 hour at full scale (assuming normal boundary layer scaling). If the connections are assumed to be brittle and fail instantaneously once the force has exceeded the hold down (HD) resistance, $R^i_{HD}, Fv_{HD}, M_{xHD}$, the hourly mean failure velocities at roof height can be obtained from;

$$V^{R^i}_{H,O.C.,3600s} = \sqrt{\frac{2}{\rho}\frac{R^i_{HD}}{\breve{C}r^i}} \tag{8.4}$$

$$V^{Fv}_{H,O.C.,3600s} = \sqrt{\frac{2}{\rho}\frac{Fv_{HD}}{\breve{C}f}} \tag{8.5}$$

$$V^{M_x}_{H,O.C.,3600s} = \sqrt{\frac{2}{\rho}\frac{M_{xHD}}{\breve{C}m_x}} \tag{8.6}$$

Since, in general, thunderstorms winds are short lived, the stationary hourly mean commonly used for synoptic winds has little meaning. Holmes et al. (2002) found that for the Lubbock-Reese rear flank downdraft in 2002, a running mean of 40 seconds provided a good representation of the underlying wind event. With this in mind, rather than taking the absolute peak coefficient from the wind tunnel time series of $Cr(t)^n$, $Cf(t)$, and $Cm(t)_x$ the entire record was divided into 40s sections, the peak from each section

was then extracted and a Type I extreme value analysis was fit to these peaks. Typically when considering boundary layer winds the median value (50th percentile) value is selected as representative peak pressure coefficient to be used in Eq. (2a-c). However, for transient short duration events such as a gust front or down burst, it is not clear that the median peak is appropriate. As such the current analysis will use the median peak along with the 10th and 90th percentile values from the peak distribution in Eq. 8.4 to Eq. 8.6. By assuming quasi-steady theory, the gust wind speed $V_{H,O.C.,gust}^{M_x}$ can be determined from,

$$V_{H,O.C.,gust}^{M_x} = \sqrt{\frac{\breve{C}m_x}{\bar{C}m_x}} V_{H,O.C.,3600s}^{M_x} \tag{8.7}$$

where $\bar{C}m_x$ is the mean moment coefficient. Similarly $V_{H,O.C.,gust}^{Fv}$ and $V_{H,O.C.,gust}^{R^n}$ can be determined through the same procedure. The gust wind speed using the median peak coefficient will be reported, with the wind speeds calculated from the 10th and 90th percentile peak coefficients presented in brackets.

In addition, to facilitate comparison to ASCE7-05 (2006), the hourly roof height wind speeds are also converted into ASCE7-05 (2006) 3s gust wind speeds following the procedure outlined in St. Pierre et al. (2005) where;

$$V_{10m,O.C.,3s}^{ALL} = V_{H,O.C.,3600s}^{ALL} * \left( \frac{V_{10m,O.C.,3s}}{V_{10m,O.C.,3600s}} \right) \left( \frac{V_{10m,O.C.,3600s}}{V_{H,O.C.,3600s}} \right) \tag{8.8}$$

The first ratio can be obtained from Table C6-4 in ASCE7-05 (2006), while the second ratio can be obtained from the experimental wind tunnel profiles. This type of wind speed conversion assumes that the wind speed profile is similar to that of a typical

boundary layer wind. From the profile data presented by Holmes et al. (2002) it appears likely that such an approach may overestimate the wind speed at 10m. Following this analysis, the gust wind speed ($V_{H,O.C.,gust}^{M_x}$) required to fail the roof in overturning about the leeward wall is 39 m/s (34.5 m/s, 43 m/s), while the overall uplift failure wind speed ( $V_{H,O.C.,gust}^{Fv}$) is 50.6 m/s (44.5 m/s, 56.2 m/s) for a wind angle of 360°. From these results it is apparent that the governing failure mode would be the overturning of the roof about the leeward wall and not a pure uplift failure and assumes that there was "perfect" load sharing between the structural connections (i.e., toe-nails). In contrast, if it is assumed that there is no load sharing between structural elements, the first individual toe-nail connection would fail at a wind speed of 22.2 m/s (19.6, 24.4) for the same wind direction. In reality the true structural stiffness will lie somewhere between these two cases, but ultimately the current results indicate that individual connections would fail before the roof would fail in overturning about the eastern wall. However, if only the weight of the roof is considered (no toe-nail connections) the gust wind speeds $V_{H,O.C.,gust}^{M_x}$ and $V_{H,O.C.,gust}^{Fv}$ become 21.7 m/s (19.2, 23.9) and 28.1 m/s (24.7, 32.3) respectively. The wind speeds above, along with the variation based on wind angle, are presented in Table 8.2. The results presented above suggest that there may have been a sequential failure of the connections prior to the flight of the roof. However, due to the spatial variations of the wind loading on the roof of the building and that the wind speed required to remove the roof with no hold downs is nearly equal to that of the highest loaded connection, it is not likely that a sequential failure initiating at a wind speed of 22.2 m/s (19.6, 24.4) would cause the complete removal of the roof. Moreover, the debris field indicates that

the entire roof was removed from the structure as a single piece. However, it is possible that several connections failed sequentially prior to the failure of the complete roof reducing hold down capacity, ultimately reducing $V_{H,O.C.,gust}^{M_x}$.

To evaluate this hypothesis further, a sequential failure analysis was carried out where the connection with the lowest failure wind speed was assumed to have failed, the failure wind speeds for all remaining connections were recalculated with the failed connection 'missing'. This process was repeated until either $V_{H,O.C.,gust}^{M_x}$ or $V_{H,O.C.,gust}^{Fv}$ was less than the wind speed required to fail the next connection, or all the connections had failed. Fig. 6 shows the sequential analysis for a wind angle of 360°. The horizontal axis represents the sequence of failed connections i.e., 0 meaning no connections have failed, 1 meaning a single connection has failed, and so on. Once a connection has failed its load is redistributed to adjacent connections but because of the high spatial variation of the wind these connections may actually require a higher wind speed to fail. For example, in Fig. 6, once the wind speed has passed 22.2 m/s (19.6, 24.4) the connections corresponding to steps 0-8 would have failed; however, to continue the failure (step 9) a higher wind speed would be required. In contrast, the overturning moment remains constant while the hold down force has diminished, reducing the wind speed required to overturn the entire roof at each failure step. Ultimately, the wind speed required to overturn the entire roof becomes less than the wind speed required to fail the next connection, and the estimate for the failure wind speed for this wind angle is found, 25.3 m/s (22.2, 28.0) for the a wind angle of 360°. For synoptic winds it would be possible for this type of failure to

occur over several different wind gusts, in this particular case, where a gust front is moving past the building all the failures would likely occur in the same ‘gust’ as the front passes.

The wind speeds presented in Table 8.2 showed a large variation based on wind angle, however, for the sequential failure analysis the wind speeds varied from 21.0 m/s (18.1, 22.5) at an angle of 320° to 25.3 m/s (22.2, 28.0) at an angle of 360°. This is equivalent to a 3 second gust speed at 10m (i.e., equivalent to the wind speed provided in ASCE7-05 2006) of 24.3 to 29.3 m/s, using Eq. (8.8). Increasing and decreasing the building weight and toe-nail strength, as described above, causes these estimates to vary by approximately ±2 m/s.

It should be noted that the design 3s gust failure wind speeds at 10 m above are less than those specified in NBCC (2005) of 36.5 m/s for a return period of 10 years or 42.3 m/s for a 50 year return period (converted from mean hourly to 3s gust at 10m in an open country terrain), or in ASCE7-05 (2006) of 40 m/s (for Michigan).

The ultimate failure velocities found using this method provide an estimate of the lower bound of the peak velocity for this storm. The actual peak velocity for this storm could have been much higher, but in order to place an upper bound on the wind speed, other indicators would have to be used such as analysis of nearby structures that have not failed or debris flight analysis, which will be discussed in more detail below. We do note, however, that there were no other failures in the town of Tupperville, except for tree branches.

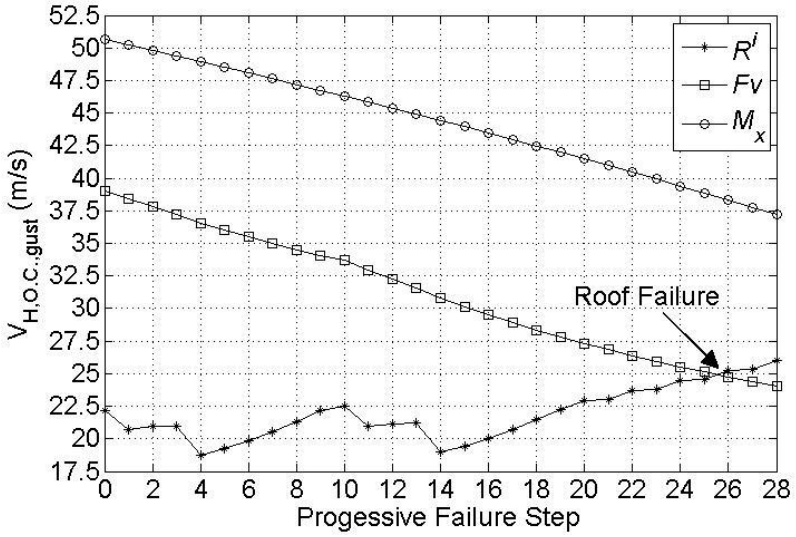


Figure 8.5 Failure wind speeds for the progressive structural failure

Table 8.2 Maximum and Minimum wind speeds calculated for the range of angles considered

| | Peak 50% | Peak 10% | Peak 90% | Wind Angle |
|---|---|---|---|---|
| | Maximum Wind Speed (m/s) | | | |
| $V_{H,O.C.,gust}^{M_x}$ | 39.0 | 34.5 | 43.0 | 360° |
| $V_{H,O.C.,gust}^{M_x}$ (weight only) | 21.7 | 19.2 | 23.9 | 360° |
| $V_{H,O.C.,gust}^{Fv}$ | 50.6 | 44.5 | 56.2 | 360° |
| $V_{H,O.C.,gust}^{Fv}$(weight only) | 28.1 | 24.7 | 31.3 | 360° |
| | Minimum Wind Speed (m/s) | | | |
| $V_{H,O.C.,gust}^{M_x}$ | 33.6 | 30.3 | 36.3 | 315° |
| $V_{H,O.C.,gust}^{M_x}$(weight only) | 18.7 | 16.9 | 20.2 | 315° |
| $V_{H,O.C.,gust}^{Fv}$ | 36.4 | 32.9 | 39.3 | 315° |
| $V_{H,O.C.,gust}^{Fv}$(weight only) | 20.2 | 18.3 | 21.8 | 315° |

### 8.1.3 Final Remarks

Analysis of Radar data discussed by Kopp et al. (2010) for the gust front that caused the failure of the Co-op building estimated the upper level wind speeds at a height of 550 m to be 33 m/s, while analysis of the flight of the roof also discussed in Kopp et al. (2010) estimate the wind speed to be in the range of 19 to 24 m/s. The estimate of the debris flight suggests that the failure wind speed is closer to that of the progressive connection failure analysis. In any case both the debris analysis and radar data indicate that the wind speeds have shown that the calculated global overturning moment wind speed $V_{H,O.C.,gust}^{M_x}$ is too high unless there were no RTWC at all and the only hold down was the weight of the roof. The analysis above illustrates that for flexible systems it is possible to have progressive failures of the structure, whereby individual connections fail causing increased loading on the remaining connections. This type of progressive failure has a substantially lower wind speed of failure than the global roof failure.

# 9.0 CONCLUSIONS AND RECOMMENDATION

During severe wind storms, the roofs of low-rise buildings are subjected to large uplift. Damage investigations following these severe wind events have identified roof-to-wall connections (RTWC) as a common failure mode. While damage surveys identify what has failed they are unable to explain what the loading was that caused the failure and in many cases the failure process. In contrast, the loads on buildings can be obtained from surface pressure data obtained from wind tunnel experiments, however they are unable to determine which component and at what load will initiate failure. The current study was undertaken to link the aerodynamic loading to the initiation of failures that are observed during damage investigations for wood frame residential houses. Specifically, the failures of toe-nailed RTWC were investigated in detail, both individually and as part of a complete structural system. This Chapter outlines the key findings from the current work along with the implications and areas where further research is required.

## 9.1 Key Findings from the current work

Through the current investigation, the following conclusions can be made:

- Toe-nail connections, individually or as part of a structural system, fail incrementally when subjected to a realistic fluctuating wind loads. This means that many peaks are required to cause ultimate failure (except perhaps for rapidly increasing loads as may happen in tornadoes).
- The maximum capacity of individual toe-nail connections is nearly identical under ramp loading or a realistic fluctuating loading. The capacity found in the current investigation is within a similar range to that found for previous investigations of toe-nail connections. This study has demonstrated the failure

load is independent of ramp rate, and that fatigue is not playing a significant role for the realistic loading used in this study.

- The loads applied to the roof of the house on a per connection basis are significantly larger than the mean maximum capacity determined from the individual connection experiments. This indicates that there is significant load sharing through the roof of the house and that failure will not initiate at a single connection but over many connections, up to the entire roof, depending on the structural stiffness.
- Significant hysteresis was observed during the movement of the toe-nails during the full roof tests, while it was not observed in the single toe-nail tests. In addition, the toe-nails responded coincidently with the increased load during peaks, while during the decreasing peaks, it dropped more slowly.
- The transfer function between the displacements of the RTWC and the applied load has shown that there is not a clear amplification or attenuation of the response of the house at any specific frequency. Overall, a general attenuation of the response at higher frequencies is observed, however, since the reactions at the connections were not measured, a definitive conclusion of the frequency response of the house cannot be made.
- Despite the large displacements experienced by the RTWC there is very little damage observed to the interior of the house. Only hairline cracks appeared following testing; however, the size of these cracks would be expected in wood frame houses even those who have not experienced significant wind loads. Thus, damage to the connections is relatively hidden until the entire

roof comes off. It is not clear whether racking (shear) loads, not included in the current study, would alter this.

- For cornering wind angles, the failure of the roof will initiate at RTWC on the leeward side of the house. This leads to the roof overturning into the wind. In this configuration as the roof lifts the aerodynamic coefficients would not change with angle of attack in such a way as to lift the roof further. As such, it is unlikely that the roof would "fly" off the house at the current wind angle.

## 9.2 Implications and Recommendations from the Current Work

The findings from the current work have implications for future research into the performance of wood frame houses under wind loads.

- Toe-nail connections have been shown to fail in increments. Since the load sharing through the structural system will change as connections accumulate damage. Consequently static influence function obtained on an undamaged structure, likely does not reflect how the loads are being transferred to the connections at failure.
- Roofs with higher lateral (along the ridge) stiffness have a greater amount of load sharing between the connection, requiring a higher wind speed to cause failure, and that failure will initiate at multiple connections. This suggests a cost effective retrofitting strategy of increasing the stiffness of the roof and strengthening critical connections. Further work would be needed to establish this.
- As stated above with increasing lateral stiffness the larger the number of connections that will fail together. This suggests that the factor of safety used for

the design of the entire roof can be reduced from that used for an individual toe-nail connection, with increasing stiffness of the roof.

- Static testing for individual toe-nail connections appears to be suitable to determine the capacity of toe-nail connections to withdrawal loads. However, because the failure mechanism is different between fluctuating wind loads and static loads, realistic wind loading must be used when considering the entire structure. Since toe-nail connections fail incrementally, the structural system changes continuously as connections are damaged intermittently meaning that the failure of the structure under fluctuating loads will be likely different than those predicted under static loading.
- The current test house was found to be able to withstand design wind loads for almost all wind regions in the United States, provided that no internal pressures are considered. Internal pressures were found to drastically reduce the failure wind speeds applied to the house. This suggests that global roof failures observed in the field (except for tornadoes) for a similarly built house likely initiate as the result of internal pressurization of the structure due to a breach in the building envelope.
- For the current roof construction, design pressure coefficients should be for tributary areas substantially larger than that of a single truss, with values ranging from approximately half the roof (6 trusses) to the full roof.

## 9.3 Recommendations for Future Research

While this study has identified some key aspects of the behaviour of toe-nail connections, tested both individually and as part of a complete structural system, further aspects

should be addressed through further research.

- The individual toe-nail experiment conducted in the current study determined the capacity for a single type of toe-nail connection. More importantly the study has indentified how toe-nail connections respond under fluctuating loads. However, further experiments that should be conducted on individual toe-nail connections are detailed below:
    - The current results have shown that under fluctuating wind loads the load that caused failure is less than the maximum applied load indicating that the capacity of the toe-nail connection has been reduced. For the applied fluctuating loading trace, this reduction has been found to be relatively small; however this trace was designed to on average increase the load over time. Understanding if fluctuating wind loading with a longer duration but a lower load level can cause failure may be critical to assess fatigue characteristics of toe-nail connections, which may be important for longer duration storms.
    - Additional experiments on a variety of different connections such as different nails, wood species, to encompass the variety of connections that exist in construction.
    - Toe-nail connection constructed using hand driven nails should be tested to document any difference in capacity as compared to the pneumatically driven nails in the current investigation.

- The current experiments have shown that the stiffness of the structural system plays an important role in the failure of the entire roof. However, there is still a significant amount of research required to fully understand these types of failures.
    - The current results have shown that the failure of the roof will initiate by over turning about the leeward wall. Once the roof has lifted sufficiently, the aerodynamics will change forcing the roof back down. Scaled aeroelastic models in the wind tunnel may help to evaluate these effects in greater detail.
    - The current investigation has shown that the influence functions for the RTWC on the roof change as the connections become increasingly damaged. However, the current investigation did not measure the reactions at each connection. As such, the results from the current experiment cannot quantify how the influence functions are changing with time (i.e., as the toe-nail connections become increasingly damaged). Therefore, future experiments should install load cells below the top-plate of the house which can be used to determine the reactions at each RTWC without changing the failure characteristics of the toe-nail connections.
    - The current study examined the response of a gable roof, which is a common style of roof. However, there are numerous other types of roof geometries used in practice. Hip roofs are also widely used through residential construction and not only have a significantly different structural system that gable roofs but also have very different aerodynamic

loads. As such, testing of a different style of roof would be useful to contrast the current results obtained from the current testing.

- Finally, the ultimate goal of these experiments should be to obtain sufficient understanding of the interaction of the wind loads and the structural system so that models can be developed to predict the response of roofs without having to test every different roof configuration. To this end, Finite Element Models, are needed to model both the failure behaviour observed for toe-nail connections, and the behaviour of the overall structural systems. The data generated from this study can be used as benchmark data to validate such models.

# REFERENCES

ASCE, 2006 ASCE7-05: Minimum Design Loads for Buildings and Other Structures. *American Society of Civil Engineers*, Reston, VA.

ASTM. (2001). "Standard test method for structural performance of sheet metal roof and siding systems by uniform static air pressure difference." *Designation E 1592-01*, Philadelphia, USA.

Baskaran, A., Chen, Y. (1998). "Wind load cycle development for evaluating mechanically attached single-ply roofs." *Journal Wind Engineering Industrial Aerodynamics*, 77-78, 83-96.

Boughton, G.N., 1988. "An investigation of the response of full scale timber framed houses to simulated cyclonic wind loads" PhD Thesis, James Cook University of North Queensland, Townsville, Queensland, Australia.

Department of Housing and Urban Development (HUD). (1993). "Assessment of Damage to Single-Family Homes Caused by Hurricanes Andrew and Iniki." *U.S., Office of Policy and Development and Research*, HUD-0006262.

Board on Natural Disasters, et al., (1999). "Mitigation Emerges as Major Strategy for Reducing Losses Caused by Natural Disasters." *Science* 284, 1943-1947. (DOI:10.1126/science.284.5422.1943)

Chay M.T., Letchford C.W., (2002). "Pressure distributions on a cube in a simulated thunderstorm downburst—Part A: stationary downburst observations." *Journal of Wind Engineering and Industrial Aerodynamics*, 90(7), 711-732.

Cheng, J., (2004). "Testing and analysis of the toe-nailed connection in the residential roof-to-wall system." *Forrest Products Journal*, 54, 58-65.

Cochran, L.S., Cermak, J.E., (1992). "Full- and model-scale cladding pressures on the Texas Tech University experimental building". *Journal of Wind Engineering and Industrial Aerodynamics*, 41-44, 1589-1600.

Cook, N.J., Keevil, A.P., Stobart, R.K., (1988). "Brerwulf – the big bad wolf." *Journal of Wind Engineering and Industrial Aerodynamics*, 29, 99-107.

Emanuel, K., (2005). "Increasing destructiveness of tropical cyclones over the past 30 years." Nature, 436, 686-686. (DOI:10.1038/nature03906)

Engineering Science Data Unit (ESDU), Strong winds in the atmosphere boundary layer. Part 1:Mean-hourly wind speeds. Data Item 82026, 1982.

Guikema, S.D., (2009). "Infrastructure Design Issues in Disaster-Prone Regions." *Science*, 323, 1302-1303. (DOI:10.11206/science.1169057)

Gurley, K., Davis, R.H., Ferrera, S.P., Burton, J., Masters, F., Reinhold, T., Abdullah, M., (2006). "Post 2004 hurricane field survey – an evaluation of the relative performance of the Standard Building Code and the Florida Building Code." *Proc. 2006 ASCE/SEI Structures Congress*, St. Louis.

Hann F.L., Balaramudu, V.K., Sarkar, P.P., (2010). "Tornado-Induced Wind Loads on a Low-Rise Building", *Journal of Structural Engineering*, 136(1), 106-116.

He M., Lam F., Foschi R.O., (2001). "Modeling Three-Dimensional Timber Light-Frame Buildings." *Journal of Structural Engineering*, 127(8), 901-913.

Henderson, D.J., Ginger, J., Morrison, M.J. and Kopp, G.A. (2009). "Simulated cyclonic winds for low cycle fatigue loading of roofing." *Wind Struct.*, 12, 383-400.

Ho, T.C.E., Surry, D., Morrish, D., Kopp, G.A., (2005) "The UWO contribution to the NIST aerodynamic database for wind loads on low buildings: Part1. Archiving format and basic aerodynamic data." *Journal of Wind Engineering and Industrial Aerodynamics*, 93, 1-30.

Holmes, J.D., Hangan, H., Schroeder, J.L., Letchford, C.W., and Orwig, K.D., (2008). "A forensic study of the Lubock-Reese downdraft of 2002." *Journal of wind and structures*, 11(2), 137-152.

Keith, E.L., Rose, J.D., (1994). "Hurricane Andrew – structural performance of buildings in South Florida." *Journal of Performance of Constructed Facilities*, 8, 178-191.

Kordi, B., Traczuk, G., Kopp, G.A., (2010). "Effects of wind direction on the flight trajectories of roof sheathing panels under high winds". *Journal of Wind and Structures*, 13(2), 145-167.

Kopp, G.A., Mans, C., Surry, D., (2005). "Wind effects of parapets on low buildings: Part 1. Basic aerodynamics and local loads." *Journal of Wind Engineering and Industrial Aerodynamics*, 93, 817-841.

Kopp G.A., Morrison M.J., Kordi B., Miller C., "A Method to Assess Peak Storm Wind Speeds Using Detailed Damage Surveys", *Engineering Structures*, Submitted April 2010.

Kopp, G.A., Oh, J.H., Inculet, D.R., (2008). "Wind-induced internal pressures in houses." *Journal of Structural Engineering*, 134, 1129-1138.

Levitan M.L., Mehta K.C., (1992a). "Texas Tech field experiments for wind loads part I: meteorological instrumentation and terrain parameters", *Journal of Wind Engineering*

*and Industrial Aerodynamics*, 43, 1565-1576.

Levitan M.L., Mehta K.C., (1992b). "Texas Tech field experiments for wind loads part II: Building and pressure measuring system", *Journal of Wind Engineering and Industrial Aerodynamics*, 43, 1565-1576.

Lin J.X., Surry D., (1998). "The variation of peaks loads with tributary area near corners on flat low building roofs", *Journal of Wind Engineering and Industrial Aerodynamics*, 77&78, 185-196.

Liu, Z., Prevatt, D.O., Aponte-Bermudez, L.D., Gurley, K.R., Reinhold, T.A. and Akins, R.E., (2009). "Field measurement and wind tunnel simulation of hurricane wind loads on a single family dwelling." *Engineering Structures*, 31, 2265-2274.

Lombardo F.T., (2009). "Analysis and Interpretation of Thunderstorm Wind Flow and its Effects on a Bluff Body." *Phd Dissertation*, Texas Tech University, Lubbock TX.

Mahendran, M., (1995). "Simulation of cyclonic wind forces on roof claddings by random block load testing." *Technical Report* 38, Cyclone Testing Station, James Cook University, Australia.

Mani, S., (1997). "Influence functions for evaluating design loads on roof-truss to wall connections in low-rise buildings." M.S. Thesis, Clemson University, Clemson, South Carolina, United States.

Minor, J.E., (1994). "Windborne debris and the building envelope." *Journal of Wind Engineering and Industrial Aerodynamics* 53, 207-227.

Morrison M.J. Kopp G. A., (2010). "Analysis of Wind-Induced Clip Loads on Standing Seam Metal Roofs." *Journal of Structural Engineering*, 136(3), 334-337.

Morrison M.J., Kopp, G.A., Gavanski E., Miller, C., "Damage to residential construction from the tornadoes in Vaughan, Ontario on August 20, 2009", Canadian Journal of Civil Engineering, Submitted January 2010.

NRCC 2005. "National building code of Canada 2005 (NBCC (2005)); includes user's guide –NBCC 2005 structural commentaries (Part 4), NRCC, Ottawa, Canada.

Pielke, R.A. Jr., Gratz, J., Landsea, C.W., Collins, D., Saunders, M.A., Musulin, R., (2008). "Normalized Hurricane Damage in the United States: 1900-2005." *Natural Hazards Review*, 9, 29-42. (DOI:10.1061/(ASCE)1527-6988(2008)9:1(29))

Reardon, G., Henderson, D., Ginger, J., (1999). "A structural assessment of the effects of Cyclone Vance on houses in Exmouth WA", CTS, James Cook University Australlia, Technical Report No. 48.

Reardon, G., (1996). "Simulated Wind Load Testing of Full Size Houses", *Joint IStructE/City University International Seminar,* London UK, pp 101.1-101.8.

Reed, T.D., Rosowsky, D.V., Schiff, S.D., (1997). "Uplift capacity of light-frame rafter to top plate connections." *Journal of Architectural Engineering*, 3, 156-163.

Riley, M.A., Sadek, F., (2003). "Experimental Testing of Roof to Wall Connections in Wood Frame Houses." *National Institute of Standards and Technology*, Technical Report NISTIR 6938.

Rosowsky, D.V, Reinhold, T.A., (1999). "Rate-of-Load and Duration-of-Load Effects for Wood Fasteners", *Journal of Structural Engineering*, 125(7), 719-724.

Saathoff, P.J., Melbourne, W.H., (1997). "Effects of free-stream turbulence on surface pressure fluctuations in a separation bubble." *Journal of Fluid Mechanics*, 337, 1-24.

Shanmugam, B., Nielson, B.G., Prevatt, D.O., (2009). "Statistical and analytical models for roof components in existing light-framed wood structures." *Engineering Structures* 31, 2607-2616. (DOI:10.1016/j.engstruct.2009.06.009)

Sparks, P.R., Schiff, S.D., Reinhold, T.A., (1994). "Wind damage to envelopes of houses andconsequent insurance losses." *Journal of Wind Engineering and Industrial Aerodynamics* 53, 145-155.

Stathopoulos, T. (1979). "Turbulent Wind Action on Low-rise Buildings." PhD Thesis, The University of Western Ontario, London, Ontario, Canada.

Stathopoulos T., Surry D., (1983). "Scale effects in wind tunnel testing of low buildings." *Journal of Wind Engineering and Industrial Aerodynamics*, 13, 313-326.

St. Pierre, L.M., Kopp, G.A., Surry, D. and Ho, T.C.E., (2005). "The UWO contribution to the NIST aerodynamic database for wind loads on low buildings: Part 2. Comparison of data with wind load provisions." *Journal of Wind Engineering and Industrial Aerodynamics*, 93(1), 31-59.

Surry, D., (1991). "Pressure measurements on the Texas tech building: Wind tunnel measurements and comparisons with full scale." *Journal of Wind Engineering and Industrial Aerodynamics*, 38, 235-247.

Surry, D., (1999). "Wind loads on low-rise buildings: past, present and future." *Proc. 10th Inernational Conference Wind Engineering*, Copenhagen, Denmark, 105-114.

Surry, D., Sinno, R.R., Nail, B., Ho, T.C.E., Farquhar, S., Kopp, G.A., (2007). "Structurally effective static wind loads for roof panels." *Journal of Structural*

*Engineering*, 133, 871-885.

Tieleman H. W., (2003). "Wind tunnel simulation of wind loading on low-rise structures: a review." *Journal of Wind Engineering and Industrial Aerodynamics*, 91, 1627-1649.

Trenberth, K., (2005). "Uncertainty in Hurricanes and Global Warming." *Science*, 308, 1753-1754. (DOI:10.1126/science.1112551)

Visscher B.T., Kopp G.A., (2007). "Trajectories of roof sheathing panels under high winds." *Journal of Wind Engineering and Industrial Aerodynamics*, 95, 697-713.

Walker, G.R., (1975). "Report on Cyclone Tracy – Effect on buildings – Dec 1974." *Department of Housing and Construction,* Australia.

Wolfe, R.W., McCarthy M., (1989). "Structural Performance of Light-Frame Roof Assemblies I. Truss Assemblies with High Truss Stiffness Variability", *Forrest Products Laboratory*, Research Paper: FPL-RP-492.

Wolfe, R.W., LaBissoniere T, (1991). "Structural Performance of Light-Frame Roof Assemblies II. Conventional Truss Assemblies", *Forrest Products Laboratory*, Research Paper: FPL-RP-499.

Xu, Y.L., Reardon, G.F., (1996). "Full-Scale and Model-Scale Wind Pressures and Fatigue Loading on the Texas Tech University Building", CTS, James Cook University, Townsville Australia, Technical Report No. 42.

# APPENDIX A VIDEO OF WIND PRESSURES ON THE ROOF OF A LOW-RISE BUILDING

Video is provided in the APPENDIX A directory on the included DVD or the online archive.

# APPENDIX B PHOTOGRAPHS OF THE TOE-NAIL RTWC PRIOR TO TESTING

Photographs are provided in the APPENDIX B directory on the included DVD or the online archive. The filename represents which connection is being photographed as well as the side of the truss the photograph was taken from. The truss numbering is consistent with the truss numbering of Figure 2.5. For example the filename "S3-East.jpg" refers to the toe-nail connect on the south side of truss 3 with the picture taken from the East side of the connections facing West. The grid shown in the figure is 1.5 cm by 1.5 cm. The author would like to thank Dr. Hong, for providing these photographs.

# APPENDIX C RAW WIND TUNNEL PRESSURE DATA

The raw wind tunnel data obtain has been archived in Hierarchical Data Format (HDF) version 4 (HDF4) files and are designed to be self sufficient archives with minimal if any external information required by the user. The conventions used are similar to those used in the NIST aerodynamic database discussed by Ho et al. (2005). The HDF files are located in the APPENDIX C folder on the included DVD or the online archive.

# APPENDIX D ESTIMATES OF THE NET LOAD ON EACH RTWC

## D.1 Dead Load of the roof

Since the reactions at the RTWC are not measured directly they must be computed from the applied loads from the roof. In order to accomplish this, the weight of the roof must be accounted for, since the weight of the roof was not measured directly during construction an estimate must be calculated by assuming physical properties of the components. Table D. 1 lists the components that make up the weight of the roof and the assumed densities for each component. It should be noted that the weight of the shingles were not included in this calculation since they were removed prior to testing. Since with the exception of the gable end walls the weight of the roof is evenly distributed, the reaction at each RTWC due to the weight of the roof will be the same. The RTWC of the gable end walls are assumed to support the added weight due to the end walls. While the brick veneer is attached to the gable end wall using brick ties, the weight is largely supported by the foundation wall, as such, it is assumed that the brick does not add to the weight of the roof. Using the density for wood assumed in Table D. 1, the resultant force at the interior RTWC due to the weight of the roof is 0.53 kN, and 0.95 kN for the RTWC on a gable end wall and an overall weight of the roof of 18.4 kN.

Table D. 1 Assumed Densities of components on the roof of the house

| Component | Density |
|---|---|
| Plywood Sheathing | 0.046 ($kN/m^2$) |
| Truss wood Density | 530 ($kN/m^3$) |
| Gypsum | 0.077 ($kN/m^2$) |

## D.2 Calculation of the reactions loads at each RTWC

The following section outlines the calculation of the reactions at the roof to wall connections using the sum of moments about the Northern wall of the house. Each truss is assumed to act independently of each other, with the wind loads calculated based on the geometric tributary areas. Figure D. 1 provides a schematic of the cross section of a typical truss, the reactions at the nails are shown as $R^{y}_{S\text{-}i}$, $R^{z}_{S\text{-}i}$, $R^{y}_{N\text{-}i}$, and $\underline{R^{z}_{N\text{-}i}}$, where the super script "*y*" or "*z*" denote the direction of the force, the subscript *N* or *S* denotes where the reaction is on the North or South side and the subscript *i* denotes the truss number. The applied forces to the truss is defined as $P_k A_{k\text{-}i}$, where $P_k$ denotes the pressures applied to the roof by box number *k* and $A_{k\text{-}i}$ is the overlapping area between the airbox and the tributary area of the truss *i*. Finally the weight of the roof on a per truss basis is represented by $W_i$ and acts at the center of the truss. By summing forces in both the y and z directions yields:

$$\sum F_i^{\,z} = m_i a_i^{z}(t) = \sum_{k=1}^{58} P(t)_k A_{k-i} \cos\theta + R^{z}_{S-i}(t) + R^{z}_{N-i}(t) - W_i \qquad \text{(D.1)}$$

$$\sum F_i^{\,y} = m_i a_i^{y}(t) = \sum_{k=36}^{58} P(t)_k A_{k-i} \sin\theta - \sum_{k=1}^{35} P(t)_k A_{k-i} \sin\theta + R^{y}_{S-i}(t) + R^{y}_{N-i}(t) \qquad \text{(D.2)}$$

While summing moments about the Northern wall as indicated by the red dot in Figure D. 1 yields:

$$\begin{aligned} \sum M^{x}_{N-i} = \bar{I}\alpha_i(t) &= R^{z}_{N-i}(t) * \frac{d}{2} + R^{z}_{S-i}(t) * \left(\frac{3d}{2} + w'\right) \\ &+ \sum_{k=1}^{58} P(t)_k A_{k-i} \cos\theta * (y_k) - \sum_{k=36}^{58} P(t)_k A_{k-i} \sin\theta * z_k \\ &+ \sum_{k=1}^{35} P(t)_k A_{k-i} \sin\theta * z_k - W_i * \left(\frac{w'}{2} + d\right) \end{aligned} \qquad \text{(D.3)}$$

Assuming that the accelerations are negligible, and combining Eq. D.1 and D.3, the reactions at both the North ($R^z_{N-i}$) and South ($R^z_{S-i}$) RTWC can be obtained from:

$$R^z_{S-i} = \frac{1}{w' + d}\left(\begin{array}{l} W_i * \left(\frac{w'}{2} + \frac{d}{2}\right) + \sum_{k=36}^{58} P(t)_k A_{k-i} \sin\theta * z_k \\ - \sum_{k=1}^{58} P(t)_k A_{k-i} \cos\theta * \left(y_k - \frac{d}{2}\right) - \sum_{k=1}^{35} P(t)_k A_{k-i} \sin\theta * z_k \end{array}\right) \quad \text{(D.4)}$$

$$R^z_{N-i} = W_i - \sum_{k=1}^{58} P(t)_k A_{k-i} \cos\theta - R^z_{S-i}(t) \quad \text{(D.5)}$$

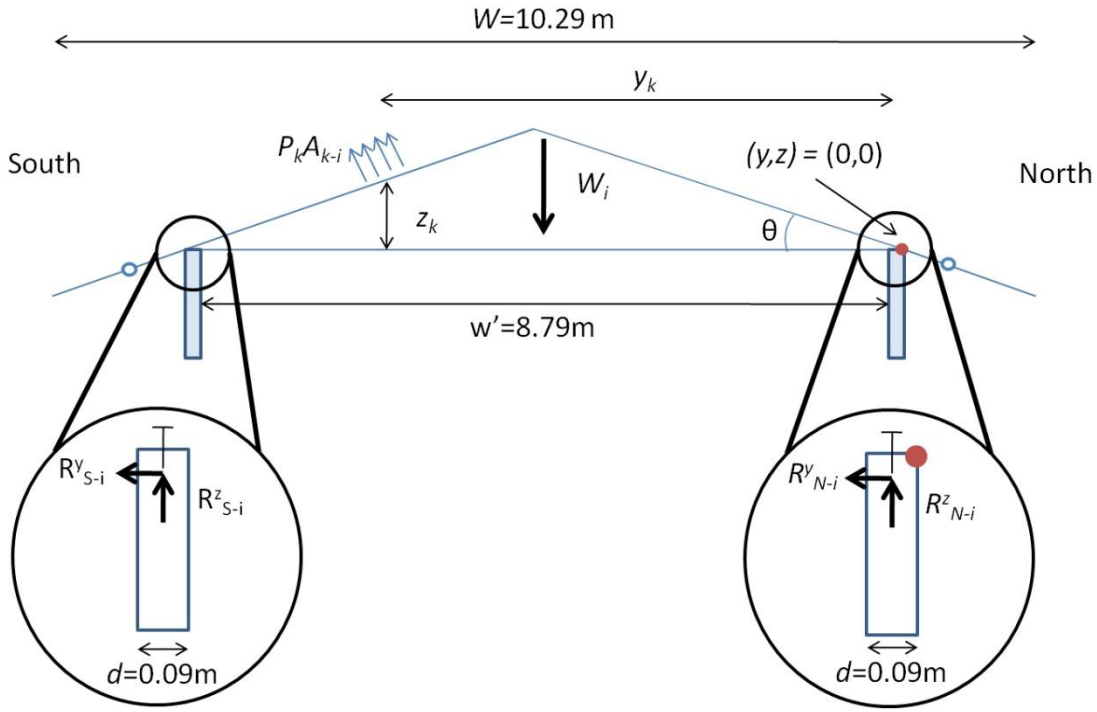


Figure D. 1 A schematic of a typical roof truss and the applied loads.

# APPENDIX E DISPLACEMENT TIME SERIES FOR ALL 6 FULL SCALE HOUSE TESTS

The displacement time histories for the RTWC during all 6 tests are shown below. For RTWC "S12" the displacement transducer did not record data for tests 2 through 6 due to a mechanical malfunction, as such the displacements for this connections are not shown.

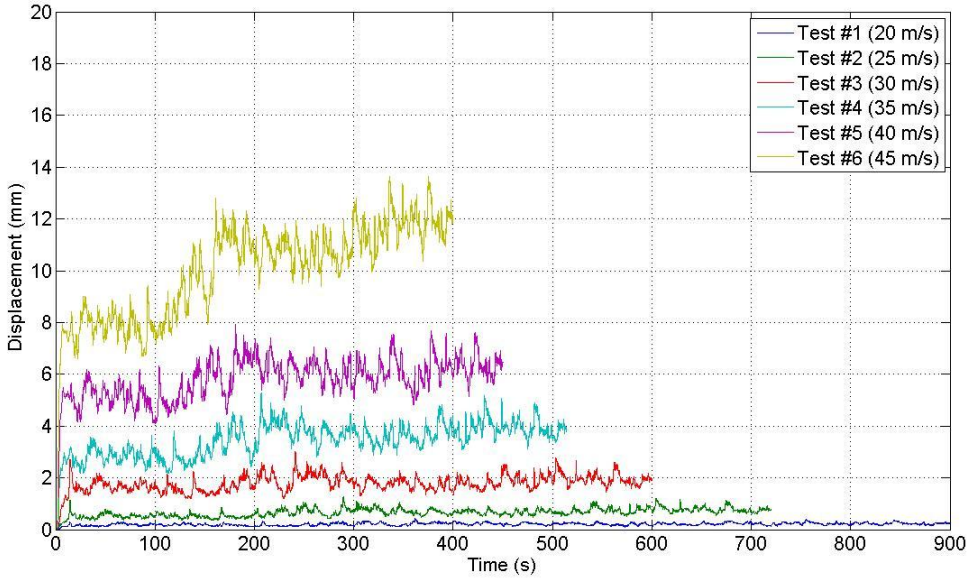


Figure E. 1 Displacement Time Series for all 6 tests for RTWC "S7"

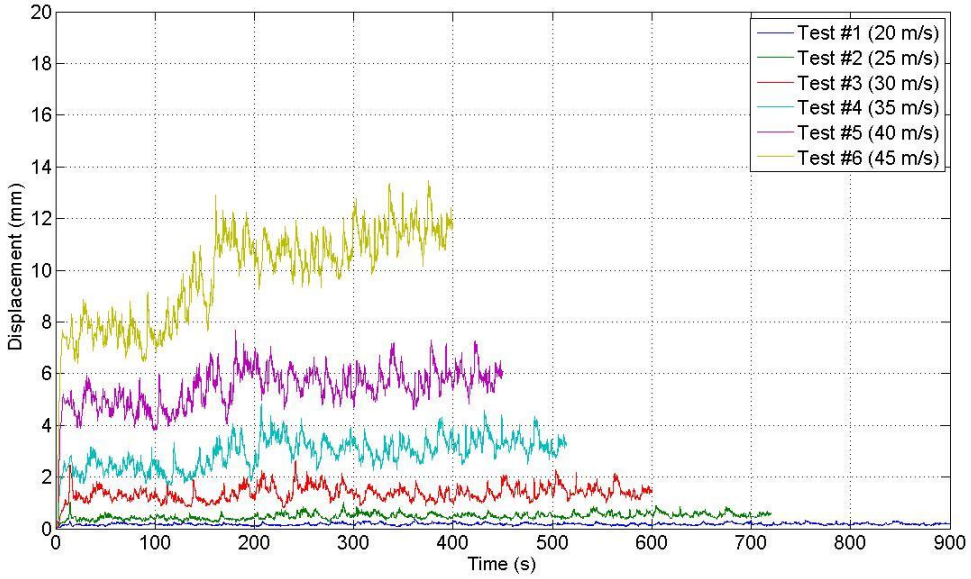


Figure E. 2 Displacement Time Series for all 6 tests for RTWC "S8"

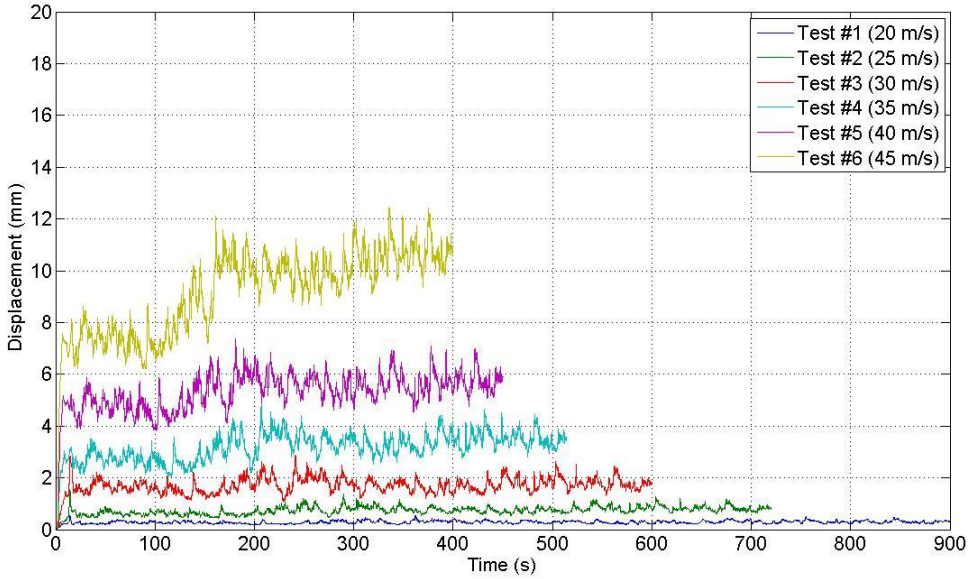


Figure E. 3 Displacement Time Series for all 6 tests for RTWC "S9"

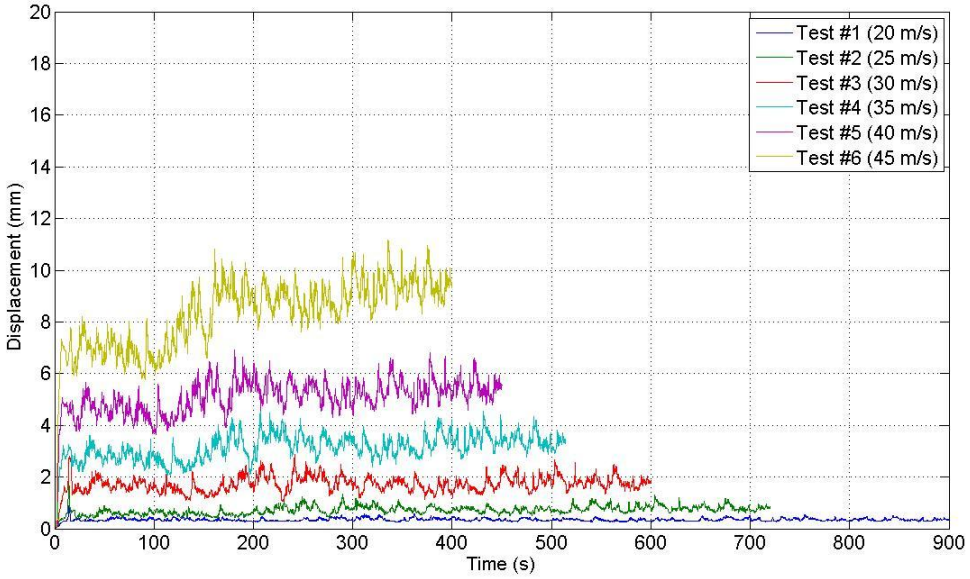


Figure E. 4 Displacement Time Series for all 6 tests for RTWC "S10"

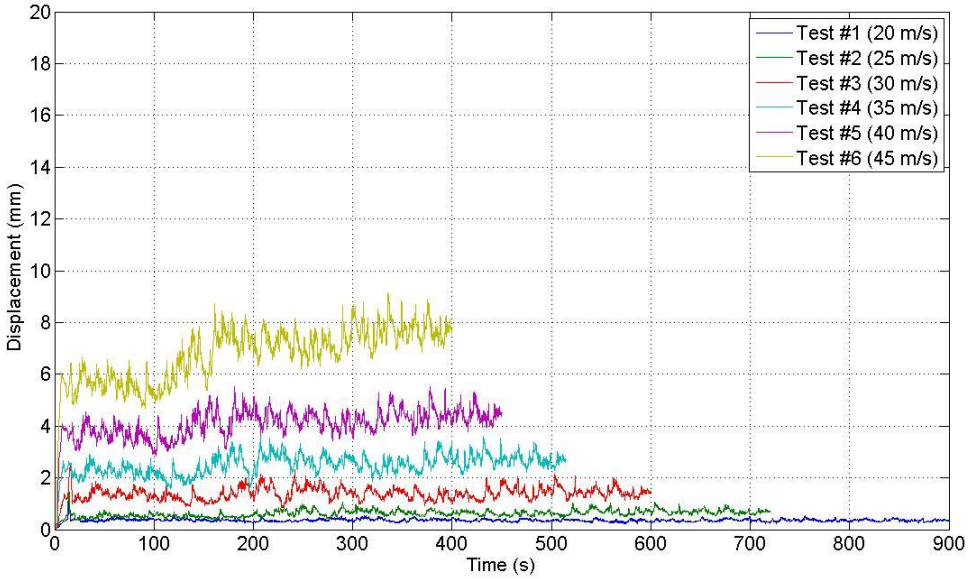


Figure E. 5 Displacement Time Series for all 6 tests for RTWC "S11"

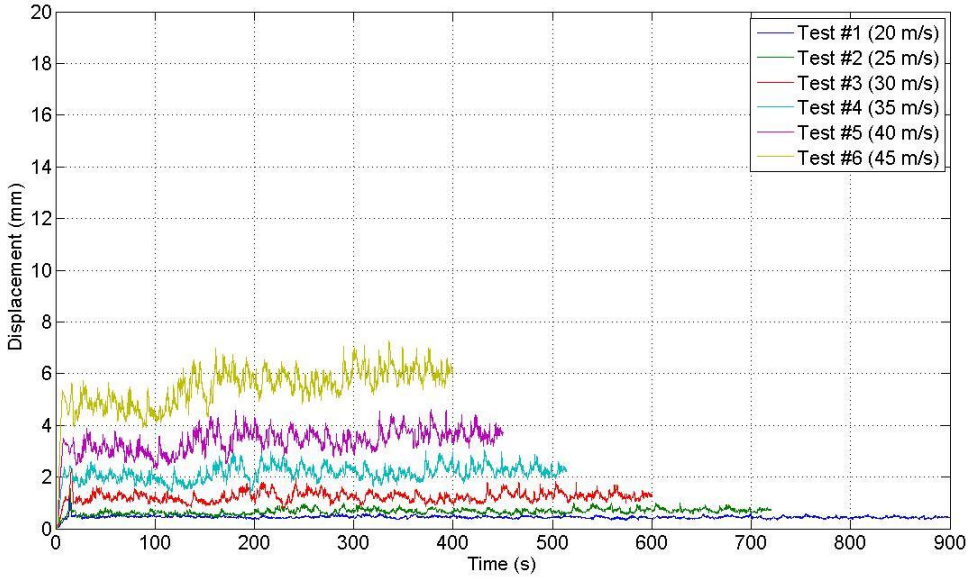


Figure E. 6 Displacement Time Series for all 6 tests for RTWC "S13"

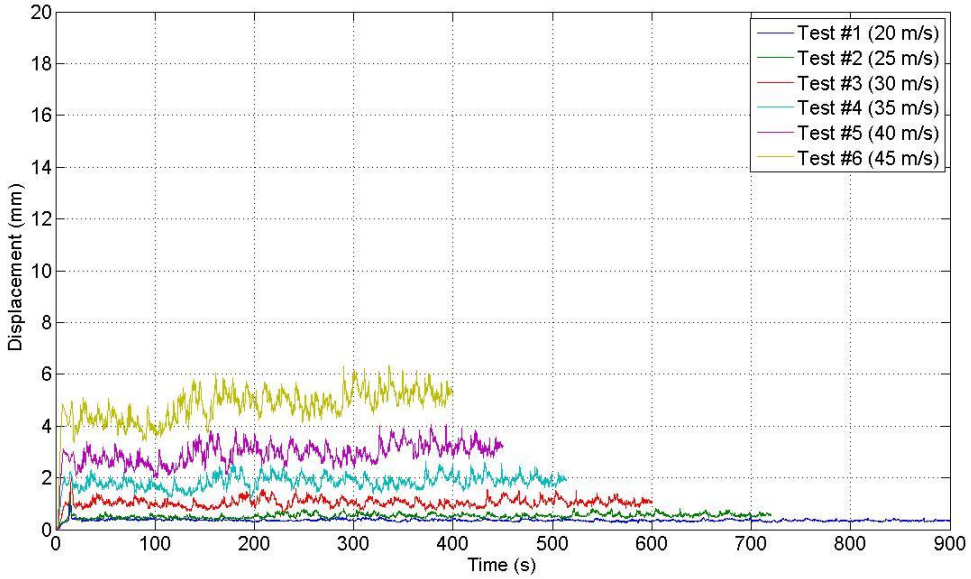


Figure E. 7 Displacement Time Series for all 6 tests for RTWC "S14"

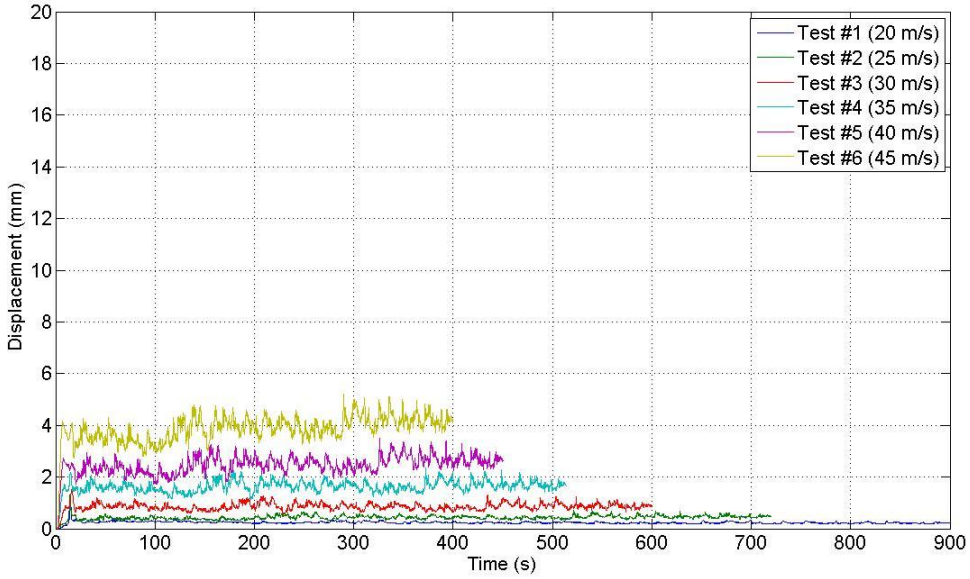


Figure E. 8 Displacement Time Series for all 6 tests for RTWC "S15"

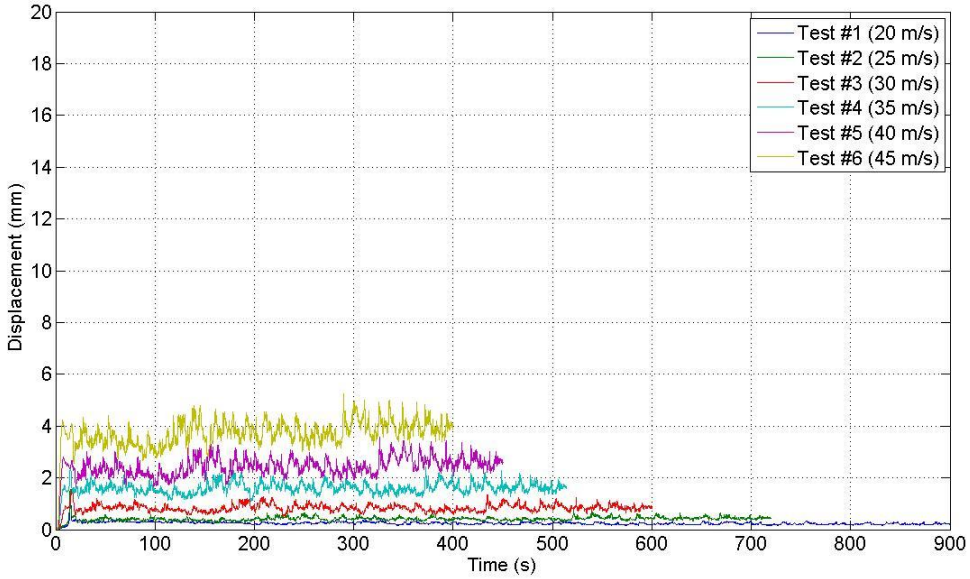


Figure E. 9 Displacement Time Series for all 6 tests for RTWC "S16"

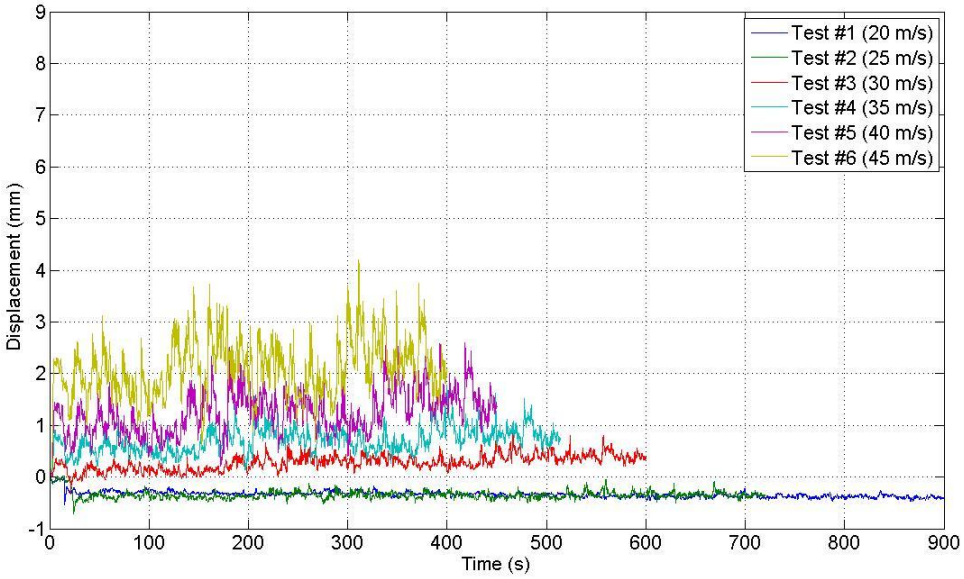


Figure E. 10 Displacement Time Series for all 6 tests for RTWC "N7"

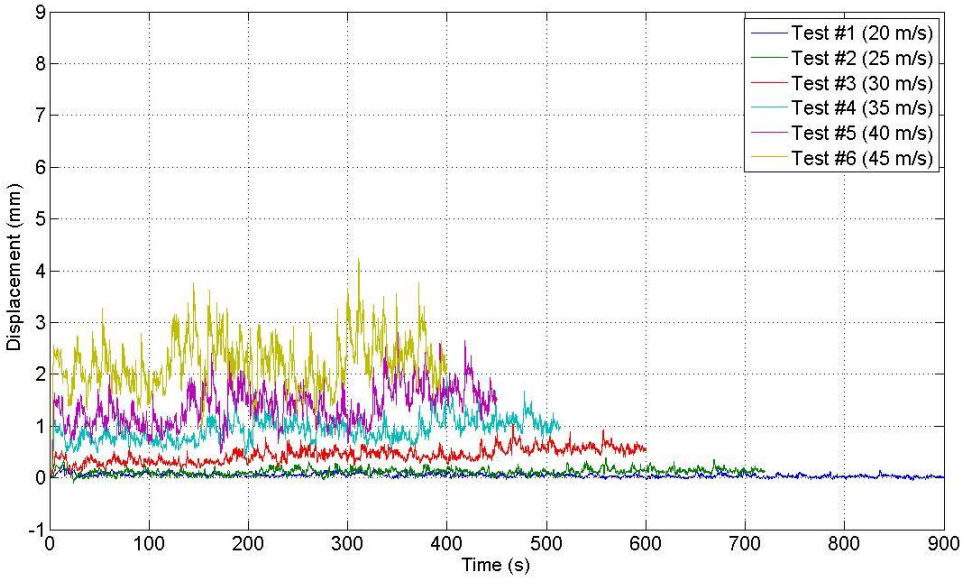


Figure E. 11 Displacement Time Series for all 6 tests for RTWC "N8"

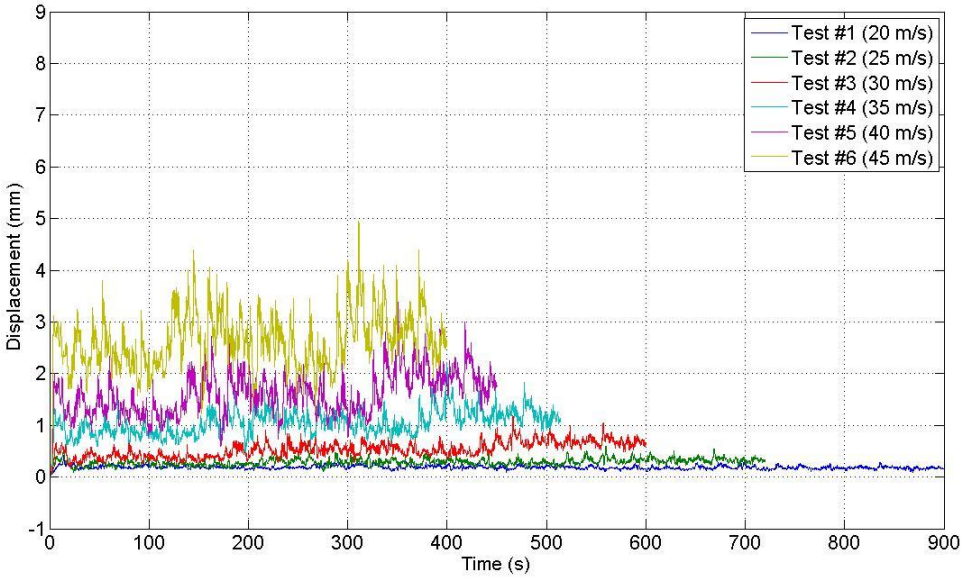


Figure E. 12 Displacement Time Series for all 6 tests for RTWC "N9"

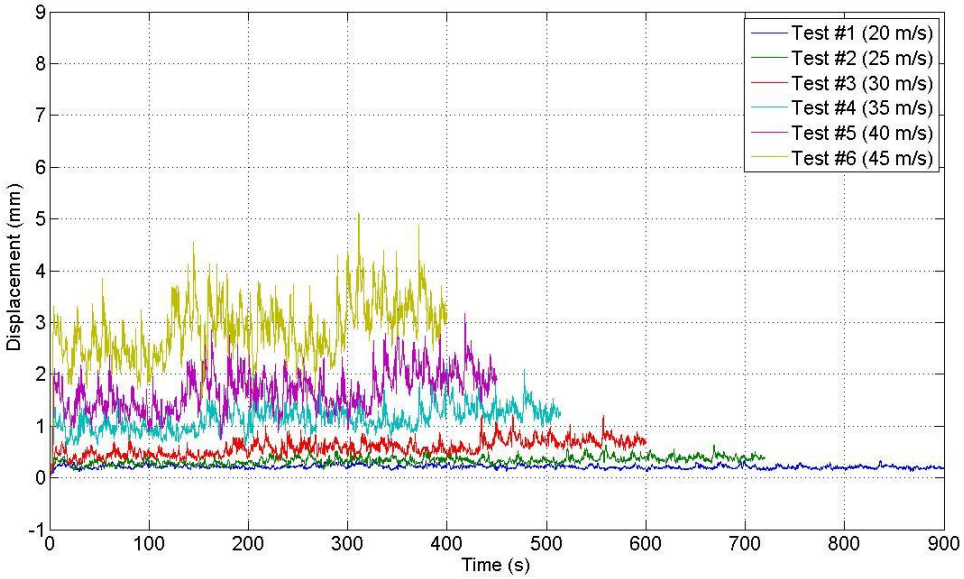


Figure E. 13 Displacement Time Series for all 6 tests for RTWC "N10"

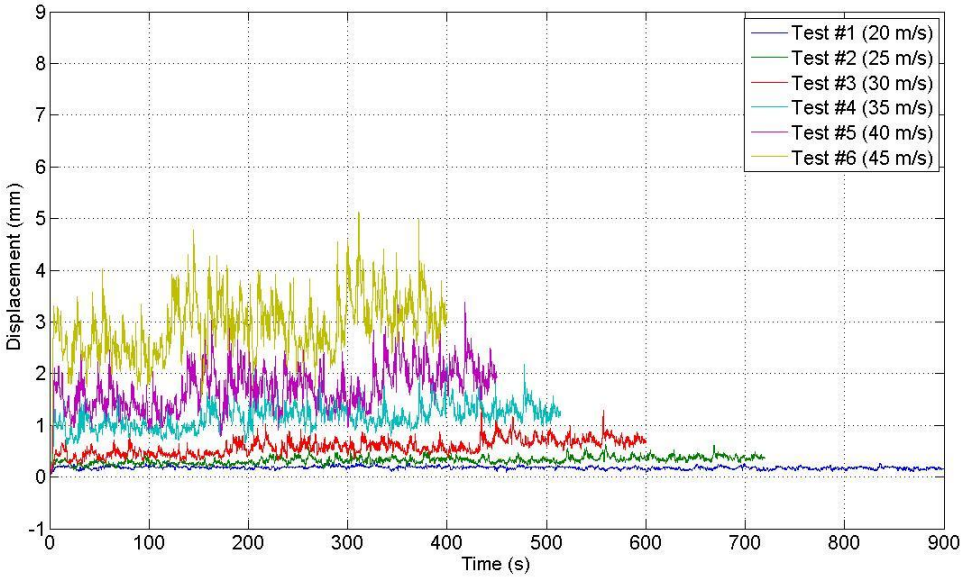


Figure E. 14 Displacement Time Series for all 6 tests for RTWC "N11"

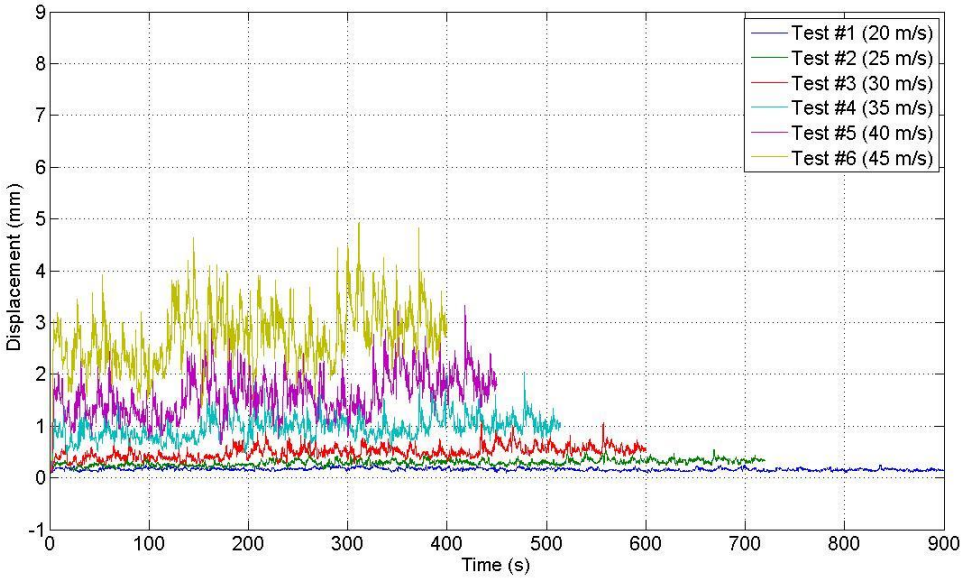


Figure E. 15 Displacement Time Series for all 6 tests for RTWC "N12"

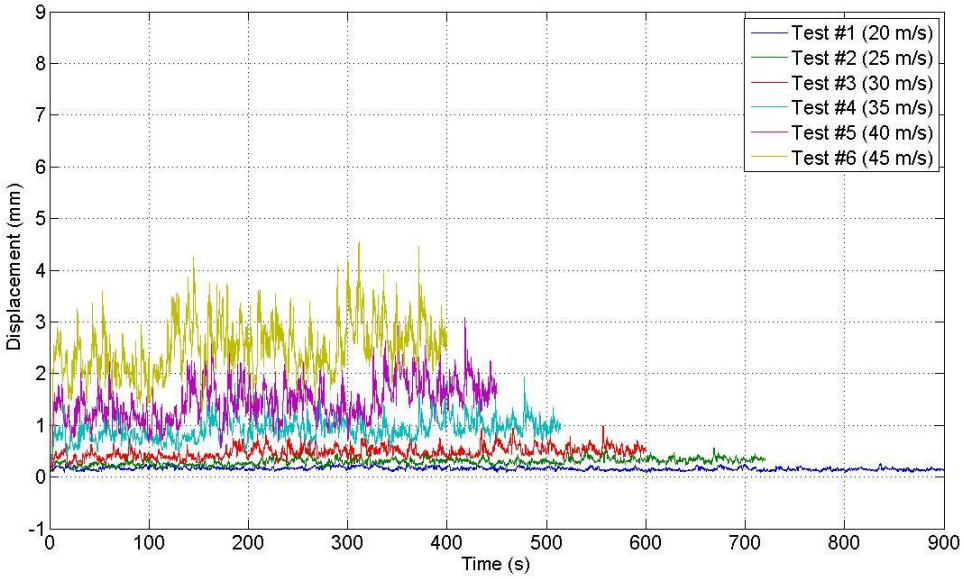


Figure E. 16 Displacement Time Series for all 6 tests for RTWC "N13"

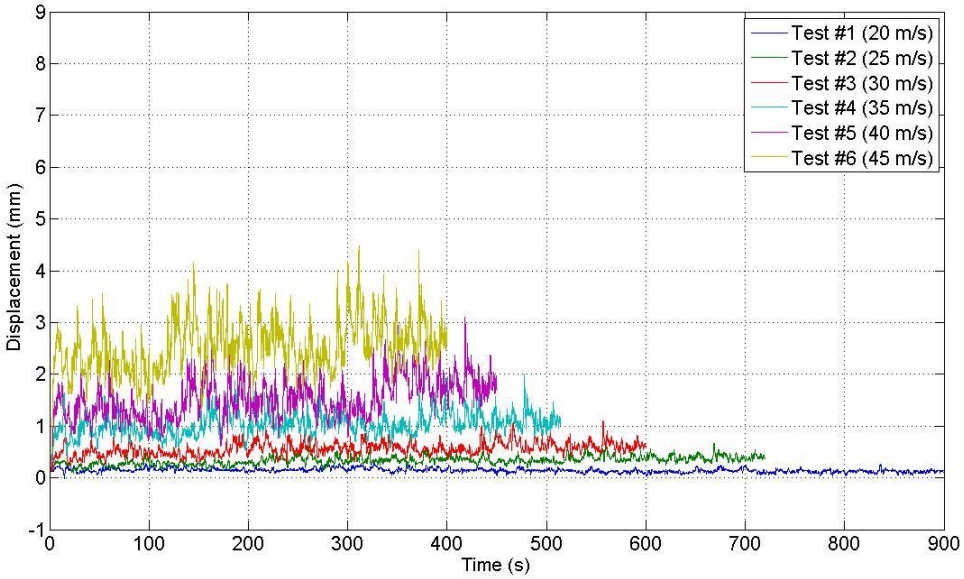


Figure E. 17 Displacement Time Series for all 6 tests for RTWC "N14"

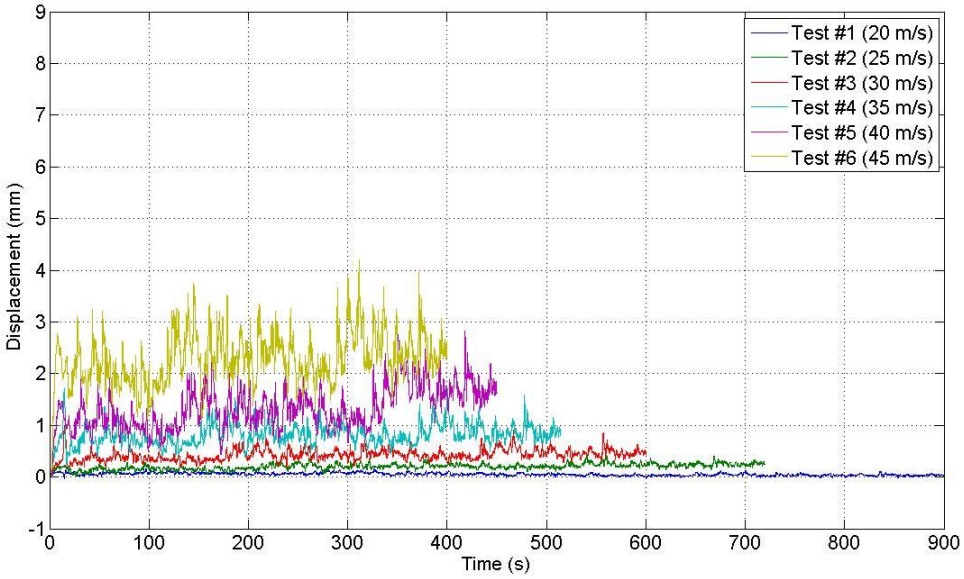


Figure E. 18 Displacement Time Series for all 6 tests for RTWC "N15"

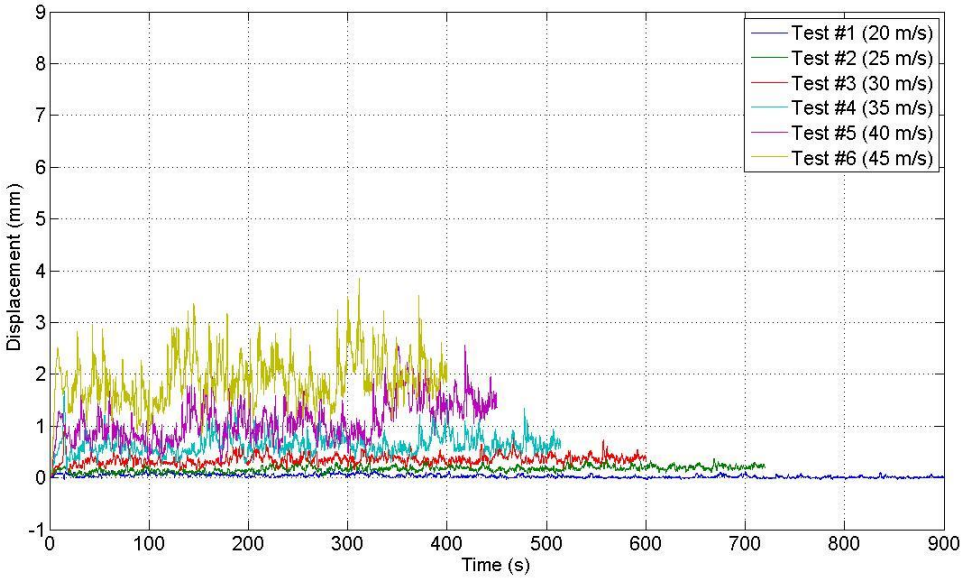


Figure E. 19 Displacement Time Series for all 6 tests for RTWC "N16"

# APPENDIX F LOAD DISPLACEMENT CURVES FOR ALL RTWC

The load versus displacement curves for the RTWC during all 6 tests are shown below. For RTWC "S12" the displacement transducer did not record data for tests 2 through 6 due to a mechanical malfunction, as such the displacements for this connections are not shown.

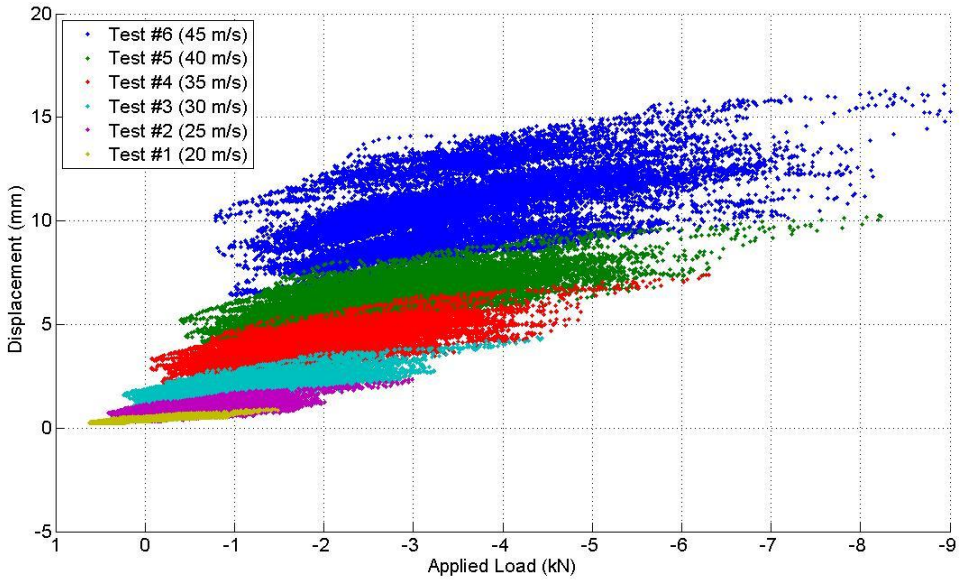


Figure F. 1 Load Displacement data for connection "S2" for all 6 tests.

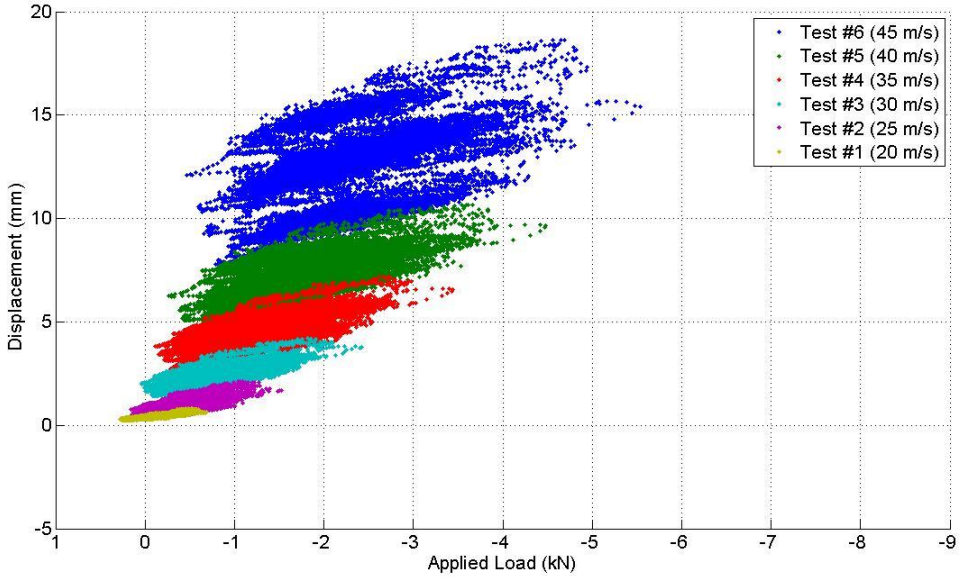


Figure F. 2 Load Displacement data for connection "S4" for all 6 tests.

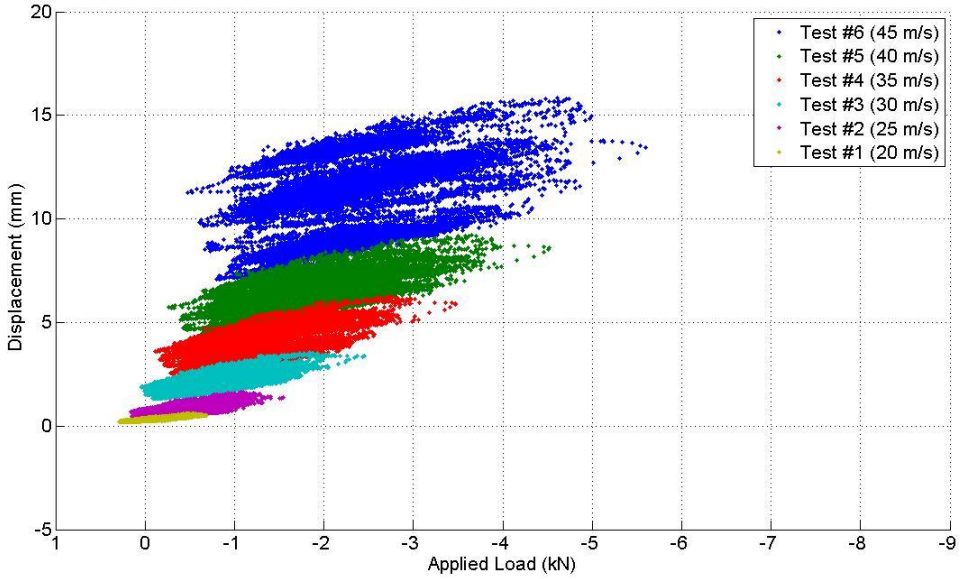


Figure F. 3 Load Displacement data for connection "S5" for all 6 tests.

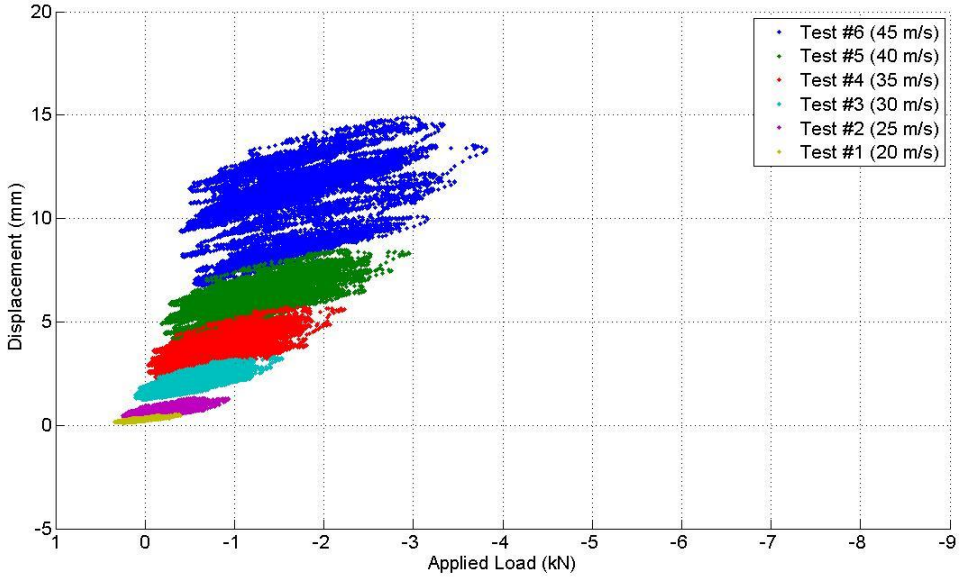


Figure F. 4 Load Displacement data for connection "S6" for all 6 tests.

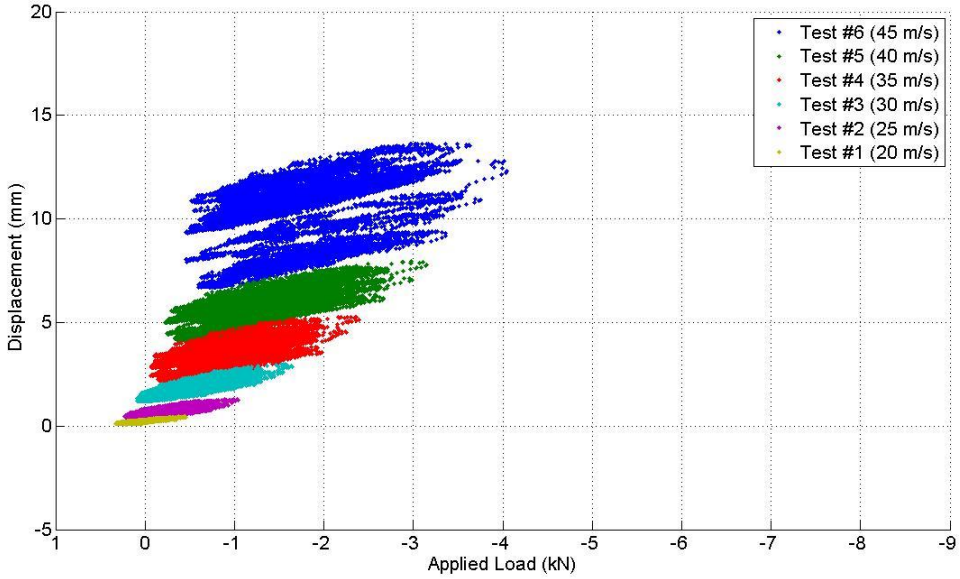


Figure F. 5 Load Displacement data for connection "S7" for all 6 tests.

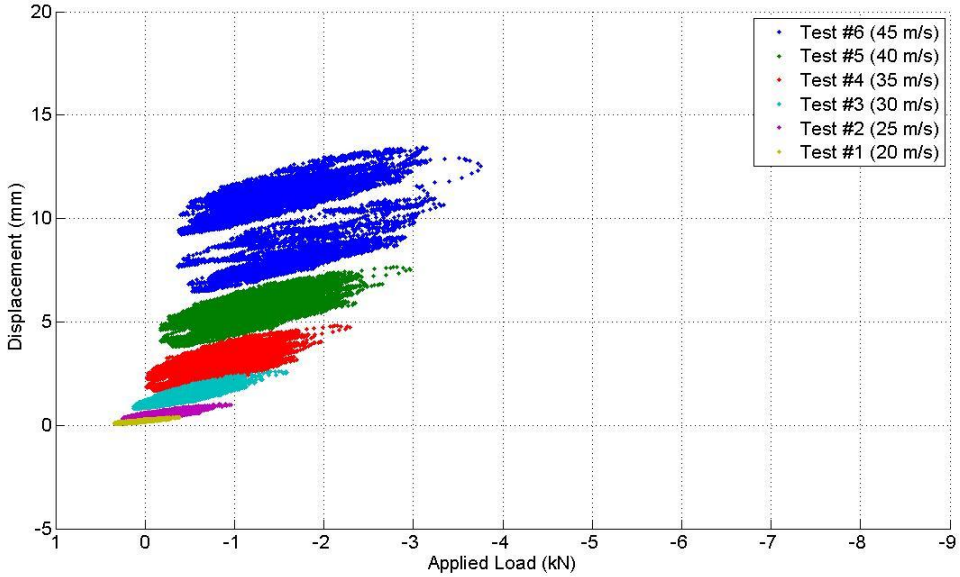


Figure F. 6 Load Displacement data for connection "S8" for all 6 tests.

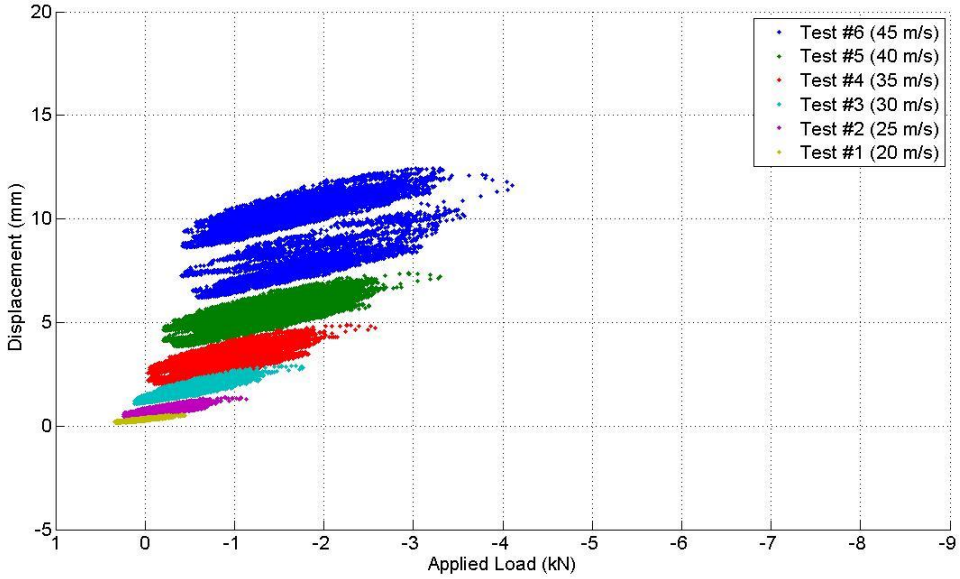


Figure F. 7 Load Displacement data for connection "S9" for all 6 tests.

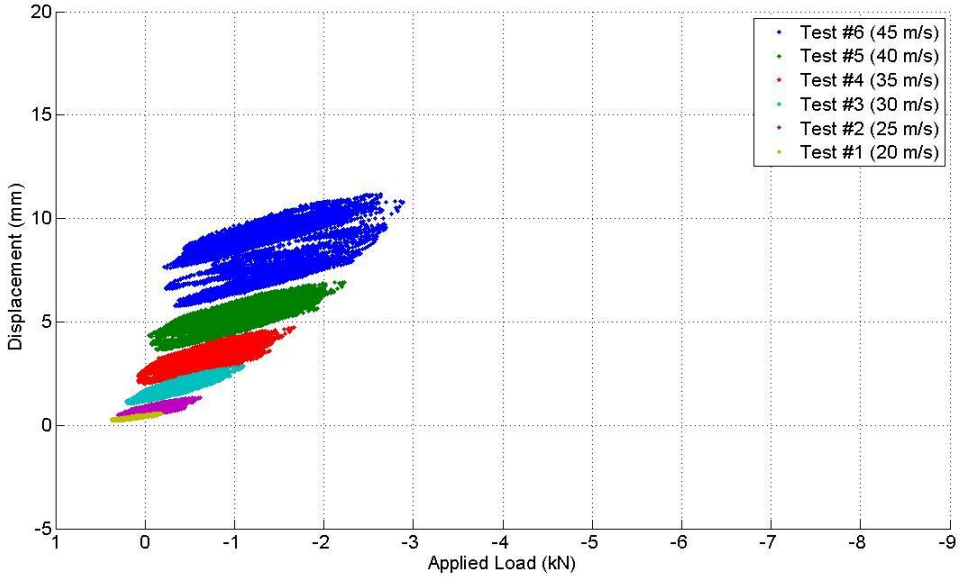


Figure F. 8 Load Displacement data for connection "S10" for all 6 tests.

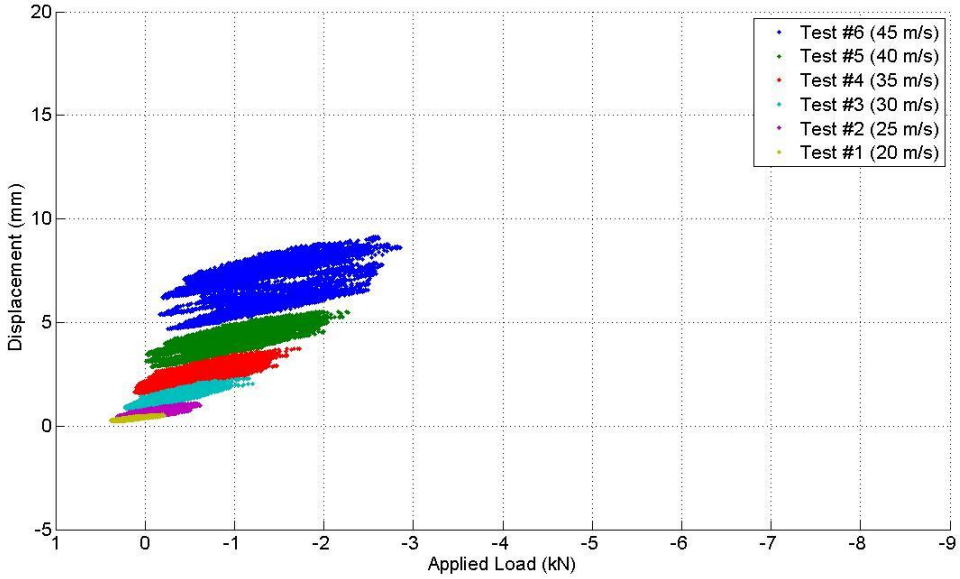


Figure F. 9 Load Displacement data for connection "S11" for all 6 tests.

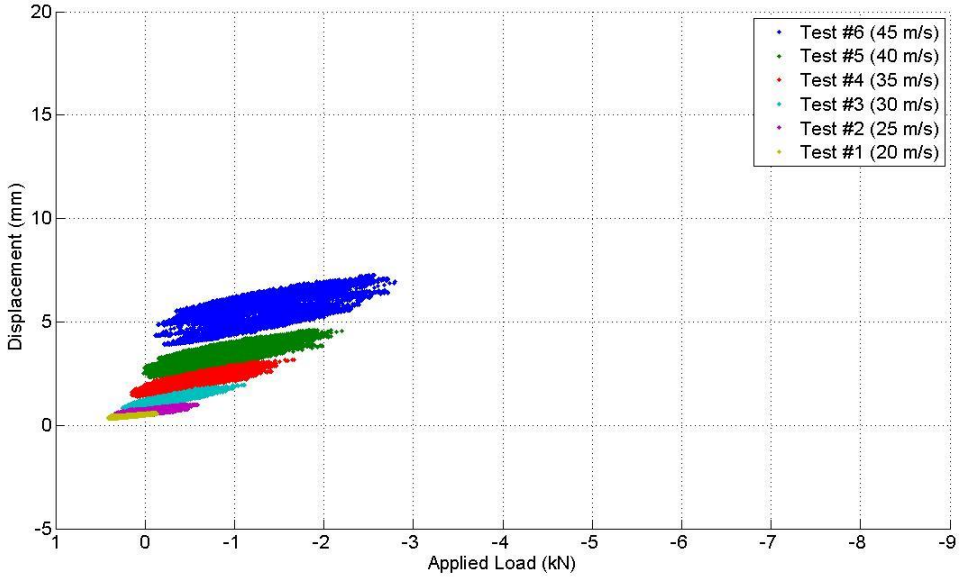


Figure F. 10 Load Displacement data for connection "S13" for all 6 tests.

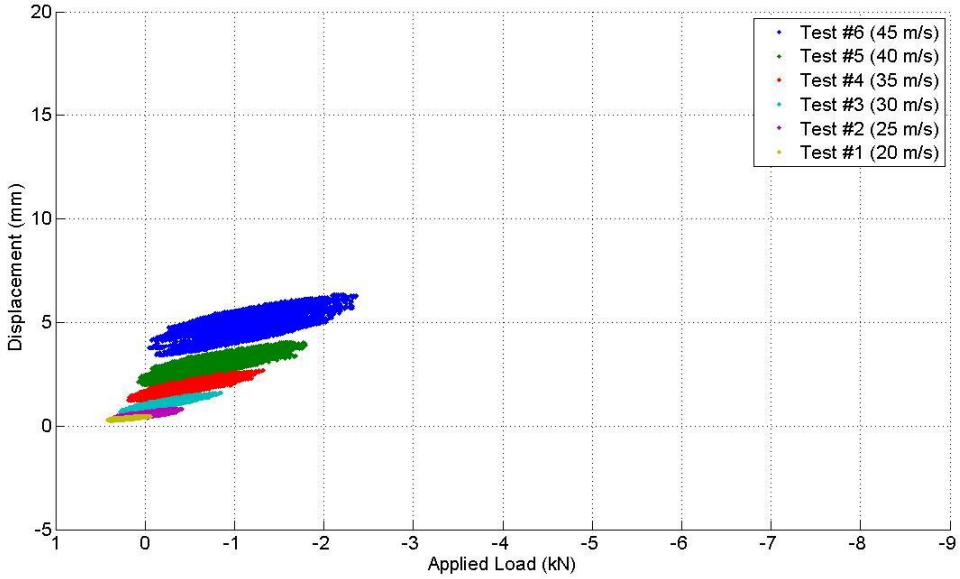


Figure F. 11 Load Displacement data for connection "S14" for all 6 tests.

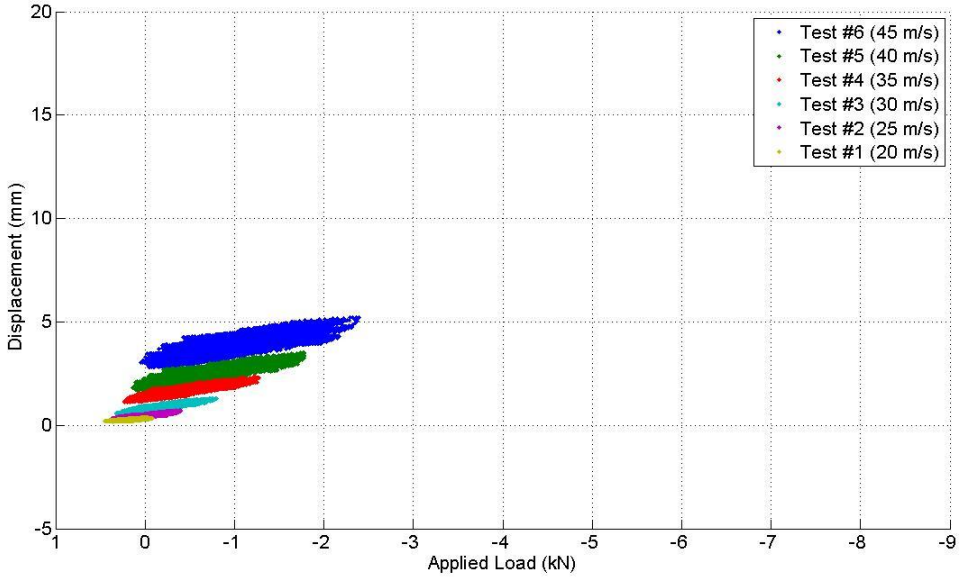


Figure F. 12 Load Displacement data for connection “S15” for all 6 tests.

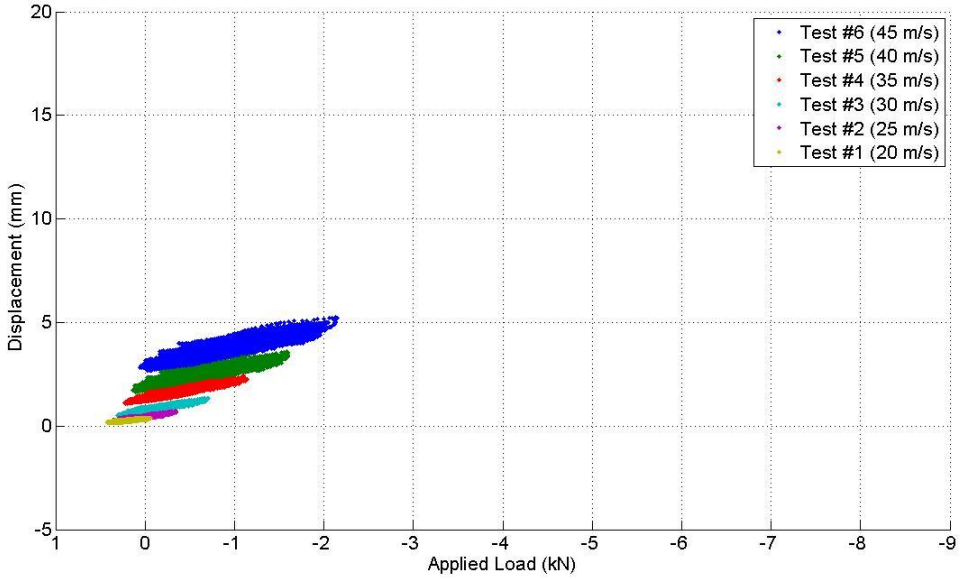


Figure F. 13 Load Displacement data for connection “S16” for all 6 tests.

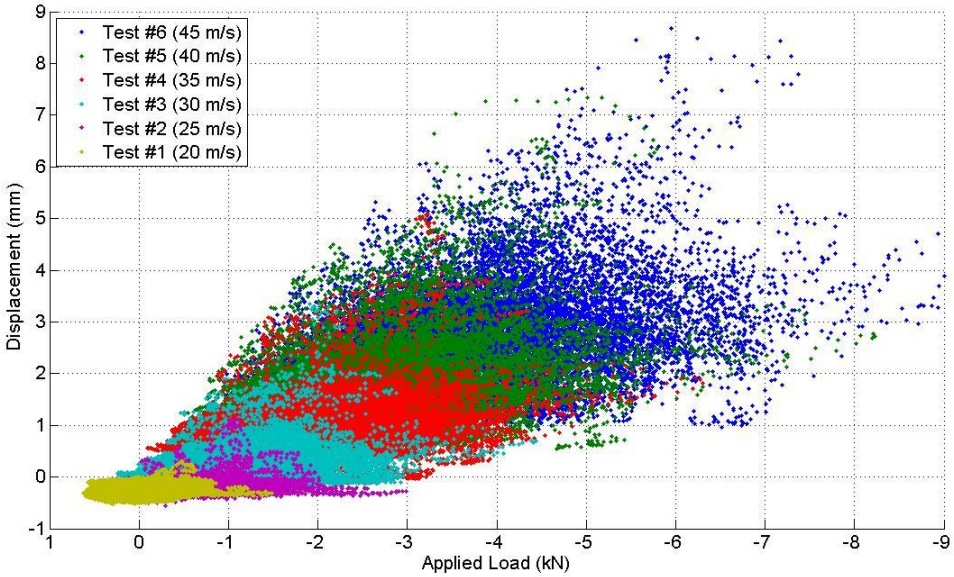


Figure F. 14 Load Displacement data for connection "N2" for all 6 tests.

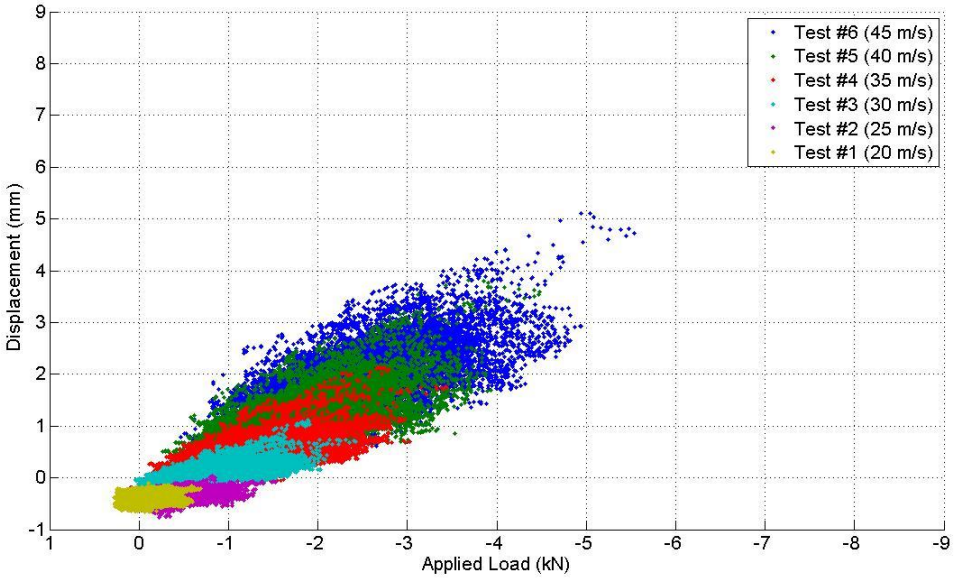


Figure F. 15 Load Displacement data for connection "N4" for all 6 tests.

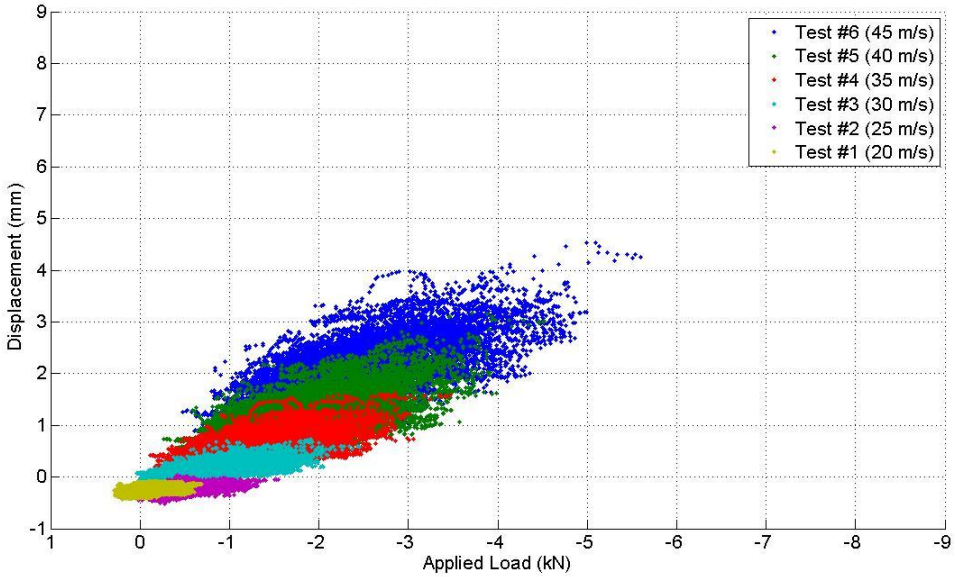


Figure F. 16 Load Displacement data for connection "N5" for all 6 tests.

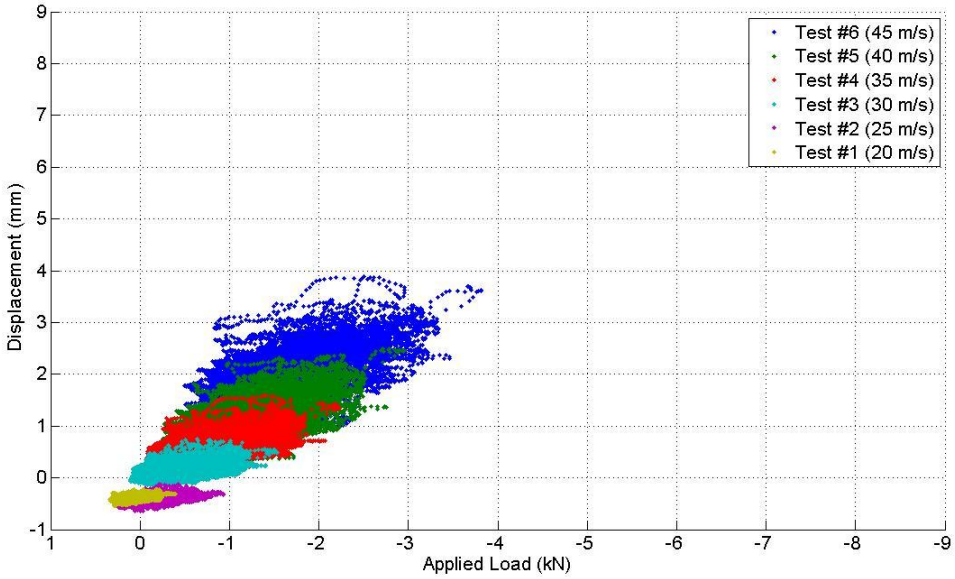


Figure F. 17 Load Displacement data for connection "N6" for all 6 tests.

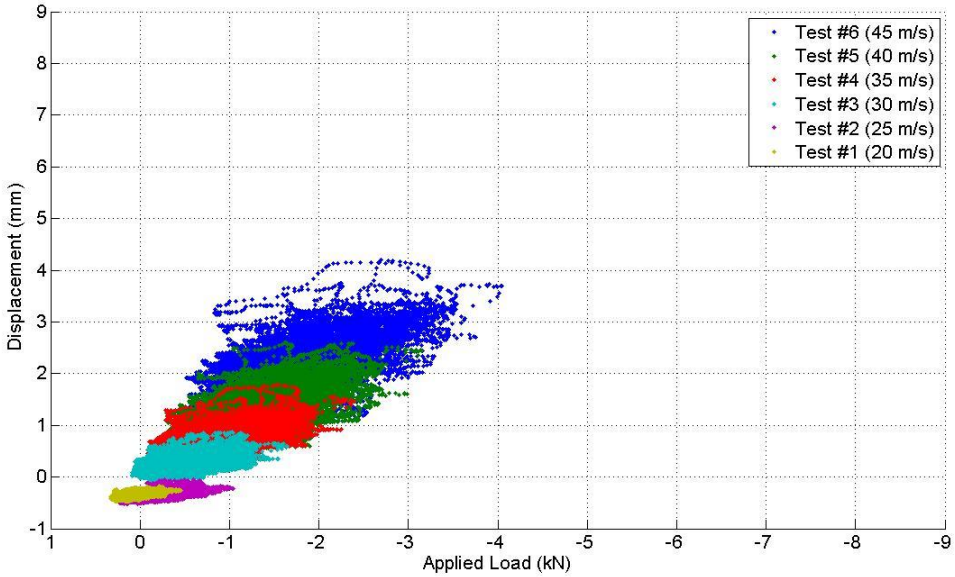


Figure F. 18 Load Displacement data for connection "N7" for all 6 tests.

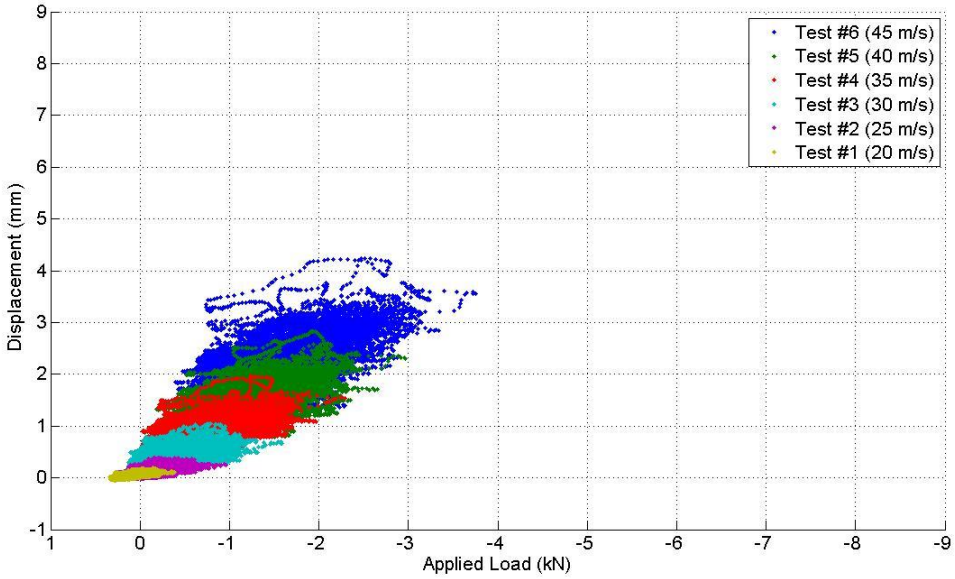


Figure F. 19 Load Displacement data for connection "N8" for all 6 tests.

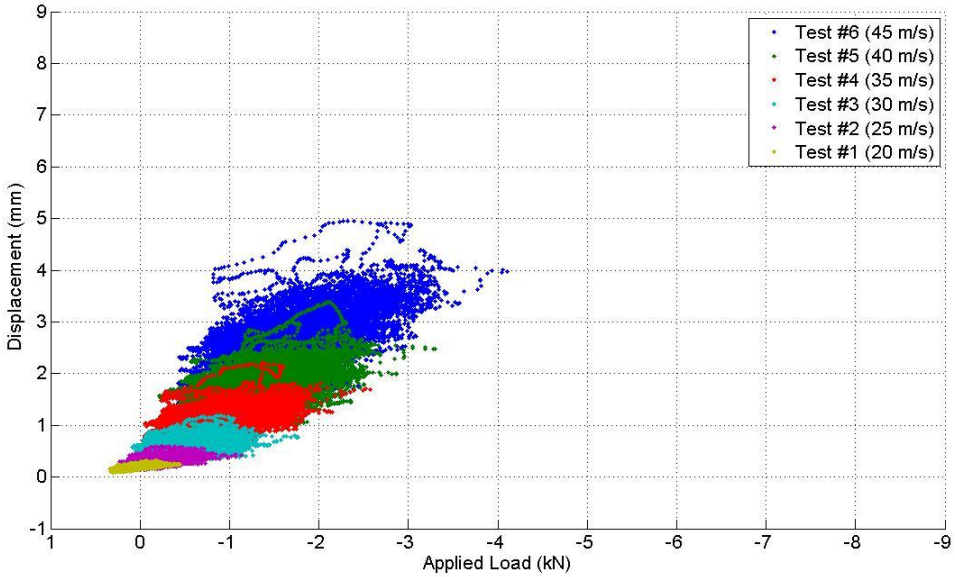


Figure F. 20 Load Displacement data for connection "N9" for all 6 tests.

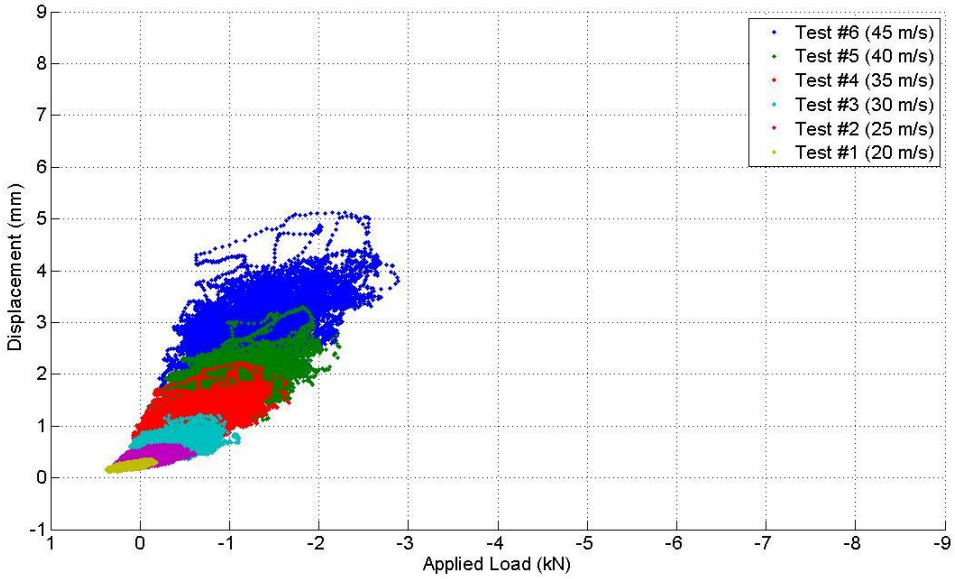


Figure F. 21 Load Displacement data for connection "N10" for all 6 tests.

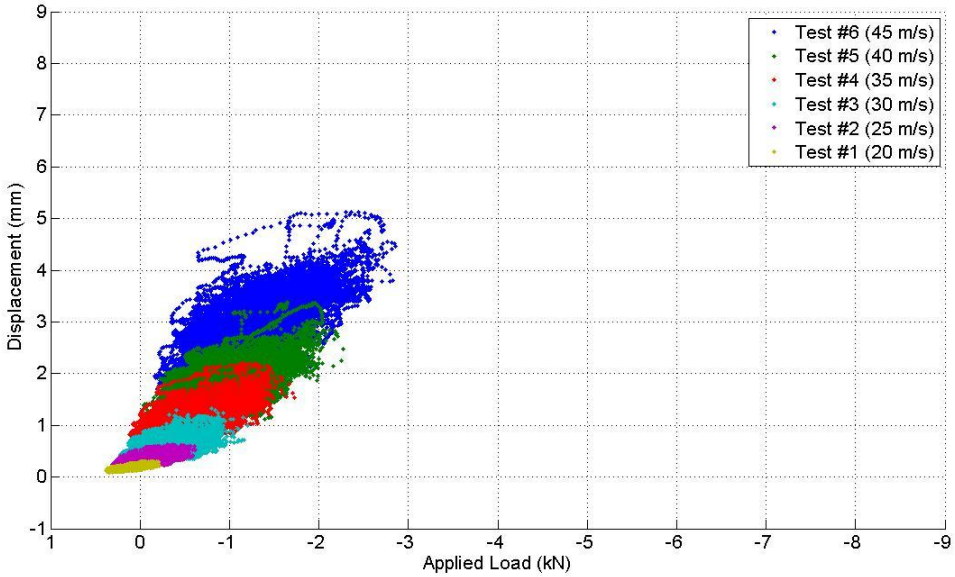


Figure F. 22 Load Displacement data for connection "N11" for all 6 tests.

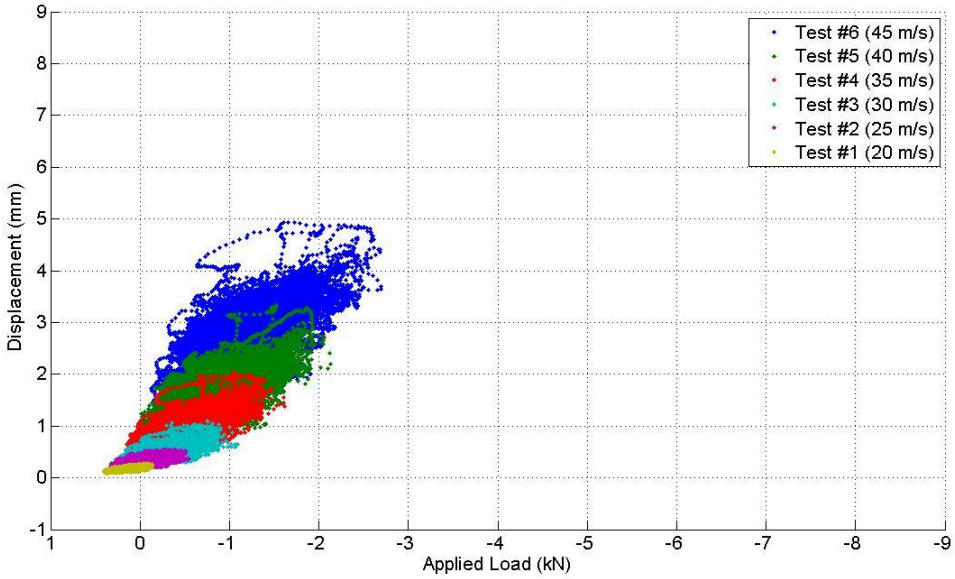


Figure F. 23 Load Displacement data for connection "N12" for all 6 tests.

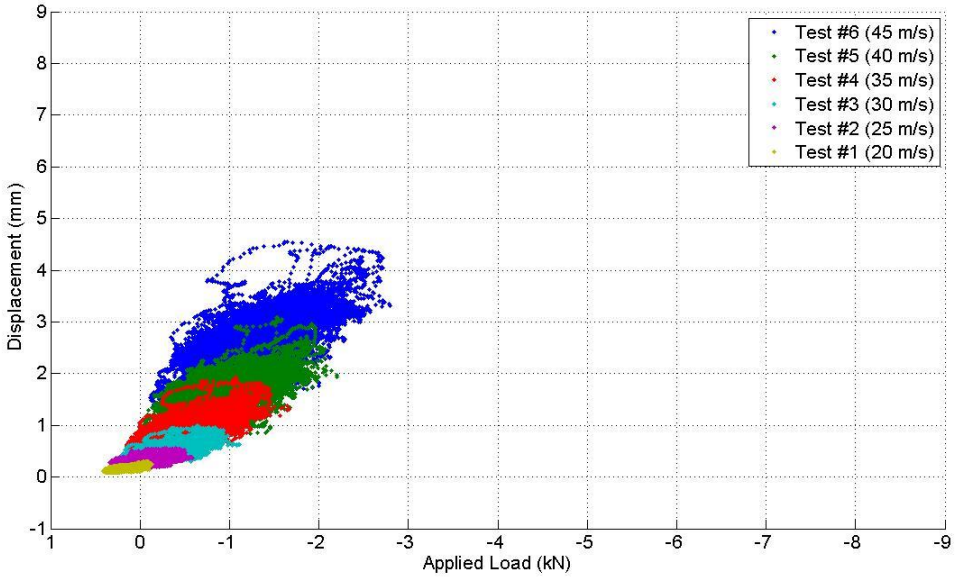


Figure F. 24 Load Displacement data for connection "N13" for all 6 tests.

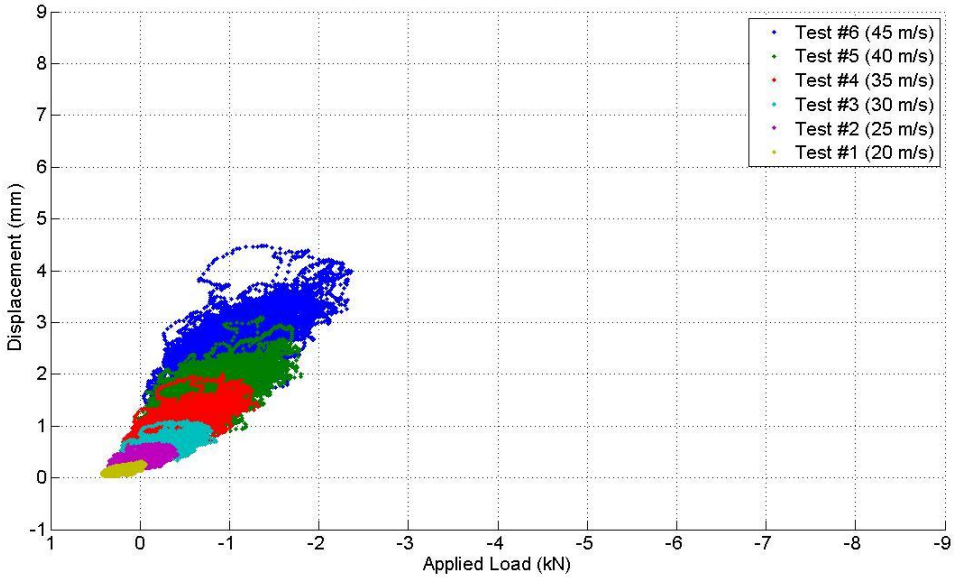


Figure F. 25 Load Displacement data for connection "N14" for all 6 tests.

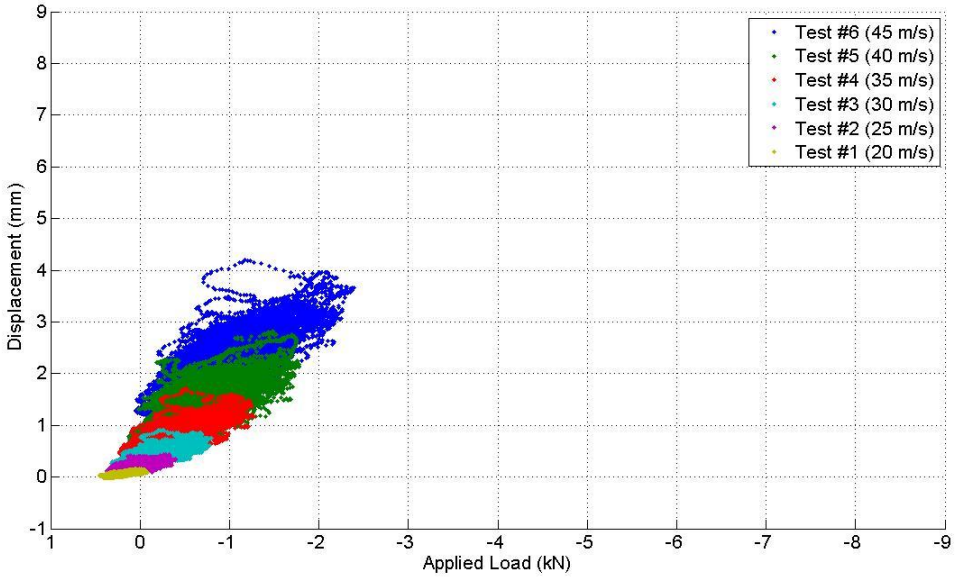


Figure F. 26 Load Displacement data for connection "N15" for all 6 tests.

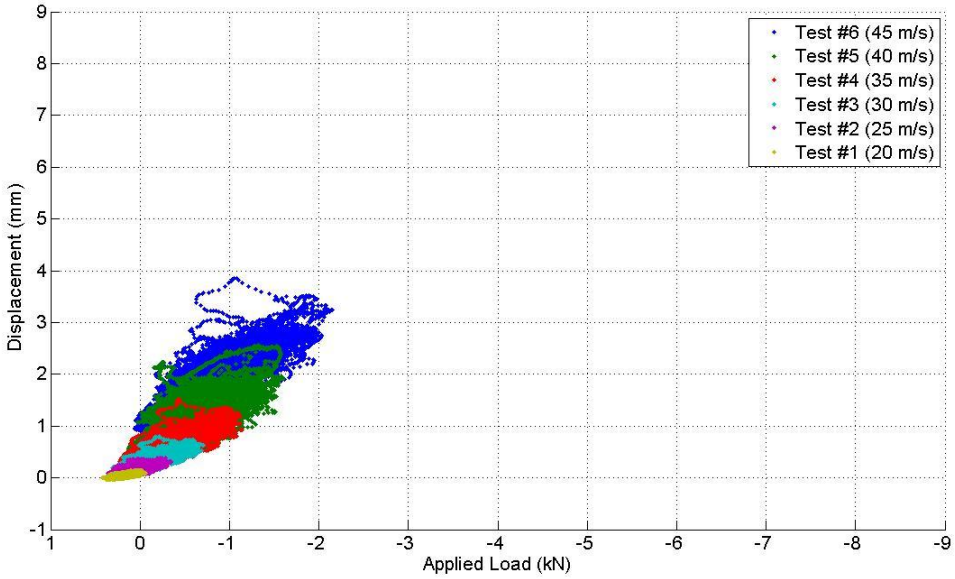


Figure F. 27 Load Displacement data for connection "N16" for all 6 tests.

# VITA

**Name**

Murray J. Morrison

**Post-Secondary Education and Degrees**

Department of Mechanical and Materials Engineering
The University of Western Ontario
London, Ontario, Canada
2000 – 2004, BESc

Department of Mechanical and Materials Engineering
The University of Western Ontario
London, Ontario, Canada
2004 – 2006, MESc

**Honours and Awards**

Dean's Honour List
2002-2004

NSERC USRA Scholarship
Summer 2003

Graduated with Distinction
2004

Ontario Graduate Scholarship
2004-2005

NSERC PGS M Scholarship
2005-2006

Outstanding Teaching Assistant
Department of Mechanical and Materials Engineering
The University of Western Ontario
2006

OGSST Scholarship
2006-2007

NSERC PGS D Scholarship
2007-2010

**Related Work Experience**

Teaching Assistant
Department of Mechanical and Materials Engineering
The University of Western Ontario
2004-2006

Teaching Assistant
Department of Civil and Environmental Engineering
The University of Western Ontario
2006-2008

Technology Coordinator
The Insurance Research Lab for Better Homes
The University of Western Ontario
2008-2010

**Publications:**

Journal Publications

**Morrison M.J.** Kopp G. A. (2010). "Analysis of Wind-Induced Clip Loads on Standing Seam Metal Roofs", *Journal of Structural Engineering*, 136(3), 334-337.

Kopp G.A., **Morrison M.J.**, Gavanski E., Henderson D., Hong H. (2010). "The 'Three Little Pigs Project: Hurricane Risk Mitigation by Integrated Wind Tunnel and Full-Scale Laboratory Tests", Natural Hazards Review; (doi:10.1061/(ASCE)NH.1527-6996.0000019).

Henderson, D., Ginger J., **Morrison M.J.**, Kopp G.A. (2009). "Simulated tropical cyclonic winds for low cycle fatigue loading of steel roofing", *Journal of Wind and Structures*, 12(4), 383-400.

Kopp G.A., **Morrison M.J**., Kordi B., Miller C. "A Method to Assess Peak Storm Wind Speeds Using Detailed Damage Surveys", *Engineering Structures*, Accepted 2010.

Kopp G.A., **Morrison M.J.**, "Discussion of **"**Tornado-Induced Wind Loads on a Low-Rise Building" by F.L. Haan Jr.; V.K. Balaramudu; and P.P. Sarkar", *Journal of Structural Engineering*, Accepted 2010.

**Morrison M.J.**, Kopp G.A., "Performance of toe-nail connections under realistic wind loading", *Engineering Structures*, Accepted 2010.

Conference Proceedings

Mapp R., Masters F.J., Bolton S., Kopp G.A., **Morrison M.J.** "Characterization of Wind-Driven Rain Ingress Through Residential Soffit Systems". *ICBEST Vancouver Canada*, June, 2010.

**Morrison, M.J.**, Kopp, G.A. "Application of realistic wind loads to the roof of a full-scale, wood-frame house". *Proceedings of the 11$^{th}$ Americas Conference on Wind*

*Engineering*(CD-ROM), San Juan, Puerto Rico, June 2009.

Kopp, G.A., **Morrison, M.J.**, Kordi, B. & Miller, C.A. " A method to assess peak storm wind speeds using detailed damage surveys". *Proceedings of the 5th ASCE Symposium on Forensic Engineering Conference*, Washington, USA, pp. 668-677, 2009.

**Morrison M.J.**, Kopp G.A. "Performance of Toe-nail connections under realistic wind loading", *NASCC Structures Congress,* May 2010.

Kopp G.A, **Morrison M.J.**, Iizumi, E. "The 'Three Little Pigs' project: Integration of wind tunnel model scale tests and full-scale laboratory tests", *ISWE3*, Tokyo Japan, 2008.

Kopp, G.A., **Morrison M.J.**, Sarathi, P., Henderson, D., Ginger, J. "New Test Methods to Examine and Improve the Performance of Low Buildings in Extreme Winds". *International Workshop on Wind Engineering Research and Practice: CurrentState-of-the-Art and Future Needs/Plans/Policies*, Charlotte, NC, May 2010.

**Morrison M. J.**, Martinuzzi R. J., Savory E., Kopp G. A., "Vortex shedding from slender surface mounted pyramids", *The CSME Forum ,* Kananaskis, Alberta, 2006.

Henderson D.J., **Morrison M.J.**, Kopp G.A., "The spatially distributed, fluctuating loading of a full scale hip roof at 3LP", *The 2nd AAWE Workshop*, Marco Island Florida, 2010.

Henderson D.J, **Morrison M.J.**, Ginger J.D., Miller C.A, "Response of Dines Anemometer to simulated winds", *Southern Hemisphere Extreme Winds Workshop*, Canberra, Australia, 2010.

Non-Refereed Technical Reports and Articles

G.A. Kopp, **M.J. Morrison**, "All About the Nails", Canadian Underwriter, January 2009.

**M.J. Morrison**, G.A. Kopp, "Evaluation of the ASCE 7-05 Definition of Edge and Corner Zones for Low-Rise Buildings", BLWT-1-2007, March 2007.

G.A. Kopp, **M.J. Morrison**, "Extension of the Analysis of Farquhar et al.", Letter, December 2006.

G.A. Kopp, **M.J. Morrison**, *Confidential*, Report: BLWT-SS29-2008, May 2008.

**M.J. Morrison**, G.A. Kopp, *Confidential*, BLWT Letter, May 2010.

Damage Survey Reports Prepared for Environment Canada

**Morrison M.J.**, Iizumi E., Miller C., Kopp G.A., "Vaughan Ontario Damage

Investigation – The August 20, 2009 Tornadoes", *Report for Environment Canada*, September 2009.

**Morrison M.J.**, Kordi B., Kopp G.A., "Damage Observations from the Events of April 25, 2008 in Southern Ontario", *Report for Environment Canada*, May 2009.